NASA CR-188283

CSDL-T-1205

FUZZY LOGIC APPLICATION FOR MODELING MAN-IN-THE-LOOP SPACE SHUTTLE PROXIMITY OPERATIONS

by

Robert B. Brown

May 1994

Master of Science Thesis
Massachusetts Institute of Technology

(NASA-CR-188283) FUZZY LOGIC APPLICATION FOR MODELING MAN-IN-THE-LOOP SPACE SHUTTLE PROXIMITY OPERATIONS M.S. Thesis - MIT (Draper (Charles Stark) Lab.) 146 p

N94-32359

Unclas

G3/63 0010460

The Charles Stark Draper Laboratory, Inc.
555 Technology Square, Cambridge, Massachusetts 02139-3563

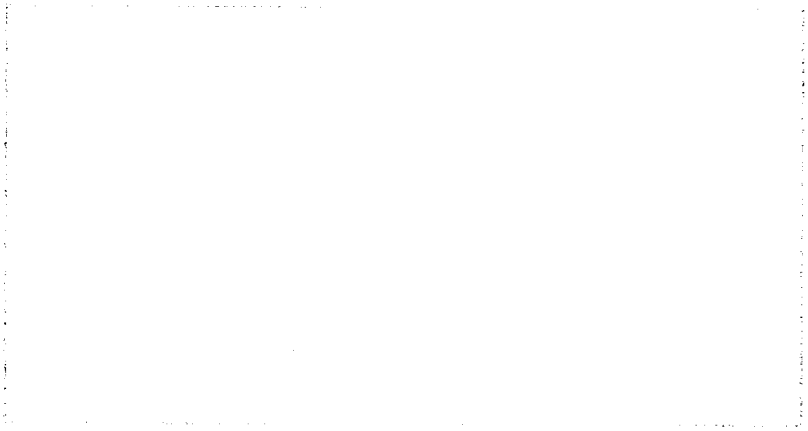

Fuzzy Logic Application for Modeling Man-in-the-Loop Space Shuttle Proximity Operations

by

Robert B. Brown

B.S. Astronautical Engineering, U.S. Air Force Academy (1986)

Master of Eng. Admin., George Washington University (1990)

SUBMITTED IN PARTIAL FULFILLMENT
OF THE REQUIREMENTS FOR THE DEGREE OF

MASTER OF SCIENCE
IN AERONAUTICS AND ASTRONAUTICS

at the
MASSACHUSETTS INSTITUTE OF TECHNOLOGY
May, 1994

Signature of Author 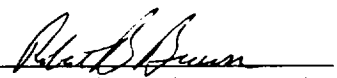
Department of Aeronautics and Astronautics
May 6, 1994

Approved by 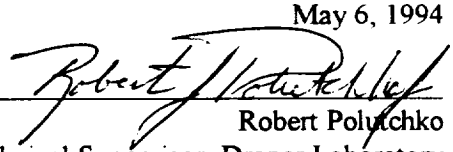
Robert Polutchko
Technical Supervisor, Draper Laboratory

Approved by 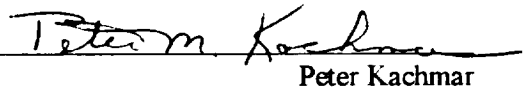
Peter Kachmar
Technical Supervisor, Draper Laboratory

Certified by 
Professor Thomas Sheridan
Thesis Supervisor, Professor of Aeronautics and Astronautics

Accepted by _____
Professor Harold Y. Wachman
Chairman, Department Graduate Committee

Fuzzy Logic Application for Modeling Man-in-the-Loop Space Shuttle Proximity Operations

by
Robert B. Brown

Submitted to the Department of Aeronautics and Astronautics on May 6, 1994
in partial fulfillment of the requirements for the degree of Master of Science.

ABSTRACT

This thesis develops a software pilot model for Space Shuttle proximity operations utilizing fuzzy logic. The model is designed to emulate a human pilot during the terminal phase of a Space Shuttle approach to the Space Station. The model uses the same sensory information available to a human pilot and is based upon existing piloting rules and techniques determined from analysis of human pilots' performance. Such a model is needed to generate numerous rendezvous simulations to various Space Station assembly stages for analysis of current NASA procedures and plume impingement loads on the Station.

The advantages of a fuzzy logic pilot model are demonstrated by comparing its performance with NASA's man-in-the-loop simulations and with a similar model based upon traditional Boolean logic. The fuzzy model is shown to respond well from a number of initial conditions, with results typical of an average human. In addition, the ability to model different individual piloting techniques and new piloting rules is demonstrated.

Technical Supervisor: Robert Polutchko
Technical Staff, Integrated Systems Section, CSDL

Technical Supervisor: Peter Kachmar
Section Chief, Integrated Systems Section, CSDL

Thesis Supervisor: Professor Thomas Sheridan
Professor of Aeronautics and Astronautics, MIT

ACKNOWLEDGMENTS

I want to express my appreciation to the many people who made this thesis and my education at MIT possible. First, I would like to thank Professor Sheridan for serving as my thesis advisor and giving freely of his time to assist me with this project. I also need to thank all of the people at the Charles Stark Draper Laboratory who have helped me with this research, particularly my advisors Pete Kachmar and Bob Polutchko. Their ideas and advice have been very valuable. I especially want to thank Bob Polutchko for the enormous amount of time he has willingly given these last two years to teach me about proximity operations, the OFS, timeliner, etc.. I have learned a tremendous amount from him.

I also want to thank the Air Force for allowing me to return to school, and Draper Laboratory for providing my fellowship.

I especially want to thank my family for all of their love and support, not just these last two years, but for my entire life. Their continual encouragement has been a tremendous reassurance wherever I have been. In particular, I want to thank my wife, and best friend, Marla. She has sacrificed a lot during these last two years, and I never could have made it without her. Her love and companionship have continually been an inspiration. She has blessed me in so many ways.

Finally, and most importantly, I want to thank my Lord Jesus Christ, for all of the prayers he has faithfully answered, and for the assurance that he holds the future in his hands.

This report was prepared at The Charles Stark Draper Laboratory, Inc., under National Aeronautics and Space Administration contract no. NAS9-18426. Publication of this report does not constitute approval by the Charles Stark Draper Laboratory, NASA, or the Massachusetts Institute of Technology of the findings or conclusions contained herein. It is published for the exchange and stimulation of ideas.

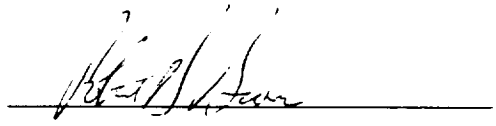

Robert B. Brown

Table of Contents

Chapter 1 : Introduction

1.1 Background

Future Shuttle rendezvous with the Space Station present some unique problems. Of particular concern is the final portion of the mission, when the Shuttle is within approximately 1,000 feet of the Station. During this phase of rendezvous, referred to as proximity operations, the relative size and distance between the vehicles become very important considerations. The Station will have large solar panels that could easily be damaged by the Shuttle's jet plume at these relatively close ranges. Also, unlike previous rendezvous targets, the Station will often not have a docking or grapple point near its center of mass, which presents some unusual problems due to orbital mechanics.

Analysis of these issues is difficult because a human pilot makes all targeting decisions during proximity operations. Every U.S. Space Program has used a manual control system during the last portion of rendezvous due to its reliability. The Shuttle's navigation sensors were designed for such a system, and are not sufficiently accurate to support computer targeting during the terminal phase of rendezvous. Therefore, an automatic trajectory controller for proximity operations is not feasible with the current Shuttle sensors. Instead, the pilot controls the Shuttle's trajectory, using the view through

a window as the primary source of information. Because a human is in the loop for such critical control functions, NASA does not currently have the capability to conduct fully computerized simulations of proximity operations. Additionally, due to the inherent variabilities associated with any human operator, parametric studies using man-in-the-loop simulations require very large Monte Carlo type analysis.

NASA intends to perform such an analysis of the Shuttle's plume induced loads on the different Space Station modular builds. To support these studies, NASA is conducting numerous proximity operations, man-in-the-loop simulations to various Space Station configurations. These simulations are conducted with a high fidelity graphic simulator flown by a human pilot in real time. While these simulations will provide important insight, they are very time consuming and cannot generate sufficient data. NASA's planning analysis shows that over 1,100 simulated approaches are required to statistically support these Monte Carlo studies, which will be used for a Station design review in December of 1994. However, due to limited simulator and pilot resources, NASA only expects to have completed 500 by this time.[14] This short term problem could become much worse if preliminary analysis indicates new piloting procedures will be necessary for Space Station missions. If this occurs, a large number of additional simulations will be required to develop and analyze each proposed change. Then, after selecting a new set of piloting procedures, NASA would have to regenerate their entire database.

A software pilot model, which duplicates the human operator's decision process and performance, is proposed as a solution to these problems. Such a model could easily supplement NASA's man-in-the-loop database. It could quickly produce a large number of simulated approaches to the Station, due to its ability to operate in "batch mode" on a main frame computer, rather than real time with a human operator on a graphic simulator. It would also be beneficial for evaluating proposed new piloting rules or techniques. Because a software model provides exact repeatability, parametric studies would require a relatively small number of runs. During these simulations, a few critical parameters could

be varied holding everything else constant. This is not possible with the man-in-the-loop simulations due to the variability associated with human pilots.

1.2 OBJECTIVE

This thesis presents a proximity operations pilot model, which is based upon fuzzy logic and is implemented using a high fidelity Space Shuttle simulator. The pilot model uses the same instrument readings and sensory information available to an astronaut. The model's fuzzy logic decision process is based upon current Space Station approach requirements and standard Shuttle piloting techniques. Analysis of over 90 NASA man-in-the-loop simulations were used to set the model's parameters, so it closely matches an actual human's performance.

There are a number of requirements for any proposed pilot model. Ideally, it should respond to various initial conditions in a manner consistent with a typical human pilot. For a large number of simulations, a pilot model should be statistically similar to an average astronaut. A software pilot should also have the ability to be modified slightly to model different individual piloting techniques. This would provide the capability to capture a broad range of potential pilots, not just one "average" pilot. Finally, a software pilot should also incorporate the flexibility to easily model potential new piloting rules or techniques by adding or modifying existing logic. The fuzzy pilot model presented in this thesis satisfies all of these essential requirements.

1.3 PREVIOUS WORK

Draper Laboratory is the only organization that has developed a computer pilot model based upon actual human performance.[4] The author participated in the development of

this model, which is based upon traditional, Boolean logic, using "crisp" thresholds. This thesis is an outgrowth of that pilot model. The primary difference is the model presented in this thesis is based upon fuzzy logic. This form of logic was selected due to its successful use in modeling the natural human decision process for control functions in other fields.[12,13,22]

NASA has also developed automatic spacecraft trajectory controllers using fuzzy logic.[3,15-18] However, these controllers are not designed to emulate a human pilot, but are intended to produce superior results. Their decisions are based upon information from on-board navigation systems not available or easily processed by the Shuttle crew. They also do not use the same techniques employed by human astronaut pilots. Consequently, these controllers are not useful in analyzing how a real pilot would perform and are unable to assess the jet plume loads on the Space Station during a manned Shuttle approach. These models are therefore inappropriate for supplementing NASA's database or for evaluating proposed new piloting rules.

1.4 METHOD OF RESEARCH

The method of research used in this thesis involves an evolutionary development of the fuzzy pilot model. The initial model is relatively simple, demonstrating the potential of a fuzzy logic controller. Slight enhancements or modifications are then made to analyze different aspects of the pilot model. Each stage in the development process builds upon the previous research and conclusions.

At each stage the model's performance is compared with NASA's man-in-the-loop simulations and is evaluated using Draper Laboratory's high-fidelity On-orbit Functional Simulator (OFS). This closed loop computer simulator models all of the Shuttle's translational and rotational dynamics, sensors, and actuators. It accounts for the

aerodynamic and plume forces on the Station, and uses the same computer code as the Shuttle to emulate the navigation, guidance, and control functions performed by the on-board computers. The OFS can control sequencing of crew procedures, and models crew keyboard interfaces and displays. Its performance has been verified using flight data. Because of its accuracy, the OFS is used to validate flight software performance in support of future Shuttle missions. For this thesis, the OFS is used to evaluate the pilot model's performance on a realistic Shuttle.

1.5 THESIS OUTLINE

Chapter 2 gives an overview of fuzzy logic. It explains the difference between traditional logic and fuzzy logic, and describes fuzzy sets, fuzzy operations, and fuzzy rules pertinent to this thesis.

Chapter 3 provides a description of Shuttle proximity operations, explaining the reference frames used and the sensory information available to a pilot. It also covers the piloting requirements and techniques used by astronauts. This provides the basis for the fuzzy rules presented in the following chapters.

Chapter 4 presents the initial fuzzy pilot model, which assumes the Shuttle does not have any rotational motion. This model's performance is evaluated in a simplified simulation environment and also with Draper Laboratory's OFS. Results are compared with four of NASA's man-in-the-loop simulations.

Chapter 5 presents an enhanced pilot model that accounts for the Shuttle's attitude motion. This model's results are compared with man-in-the-loop simulations, demonstrating the model's ability to match an "average" human pilot. The fuzzy model is also compared with a similar model, developed at Draper Laboratory, based upon "crisp"

logic. This comparison illustrates some of the benefits of fuzzy logic for duplicating a human's performance.

Chapter 6 demonstrates the fuzzy model's ability to match different piloting techniques by adjusting fuzzy set boundaries.

Chapter 7 presents a fuzzy pilot model with different parameters that model a human pilot operating with new piloting rules, which define a smaller approach corridor. The results from this pilot model are compared with eight man-in-the-loop runs. This comparison demonstrates the robust qualities of the pilot model.

Chapter 8 contains a summary of this project and outlines some areas for further research, which would likely enhance the fuzzy pilot model's performance and potential.

1.6 List of Terms and Variables

The following acronyms, terms, and variables are used throughout this thesis. They are defined in greater detail in the text, and are provided here as a reference.

1.6.1 List of Acronyms and Common Terms

COAS	Crew Optical Alignment Sight: a sight reticle mounted in an overhead window, which assists the pilot when measuring the line-of-sight angles and rates to the target vehicle.
COAS target	A target mounted on the Space Station, which is used by the pilot as a reference when looking through the Shuttle's COAS.
DAP	Digital Autopilot: Shuttle software that automatically maintains the Shuttle's attitude and selects specific jets to be fired.
DAP A	Digital Autopilot mode that allows the pilot to make large velocity changes with one THC command. Translation commands in DAP A impart approximately $.05\frac{ft}{sec}$.

DAP B	Digital Autopilot mode that allows the pilot to make small velocity changes. Translation commands in DAP B mode impart the minimum impulse to the Shuttle. For a typical Shuttle mass, this is slightly less than $.02\frac{ft}{sec}$.
LVLH	Local Vertical - Local Horizontal: target centered coordinate frame used to express the relative motion of the Shuttle with respect to the target vehicle.
Low Z	Translation burn that imparts a velocity in the $+Z_{Body}$ axis while minimizing the Shuttle's jet plume directed at the Station.
Norm Z	Normal +Z translation burn that fires jets directly along the Shuttle's $-Z_{Body}$ axis, imparting a velocity in the $+Z_{Body}$ direction.
OFS	On-orbit Functional Simulator: Charles Stark Draper Laboratory's high-fidelity Shuttle simulator, used in this thesis to evaluate the pilot models' performance.
proximity operations	The last portion of space rendezvous, which begins at a range of approximately 1,000 ft.
RMS	Remote Manipulator System: commonly called the Shuttle's "arm". This is used to grab the Station once the Shuttle is in proper position.
SC-2, SC-4	Station configuration 2 and 4: The second and fourth assembly stages for Space Station Freedom.
THC	Translation Hand Controller: device used by pilots to command translation velocity changes in the Shuttle's X, Y, and Z axes.
v-bar	The target vehicle's mean velocity vector, which is also the $\hat{i}_X$ LVLH vector.

1.6.2 List of Variables

R_L, $\dot{R}_L$	Range and range rate measured by the laser. This is the distance between the laser's mounting location and a reflector mounted on the Station near the COAS target.
R_P, $\dot{R}_P$	Range and range rate between the docking ports (the Shuttle's RMS and the grapple point on the Space Station). For the two builds addressed in this thesis $R_P = R_L - 25\text{ft}$.
$\dot{\theta}$, $\dot{\phi}$	The Shuttle's pitch and roll rates.
λ_V, λ_H, $\dot{\lambda}_V$, $\dot{\lambda}_H$	The vertical and horizontal line-of-sight angles and angle rates, measured from the Shuttle's COAS to the COAS target on the Space Station.
μ	Fuzzy logic term for the membership value of a variable in a fuzzy set. This variable also represents the truth value of a statement.
ω	Mean angular orbital motion. For low earth orbits, $\omega \approx 4\frac{\text{deg}}{\text{min}}$.

Chapter 2 : Fuzzy Logic

2.1 INTRODUCTION

Developing control systems to replace human operators is often a difficult task. Traditional methods begin by modeling the system to be controlled with mathematical equations. Then using classical control techniques, an engineer develops a suitable controller. Unfortunately, many real world systems are non-linear and are very difficult to model. Modeling these systems requires a great deal of time and often results in a very complex controller that is difficult to modify.

An additional drawback is human decisions are generally based upon relatively vague goals and constraints. Consider a control system designed to keep a room from being too *Hot* or too *Cold.* Typically engineers try to capture these imprecise terms using probability theory or by introducing stochastic variables. Well-defined thresholds for *Hot* and *Cold* are then randomized over some interval, which supposedly approximates their imprecise definitions. This however is based upon the faulty assumption that vague goals and constraints can be modeled with a random system.[2] The two are very different. For example, suppose the control system involved a person adjusting the speed of an intake fan to control the room's temperature. The person would likely determine the fan's speed

based upon the room temperature and the outside air temperature. If both of these variables are known exactly, there is no randomness. However, there are still imprecise goals and constraints in the decision process. Each person has their own "fuzzy" definitions of what temperatures are too *Hot* and too *Cold*. Vague terms such as these are used by people every day. They allow us to easily control complicated systems in an environment with inexact constraints and consequences.

In an attempt to quantify and manipulate these "fuzzy" definitions, without introducing artificial randomness, Lofti Zadeh developed fuzzy logic in 1965.[23] Fuzzy logic uses linguistic variables with simple rules to determine the required actions. As a result, fuzzy logic is relatively easy to develop, and is also a very good imitator of the human decision process. A typical fuzzy rule is:

If it is *Hot* inside *and* it is *Cool* outside then the fan speed should be *Fast*.

This chapter examines how variables such as *Hot*, *Cool*, and *Fast* are defined using fuzzy sets. It also shows how simple logic operators such as *and*, *or*, and *not* are used with fuzzy sets, and how different fuzzy rules are combined to yield a precise answer (for this example, the exact intake fan speed).

2.2 Fuzzy Sets

Traditional set theory is based upon Boolean logic; a statement is either true or false. Likewise, an element is either a member of a set or not. In contrast, fuzzy set theory allows an element to have partial membership in a set, with its degree of membership normalized to a value between zero and one. A value of one represents complete membership in the set, and zero means the element is completely excluded from the set. A value between zero and one indicates the degree of partial membership.

Fuzzy sets are usually defined over a range of a variable, referred to as a fuzzy partition. As an example, consider the membership of room temperatures. In classical set theory there is a single temperature above which the room is considered *Hot* and another temperature below which the room is *Cold*. This is depicted graphically in Figure 2-1. The temperature range is shown on the horizontal axis, and the vertical axis shows the degree of membership in a given set, commonly denoted μ. Because this figure determines the membership value for any specified temperature, it is referred to as a membership function.

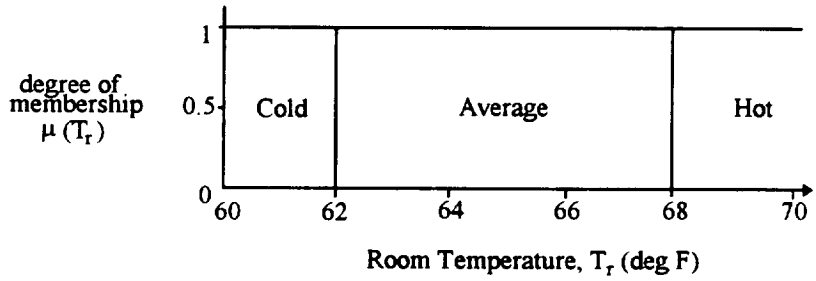

Figure 2-1 Classical sets for room temperature

Notice the sharp transitions between each set. For any given temperature, the room is considered either completely *Hot*, completely *Cold*, or completely *Average*. If the room temperature is 67.9°, $\mu_{cold} = 0$, $\mu_{average} = 1$, and $\mu_{hot} = 0$, so the temperature is *Average*. If the temperature increases to 68.1°, it is no longer *Average* but is completely *Hot* ($\mu_{cold} = 0$, $\mu_{average} = 0$, and $\mu_{hot} = 1$). These membership values can also be thought of as measure of truth. If the temperature is 68.1°, the statement, "The room temperature is *Hot.*" is completely true. At this temperature, $\mu_{average} = 0$, so the statement, "The room temperature is *Average.*" is absolutely false, and has a truth value of 0.

While this may be convenient for standard computer programming, in reality there is a gradual transition between an *Average* temperature and a *Hot* temperature. A room that is 67.9° will likely be considered somewhat *Hot*, although not as *Hot* as 68.1°. Fuzzy

set boundaries allow this partial membership. As depicted in Figure 2-2, a room at 67° is considered primarily *Average*, but it is also somewhat *Hot*. At this temperature, the membership values for each of the fuzzy sets are $\mu_{cold} = 0$, $\mu_{average} = 0.75$, and $\mu_{hot} = 0.25$.[1] As the temperature increases its membership in *Hot* grows. When the temperature is 68° the room is considered equally *Average* and *Hot*, so $\mu_{average} = \mu_{hot} = 0.5$. This is called the crossover point.[24]

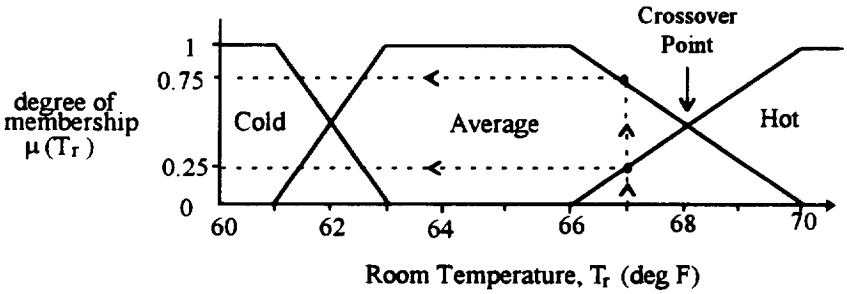

Figure 2-2 Fuzzy sets for room temperature

Because a person may have a more difficult time differentiating between *Average* and *Hot* than between *Average* and *Cold*, Figure 2-2 shows a more gradual transition between an *Average* temperature and a *Hot* temperature. In contrast, the transition between *Average* and *Cold* is not as fuzzy, so it has a steeper slope. If all of the fuzziness between two sets were removed, the boundary would become a vertical line, and the adjacent sets would be equivalent to classical sets. This special type of a fuzzy set is called a fuzzy singleton or a crisp set.[2,22]

A conditional set is another special type of fuzzy set. In this case the membership of y in fuzzy set B is conditional upon another variable, x. For example, classifying someone's height as *Tall* may be conditional upon their age. This is expressed as

[1] For these fuzzy sets, the sum of all membership values will always equal one. This is common, but it is not mandatory. Fuzzy set theory only requires individual set membership values to be normalized between zero and one. Therefore, the sum of many membership values could be greater than one.

$\mu_{Tall}(\text{height}|\text{age})$.[2,24] In addition, the variable of age can be expressed as a fuzzy set of *Young* or *Old*. When a person is *Young* they may be considered completely *Tall* if they are four feet in height. However, if they are *Old* they might have to be over six feet to be considered completely *Tall*. Given these definitions, someone who is equally *Young* and *Old* would be considered completely *Tall* if they were over five feet in height (an average of the thresholds for *Young* and *Old*). Conditional sets such as these are often used by humans to classify items and are used throughout this thesis.

2.3 FUZZY OPERATIONS

Fuzzy sets are used in conjunction with operations such as *and*, *or*, and *not*. These operations are very similar to the familiar Boolean operations and are important in evaluating fuzzy rules, of the type

"If **Antecedent** then **Conclusion**".

The antecedent is a conditional statement, which could be the function of more than one fuzzy set. For example, the antecedent may be "(It is *Hot* inside) *and* (it is *Cool* outside)". Determining the truth of this statement requires evaluating the intersection of two fuzzy sets. Other antecedents could involve unions (*or*) or complements (*not*) of fuzzy sets.

The intersection of two traditional sets is defined as all elements common to both. This simple definition is not adequate for fuzzy sets, because it does not define what should be done with the elements that have only partial membership in a set. To include this aspect of fuzzy sets, the membership value for an antecedent "(x is in A) *and* (y is in B)" is defined as the minimum value of $\mu_A(x)$ and $\mu_B(y)$. This is expressed as

$$\mu_{A\text{and}B}(x,y) = \text{Min}(\mu_A(x), \mu_B(y))$$

where μ_{AandB} represents the truth of the antecedent. Standard convention uses the symbol "$\wedge$" in place of "Min", and the expression is written

$$\mu_{\text{AandB}}(x,y) = \mu_{\text{A}}(x) \wedge \mu_{\text{B}}(y)$$

This definition is commonly called a "hard *and*", meaning it does not allow any tradeoff between $\mu_{\text{A}}(x)$ and $\mu_{\text{B}}(y)$; only the minimum value is important.[2] For example, if $\mu_{\text{A}}(x) = 0.5$ and $\mu_{\text{B}}(y) = 0.2$, then $\mu_{\text{AandB}}(x,y) = 0.2$. This value will not change for any $\mu_{\text{A}}(x) \geq 0.2$.

A "softer" interpretation of *and* is determined by the numerical product of $\mu_{\text{A}}(x)$ and $\mu_{\text{B}}(y)$. Using this definition, $\mu_{\text{AandB}}(x,y)$ is affected by the membership value in both fuzzy sets. This is denoted

$$\mu_{\text{AandB}}(x,y) = \mu_{\text{A}}(x)\mu_{\text{B}}(y)$$

Using this definition, and the above example, with $\mu_{\text{A}}(x) = 0.5$ and $\mu_{\text{B}}(y) = 0.2$, $\mu_{\text{AandB}}(x,y) = 0.1$. If either $\mu_{\text{A}}(x)$ or $\mu_{\text{B}}(y)$ change, so will $\mu_{\text{AandB}}(x,y)$. The author has opted for this "soft" interpretation of *and*, which penalizes partial membership in both fuzzy sets. Therefore, for the remainder of this thesis *and* will refer to the product of the membership values.

The union of set A and set B is the set of all elements in A *or* B. Fuzzy logic defines the union of two sets as the maximum membership value of either set. Using this definition, the truth value of "(x is in A) *or* (y is in B)" is

$$\mu_{\text{AorB}}(x,y) = \text{Max}(\mu_{\text{A}}(x), \mu_{\text{B}}(y))$$

Substituting the symbol "$\vee$" to represent the maximum, this is commonly written

$$\mu_{\text{AorB}}(x,y) = \mu_{\text{A}}(x) \vee \mu_{\text{B}}(y)$$

Although there are "soft" definitions for *or*, they are not very common and will not be used in this thesis.[2]

The fuzzy set "*Not* A" includes all elements that are not in set A. Therefore, its membership value is equivalent to the degree of nonmembership in A. This complement is simply

$$\mu_{\text{NotA}} = 1 - \mu_{\text{A}}$$

Notice, the fuzzy definitions for *and*, *or*, and *not* are identical to classical set theory if the sets are fuzzy singletons with crisp transitions.[2] Therefore, Boolean logic is really a subset of fuzzy logic that only operates on fuzzy singletons.

2.4 Evaluating Fuzzy Rules

Once the truth of the antecedent is known the resulting conclusion can be determined. This conclusion will either be expressed as another fuzzy set or as a crisp number. In either case the truth of the antecedent determines to what degree the conclusion is implemented.

2.4.1 Rules with Fuzzy Conclusions

A rule with a fuzzy conclusion is often used when the outcome is not well defined or it is difficult to determine an exact conclusion. In this case, the rule is of the form

If **(Fuzzy Antecedent)** Then **(Conclusion = Fuzzy Set)**.

The antecedent may consist of any combination of operations on fuzzy sets. These operations determine the truth of the entire antecedent. This truth value is then used as the desired membership in the conclusion's fuzzy set. This process is called a "μ cut" because everything in the conclusion's fuzzy set above the antecedent's truth value is

eliminated. As an example, the following rules, specifying an intake fan's speed as a fuzzy set, are evaluated graphically:

A. If (it is *Hot* inside *and* it is *Cool* outside) Then (the fan speed should be *Fast*).

B. If (it is *Not Hot* inside *or* it is *Warm* outside) Then (the fan speed should be *Medium*).

Assume the room temperature, $T_r = 67°$, the outside air temperature, $T_o = 60°$, and the fuzzy sets are defined as shown in Figure 2-3.

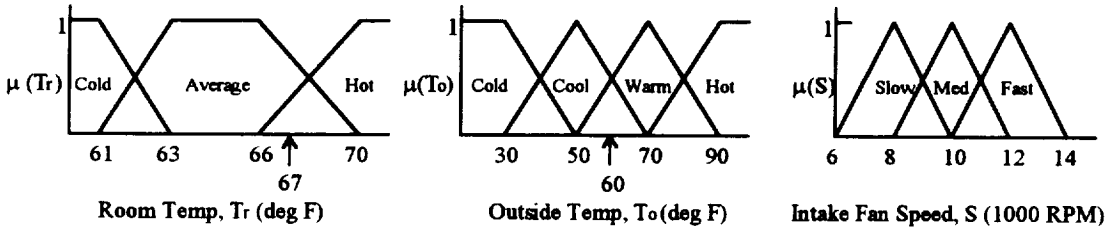

Figure 2-3 Fuzzy sets for temperatures and fan speed

The truth of the antecedent in rule A is the product of the membership values of the room temperature in the fuzzy set *Hot*, and the outside temperature in the fuzzy set *Cool*. As shown in Figure 2-4, $\mu_{hot}(67) = 0.25$ and $\mu_{cool}(60) = 0.5$; so the truth value of the entire antecedent is 0.125. This truth value is then used to define the maximum membership value in the conclusion's fuzzy set for *Fast* fan speeds.

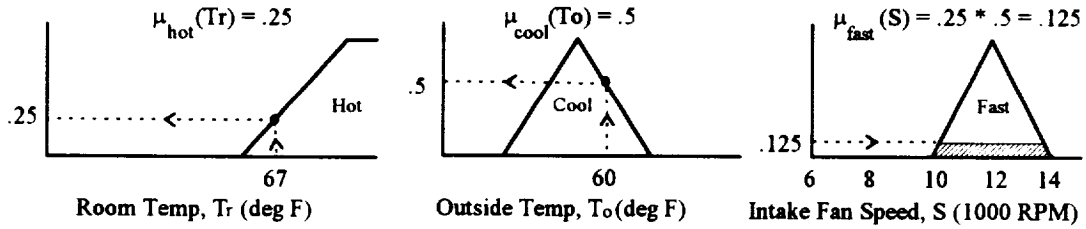

Figure 2-4 Graphical evaluation of rule A

For rule B, the truth of the antecedent is determined by the union of the fuzzy set for room temperature that is *Not Hot* and the set for a *Warm* outside temperature. Figure 2-5 shows $\mu_{not\ hot}(67) = 0.75$ and $\mu_{warm}(60) = 0.5$. Therefore, the antecedent has a truth value of 0.75. This value is used to define the desired membership for the fuzzy conclusion over the range of *Medium* fan speeds.

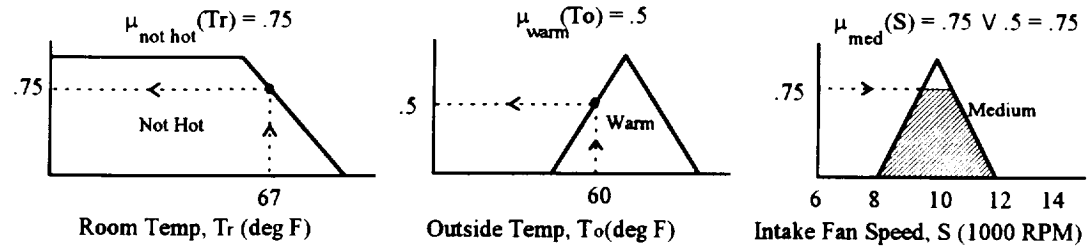

Figure 2-5 Graphical evaluation of rule B

This example is similar to many human operated control systems. People rarely control something using only one rule. Instead, they use a number of simple rules, which often have conflicting conclusions. These conclusions are blended together to yield a single output. Using fuzzy logic with the example above, the conclusions from rules A and B are combined by taking the union (or maximum) of their membership values across the domain of intake fan speeds. As previously determined, rule A specifies the fan speed should have a membership value of 0.125 in *Fast*, and rule B specifies a 0.75 membership value in the fuzzy set of *Medium* fan speeds. The union of these two sets results in an odd shaped set shown in Figure 2-6 C. Because this combined output is still a fuzzy set, it cannot be used directly as a control output. It must first be converted to a "crisp" number, specifying an exact intake fan speed, which should closely represent the aggregate fuzzy output. This process is referred to as "defuzzification". The most common method for defuzzification is to assign the domain variable the value at the centroid of the set defined

by the union of the fuzzy conclusions. This is shown graphically in Figure 2-6.[8,11,22] Using this method, the aggregate output specifies an intake fan speed 10,388 RPM.

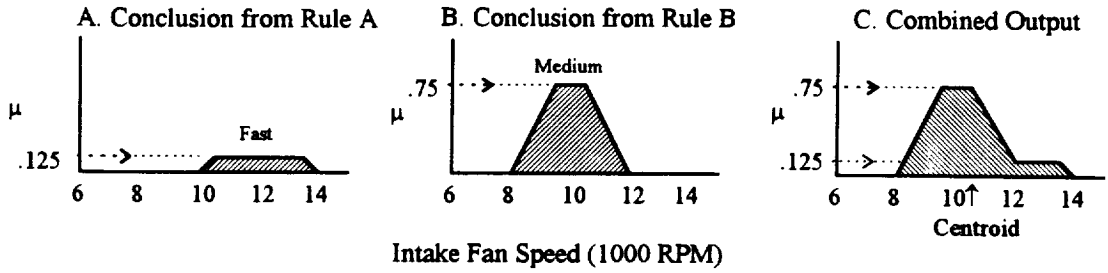

Figure 2-6 Defuzzification: A and B) Fuzzy sets after being μ cut C) Union of sets

2.4.2 Rules with Crisp Conclusions

Fuzzy rules can also specify a crisp conclusion. These rules are generally used when the exact result of some specified condition is known. They are of the form

If (Fuzzy Antecedent) Then (Conclusion = Crisp Number).

In this case, the truth of the antecedent is used to weight the crisp conclusion. Given a number of rules, the aggregate output is simply an average of the conclusions each weighted by the relative truth of its antecedent. Because this is a crisp number, defuzzification is not necessary. For a total of N rules the aggregate output is

$$\text{Aggregate output} = \frac{\sum_{n=1}^{N} \mu_n * \text{conclusion}_n}{\sum_{n=1}^{N} \mu_n}$$

where μ_n is the truth value of the nth antecedent, and conclusion_n is its corresponding crisp conclusion. For example, the previous rules A and B could be rewritten with crisp conclusions, replacing *Fast* with an exact value of 12,000 RPM, and *Medium* with 10,000 RPM.

A. If (it is *Hot* inside *and Cool* outside) Then (the speed should be 12,000 RPM).

B. If (it is *Not Hot* inside *or* it is *Warm* outside) Then (the speed should be 10,000 RPM).

Remember the truth value of the antecedent in rule A was 0.125, and the truth of the antecedent in rule B was 0.75. Therefore, the combined output is

$$\text{Aggregate output} = \frac{.125*12{,}000 \; + \; .75*10{,}000}{.125 \; + \; .75} = 10{,}285 \text{ RMP}$$

Notice, this final output is very close to the prior method when each rule had a fuzzy conclusion.

In a more general form, the outputs from different rules are weighted by a number to emphasize or de-emphasize certain rules. For crisp conclusions, the combined output is

$$\text{Aggregate output} = \frac{\sum_{n=1}^{N} w_n * \mu_n * \text{conclusion}_n}{\sum_{n=1}^{N} w_n * \mu_n}$$

where w_n is the weight of the nth rule.[22] For this thesis, however, every rule has the same weight, so $w_n = 1$.

2.5 Determining the Fuzzy Rules and Sets for this Thesis

Having covered the basic methods for evaluating fuzzy rules; the important question remaining is "How are the rules and sets chosen?". These critical decisions are very subjective and may vary depending upon the person and the circumstances. It is therefore extremely important to have some source of expert knowledge when formulating a fuzzy logic controller. A common approach is to interview people with experience controlling the system in question.[8,13,22]

For this thesis, an expert knowledge of the decision process was provided by pilot comments, documented piloting rules, piloting techniques, and simple orbital analysis. However, the primary source of information for determining the fuzzy set boundaries, came from analysis of over 90 NASA man-in-the-loop simulations. These simulations were flown by four different "engineer pilots" to four intermediate assembly stages of Space Station Freedom.[1] In many ways this type of "interview" is preferable to the more traditional face-to-face discussion. The database provides the pilots' exact response for many different sensory inputs, and it is less likely to be biased or incomplete. All of these "expert" sources were used to formulate simple fuzzy rules. Set boundaries were then determined based upon individual pilot responses. Because different pilots have different techniques and sensitivities, the boundaries defining fuzzy sets, such as *Large* and *Small*, were varied to model different individual pilots. Finally, because NASA's database provides the exact pilot responses, all of the fuzzy rules in this thesis have crisp conclusions and do not need to be defuzzified.

[1] "Engineer pilots" perform the majority of NASA's simulations because of the limited availability of astronaut pilots. Although they are not astronauts, they are trained and certified to follow NASA's proximity operations piloting procedures.

Chapter 3 : Space Shuttle Proximity Operations

3.1 INTRODUCTION

Space Shuttle rendezvous is necessary to service satellites, assemble the Space Station, and resupply the Station once it is completed. Rendezvous consists of placing and maintaining the Shuttle in a low earth orbit, which over several revolutions will intercept the target vehicle with a controlled closure rate. Maintaining this trajectory requires special navigation, guidance, and attitude control operations.

This chapter provides an overview Space Shuttle rendezvous, with an emphasis on the terminal mission phase, referred to as proximity operations. It explains the relative motion between two spacecraft, and covers the Shuttle's actuators and on-board sensors used during rendezvous. In addition, this chapter describes the operational restrictions that limit a pilot's actions and the general piloting techniques used during proximity operations. This material provides the background necessary to understand the fuzzy pilot model presented in the following chapters.

3.2 Overview of Shuttle Rendezvous and Proximity Operations

A rendezvous mission begins with a series of ground targeted burns to bring the Shuttle within the general vicinity of the target vehicle. The last two of these burns are called the Height Maneuver and Phasing Maneuver. They place the Shuttle approximately 250,000 feet behind the target at roughly the same altitude.[10]

Beginning at this point the relative position between the two vehicles is measured directly by the Shuttle's on-board sensors. Over the next three orbits, the Shuttle's computers filter this sensory data and calculate a series of impulsive velocity changes necessary to maintain the Shuttle on an intercept trajectory. This trajectory is depicted in Figure 3-1 using a target centered coordinate frame.[10] The earth is at the bottom of the figure, and the vehicles are moving right to left. Using this coordinate frame, each Shuttle orbit, which lasts approximately 90 minutes, is represented by one "loop" in Figure 3-1.

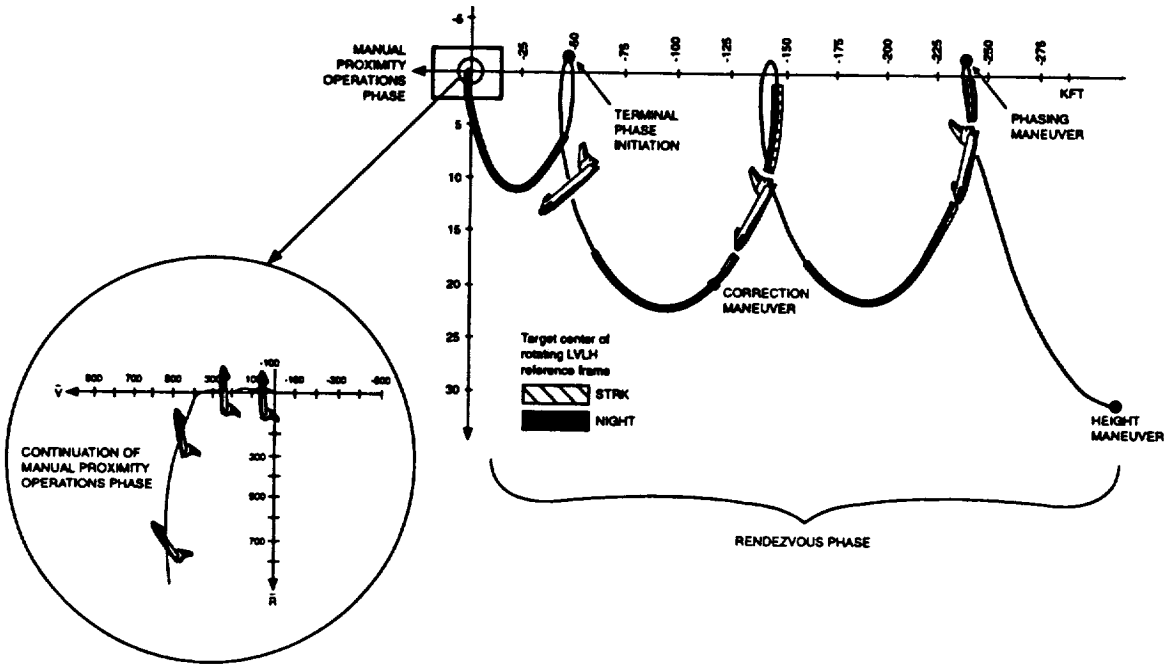

Figure 3-1 Space Shuttle rendezvous and proximity operations

During the latter half of each orbital day, when the target is illuminated by the sun, the Shuttle's star tracker accurately measures the line-of-sight angles to the target. This portion of each orbit is designated "STRK" in Figure 3-1. The measurements from the star tracker, along with data from the Inertial Measurement Unit (IMU), are fed to the Shuttle's navigation software. After the Shuttle closes to within 100,000 feet, the on-board radar begins measuring the relative range, range rate, and line-of-sight angles to the target. The computers filter all of this information to improve the navigation estimate, and calculate the necessary velocity changes using a Lambert targeting algorithm.[1] Two of these burns, the Nominal Combined Correction Maneuver and the Terminal Phase Initiation, are shown in Figure 3-1.[10]

During the last orbit, as the Shuttle passes below the target, the two vehicles are approximately one nautical mile apart, and the pilot reconfigures the Shuttle for manual operations. During this phase of the mission, computer targeting is no longer feasible due to navigational uncertainties. Instead the pilot makes small corrections to the Shuttle's trajectory to control the intercept and maintain the closure rate within acceptable levels.

During this manual phase of rendezvous, the pilot's primary sensory information comes from the view through a Crew Optical Alignment Sight (COAS) mounted in an overhead window. This allows the pilot to easily measure the line-of-sight to the target. A laser provides the pilot with the range and range rate to the target, and an IMU senses the Shuttle's attitude and inertial rotation rates, which are presented on internal computer displays.

The portion of the manual phase inside approximately 1,000 feet is referred to as proximity operations. In this region the target is susceptible to Shuttle jet plume impingement, the docking/grapple point begins to be distinguishable, and the relative size and attitude of the two spacecraft become important considerations.

During proximity operations, the pilot modifies the Shuttle's trajectory by slowing the closure rate. Instead of a direct intercept from below, the Shuttle arrives at a point

approximately 400 feet in front of the target. This begins the second half of proximity operations. From here, the pilot approaches in front of the target along, or slightly below, the target's velocity vector.

This second half of proximity operations is especially important because this is when the Shuttle's jet plume has its most significant affect on the target. For this reason, almost all of NASA's man-in-the-loop simulations cover only this second portion of proximity operations, beginning roughly 400 feet in front of the Station. Therefore, this thesis only addresses the later portion of proximity operations.

The analysis in this thesis also only covers rendezvous with two Space Station assembly stages, Station Configuration 2 (SC-2) and Station Configuration 4 (SC-4). For both of these configurations, shown in Figure 3-2, the Station is in a vertical attitude. Two solar panels are located at the top of a long truss, which points down toward the center of the earth. The grapple point is near the bottom of this truss, roughly 30 ft below the target's center of mass for SC-2, and 50 ft below the center of mass for SC-4.

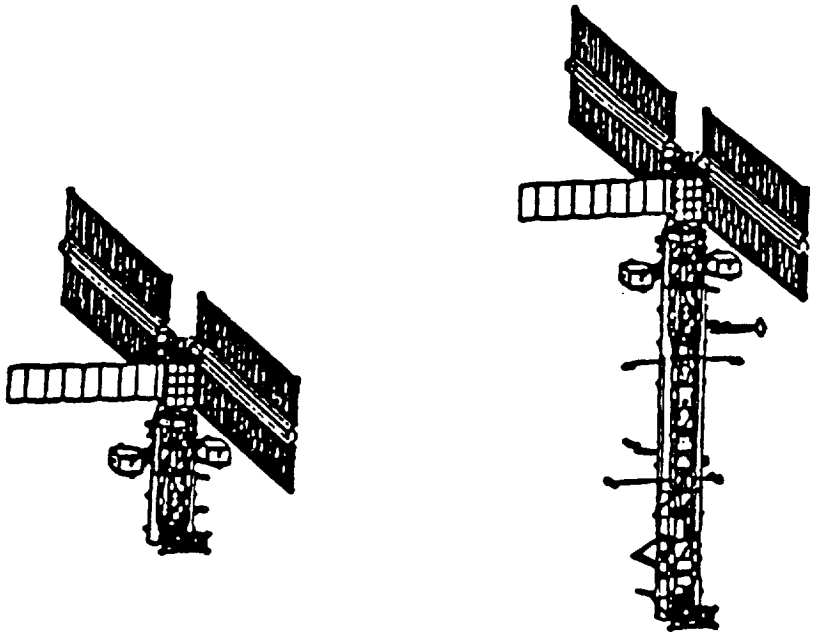

SC-2 SC-4

Figure 3-2 Station Configuration 2 and 4

3.3 Relative Motion of Two Vehicles during Rendezvous

During rendezvous, we are primarily concerned with the relative motion of the two vehicles. It is therefore convenient to define a rotating coordinate system that is centered on the target's center of mass. This "Local Vertical - Local Horizontal" (LVLH) coordinate frame was used in Figure 3-1, and is shown in more detail in Figure 3-3. The $\hat{i}_Z$ unit vector is defined to be in the direction opposite the target's orbital position vector; so it points toward the center of the earth. The $\hat{i}_Y$ vector is opposite the reference orbit's angular momentum vector, and $\hat{i}_X$ is defined to complete the right hand coordinate system ($\hat{i}_Y \times \hat{i}_Z$). For the Space Station's near circular orbit, $\hat{i}_X$ is in the direction of the Station's velocity. It is therefore often referred to as "v-bar". Because the LVLH frame is anchored to the target's orbital position vector, it rotates 360° during each orbit. For typical 90 minute orbits, this equates to a rotation rate of $4\frac{\text{deg}}{\text{min}}$. Throughout this thesis, the Shuttle's relative position in the target's orbital plane is represented by the x and z LVLH vectors, while the Shuttle's x and y LVLH vectors define its out-of-plane position.

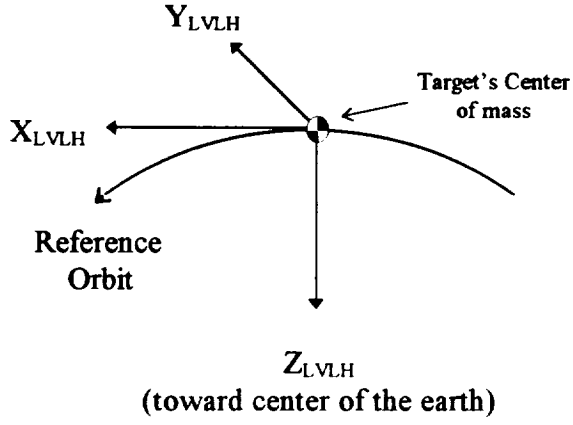

Figure 3-3 LVLH coordinate frame

The Shuttle's motion in this LVLH frame can best be described using the Clohessy-Wiltshire equations. These are linear constant-coefficient, differential equations

describing the relative motion of two small bodies in a circular orbit about a third larger body. They were originally developed in 1960,[7] and are derived by the author in Appendix A. The solution to these equations is used to determine the Shuttle's relative position and velocity with respect to the Station at time t, given the Shuttle's initial state at some reference time, $t = 0$. Equation 3-1 shows the solution to the Clohessy-Wiltshire equations in matrix form.

$$\begin{bmatrix} x \\ y \\ z \\ \dot{x} \\ \dot{y} \\ \dot{z} \end{bmatrix} = \begin{bmatrix} 1 & 0 & 6\omega t - 6\mathrm{S} & \frac{4\mathrm{S}}{\omega} - 3t & 0 & \frac{2}{\omega}(1-\mathrm{C}) \\ 0 & \mathrm{C} & 0 & 0 & \frac{\mathrm{S}}{\omega} & 0 \\ 0 & 0 & 4-3\mathrm{C} & -\frac{2}{\omega}(1-\mathrm{C}) & 0 & \frac{\mathrm{S}}{\omega} \\ 0 & 0 & 6\omega(1-\mathrm{C}) & 4\mathrm{C}-3 & 0 & 2\mathrm{S} \\ 0 & -\omega\mathrm{S} & 0 & 0 & \mathrm{C} & 0 \\ 0 & 0 & 3\omega\mathrm{S} & -2\mathrm{S} & 0 & C \end{bmatrix} \begin{bmatrix} x_0 \\ y_0 \\ z_0 \\ \dot{x}_0 \\ \dot{y}_0 \\ \dot{z}_0 \end{bmatrix} \tag{3-1}$$

where ω is the Station's orbital rotation rate, or mean motion, $C = \cos(\omega t)$, and $S = \sin(\omega t)$. In state transition form these equations are expressed

$$\mathbf{x}(t) = \Phi(\omega, t)\mathbf{x}(t_0) \tag{3-2}$$

From Equation 3-1, some general aspects about the Shuttle's relative motion are apparent. First, the equations for y and $\dot{y}$ are not affected by x_0, z_0, $\dot{x}_0$, or $\dot{z}_0$. Therefore, motion perpendicular to the orbital plane is uncoupled to the other axes. In addition, Equation 3-1 shows this out-of-plane motion is an undamped sinusoid with the same period as the Space Station ($\frac{2\pi}{\omega}$). In contrast, the x and z axes, defining the Shuttle's in-plane motion are coupled. As a result, anticipating orbital motion is a difficult task that is not at all intuitive.

Further complicating a pilot's task, it is evident from Equation 3-1 that the future position and velocity cannot be controlled simultaneously. The current position, defined by $[x_0 \quad y_0 \quad z_0]^{\mathrm{T}}$, is given. Nothing can be done to immediately change the Shuttle's initial position; the pilot can only change the Shuttle's initial velocity. This is

accomplished with translation jets, which change $[\dot{x}_0 \quad \dot{y}_0 \quad \dot{z}_0]^T$ almost instantaneously. However, because there are only three inputs, a pilot cannot simultaneously control all six variables defining the Shuttle's future position and velocity. Equation 3-1 is an overdetermined set of equations, which makes a pilot's job even more difficult. The piloting techniques used to solve these problems will be discussed in Section 3.7.

3.4 THE SPACE SHUTTLE'S ACTUATORS

Both the Shuttle's attitude rates and its translation motion are controlled using 44 jets at various locations on the vehicle. The Shuttle's body frame coordinate system is used to describe the location of these jets. For this frame, $\hat{i}_X$ is defined to be in the direction of the Shuttle's nose; $\hat{i}_Y$ is out the Shuttle's right wing; and $\hat{i}_Z$ is through the belly of the Shuttle. These vectors are shown in Figure 3-4.

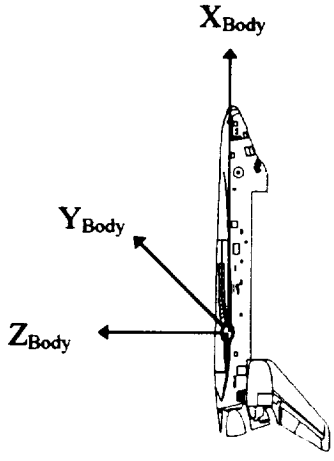

Figure 3-4 Shuttle body coordinate frame in an LVLH attitude

The Shuttle's attitude and translation motion are controlled separately.[1] The Digital Autopilot (DAP) maintains the Shuttle's attitude, and commands all of the attitude jet firings, while the pilot controls all translation jet firings.

During the first half of proximity operations, before the Shuttle arrives in front of the target (commonly called "v-bar arrival"), the DAP holds the Shuttle in an inertial attitude. However, after v-bar arrival, the Shuttle maintains an LVLH attitude, keeping the $-X_{Body}$ vector toward the center of the earth, and the Y_{Body} vector aligned with the Shuttle's angular momentum vector. This keeps the Shuttle in a tail down attitude with the cargo bay facing the target. This attitude is maintained using a 1 degree deadband and a rate limit of $0.1\frac{deg}{sec}$.

An LVLH attitude is beneficial for a pilot. Because the translation burns are referenced with respect to the Shuttle's body axes, this attitude provides a natural alignment of the Shuttle's actuators with the LVLH frame. Therefore, a pilot can easily control the Shuttle's velocity in any of the LVLH directions. For example, the X_{Body} vector points in the same direction as the $-Z_{LVLH}$ vector. Thus, a $+X_{Body}$ burn, which adds velocity in the $+X_{Body}$ direction, increases velocity in the $-Z_{LVLH}$ direction. This will tend to increase the Shuttle's altitude. Likewise, burns in the Y_{Body} axis directly affect the Y_{LVLH} velocity, and Z_{Body} burns change the Shuttle's velocity in the X_{LVLH} direction.

Translation burns in the X, Y, and Z body directions are a pilot's only control input. A pilot commands these burns by deflecting the Translation Hand Controller (THC), which fires a different number of jets depending upon the axis. These jets are generally paired to minimize the attitude disturbance. Both ±X and ±Y commands activate two jets. However, due to jet placement, -Z commands activate six jets, and +Z commands fire three or four jets, depending upon the type of burn. For a "Normal" +Z

[1] Although these functions are controlled independently, there is some unintentional coupling. Due to the location of the various jets, attitude firings cause some translation, and translation commands result in some attitude motion.

burn, three jets fire along the $-Z_{Body}$ axis to increase the Shuttle's velocity in the $+Z_{Body}$ direction. Because these jets point directly at the Station, they can create large plume forces. In contrast, a "Low" +Z burn reduces the plume loads on the Station. As shown in Figure 3-5, "Low" Z burns activate two +X jets and two -X jets simultaneously. Because these jets are not perfectly aligned with the X_{Body} axis, but are canted 7.8° toward the $-Z_{Body}$ axis, they provide a small force in the $+Z_{Body}$ direction.[20] This is extremely fuel inefficient, but it does result in less jet plume pointed directly at the Station.

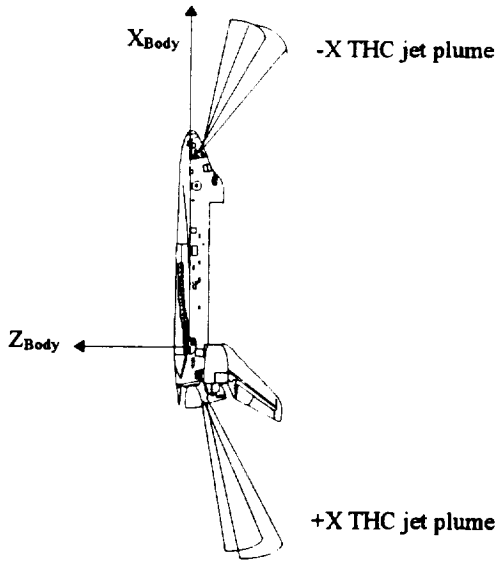

Figure 3-5 Low Z burns use ±X jets

A pilot can vary the translation pulse size by selecting "DAP A" or "DAP B". As configured for proximity operations, translation burns in DAP B impart the minimum impulse of slightly less than $.02\frac{ft}{sec}$. This small impulse is achieved by leaving the jets on for the minimum time of 80 ms.[1] In DAP A mode, the jets are left on for a longer period of time. For X and Y burns, DAP A leaves the jets on for .24 seconds, providing three

[1] Low Z burns are an exception. Due to their skewed angles, they must be left on for 0.32 seconds to achieve any meaningful force in the +Z direction.

times the minimum impulse force, or roughly $.05\frac{ft}{sec}$. For Z burns the jet on time varies considerably depending upon the number of jets activated and the Shuttle's mass. Table 3-1 summarizes all the jet on times in DAP A and DAP B for Shuttle missions to the two Station configurations discussed in this thesis, SC-2 and SC-4.[20] These numbers are used later to compare pilots' total THC activity by summing the translation jet on times from all three axes.

Table 3-1 Translation jet on time

THC Burn Axis (Body coordinates)	Number of Jets	DAP A mode		DAP B mode	
		Jet on Time (sec)	Total Jet on Time (sec)	Jet on Time (sec)	Total Jet on Time (sec)
±X Axis	2	.24	.48	.08	.16
±Y Axis	2	.24	.48	.08	.16
+Z Axis					
Normal +Z	3	.16	.48	.08	.24
Low +Z					
SC-2 (Shuttle mass 6570 lb.)	4	1.44	5.76	.32	1.28
SC-4 (Shuttle mass 6570 lb.)	4	1.28	5.12	.32	1.28
-Z Axis	6	.16	.96	.08	.48

3.5 SENSORS USED DURING PROXIMITY OPERATIONS

During proximity operations, the pilot bases THC command decisions on the information from three sensors. A Crew Optical Alignment Sight (COAS) helps the pilot measure the line-of-sight angles and angle rates to the target. These are measured in the vertical and horizontal directions, and are designated λ_V, $\dot{\lambda}_V$, λ_H, and $\dot{\lambda}_H$. The crew also uses a laser to measure the relative range and range rate, R_L and $\dot{R}_L$. In addition, most pilots also reference an IMU based attitude information display, which provides Shuttle inertial pitch

rates ($\dot{\theta}$) and roll rates ($\dot{\phi}$). These rates are used to evaluate the effect the Shuttle's rotational motion has on the line-of-sight data from the COAS. This section discusses each of these sensors.

To assist the pilot during proximity operations, a Crew Optical Alignment Sight (COAS) is mounted in an overhead window in the back of the flight deck. This is a sight reticle with vertical and horizontal crosshairs and hatch marks measuring ±5° in both directions.[21] The pilot looks out the window, through the COAS at a target mounted on the Space Station, called the COAS target. Referencing the hatch marks, the pilot can easily measure the vertical and horizontal line-of-sight angles relative the Shuttle's $-Z_{Body}$ axis. Figure 3-6 shows a pilot measuring a 3° vertical angle.

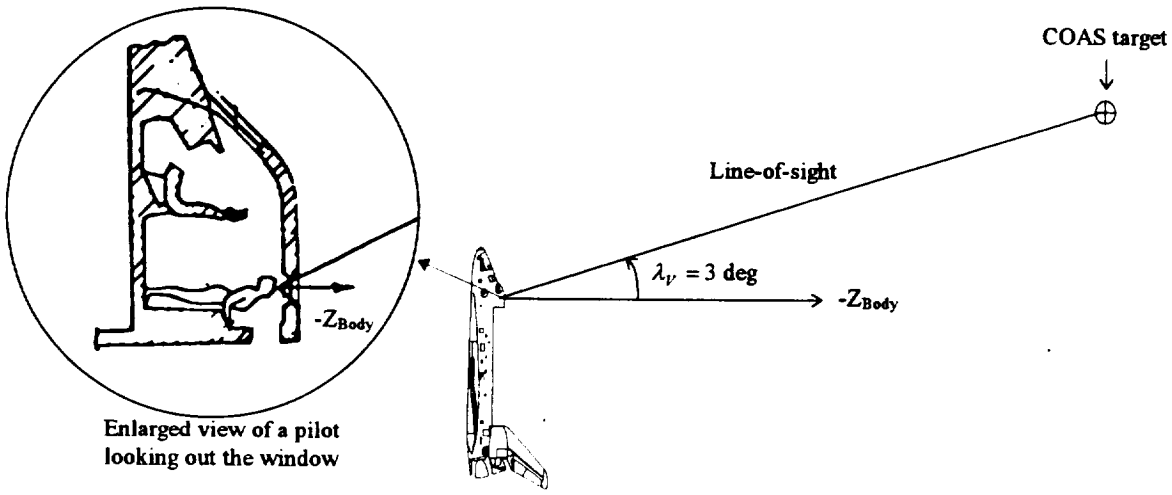

Figure 3-6 Pilot measuring a vertical line-of-sight angle

Because the COAS is fixed to the Shuttle's body, which is aligned with the LVLH frame, the COAS angles allow an estimate of the Shuttle's position relative to the Station. For example, if the COAS target is in the upper left quadrant of the COAS, the pilot is below and to the right of the COAS target. This COAS view is shown in Figure 3-7. The vertical angle, $\lambda_V = 3°$, which corresponds with the Shuttle's relative position shown in

Figure 3-6. The horizontal COAS angle, $\lambda_H = 2°$. A pilot estimates the angle rates, $\dot{\lambda}_V$ and $\dot{\lambda}_H$, by observing how fast the COAS target moves across the COAS. This information helps the pilot estimate the Shuttle's velocity in the vertical and horizontal directions.

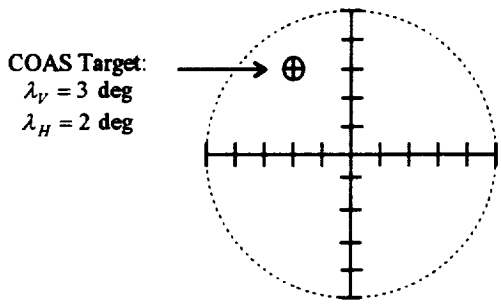

Figure 3-7 View through the COAS

If the COAS target is perfectly centered in the COAS at the conclusion of proximity operations, the Shuttle Remote Manipulator System (RMS) will be in an ideal position for grapple. For Station Configurations 2 and 4, this ideal position places the RMS end effector at the same altitude and down range position as the Station's grapple point. However, the optimum out-of-plane position is 7.5 feet to the right of the grapple point as viewed by the pilot. From this position the RMS operator only has to move the arm in the lateral direction to grab the Station. In LVLH coordinates, this final RMS position is $\begin{bmatrix} 0 & -7.5 & 0 \end{bmatrix}^T$ feet from the grapple point.

For Space Station rendezvous the crew will use a laser to measure the range and range rate. This laser has a one sigma random range rate error of $0.01 \frac{ft}{sec}$, which is displayed to the crew. It is also important to note, the laser measures the distance between its mounting location and a reflector located near the COAS target; not the distance between the end effector and grapple point. To avoid any confusion when discussing "range", R_P is used to indicate the "port-to-port" distance between the end effector and grapple point, and R_L indicates the range displayed on the laser. Pilots

generally use R_L for large ranges, but convert to R_P for smaller ranges. For rendezvous to SC-2 or SC-4, $R_L = R_P + 25$ ft. Figure 3-8 shows both of these distances as the Shuttle approaches SC-4.

Although the COAS and laser are a pilot's primary sensors, they provide no information about the Shuttle's attitude. Without this information a pilot could easily mistake attitude motion for translation motion. The DAP maintains the Shuttle in the desired LVLH attitude within $\pm$ 1° and $\pm$ 0.1$\frac{deg}{sec}$. Consequently, the Shuttle can pitch or roll up to 2° in 20 seconds. During this time, the target would appear to move through the COAS at the same rate. Because a pilot lacks external references, this perceived motion could incorrectly be attributed to a change in the Shuttle's translation. Therefore, prior to making a velocity correction most pilots reference a display of the Shuttle's body rates.

Information about the Shuttle's pitch and roll rates helps a pilot analyze target motion in the COAS. For example, if the pitch rate is relatively high, a pilot assumes a large portion of the target's perceived vertical movement is due to attitude motion, not translation. In the same way, the roll rate helps the pilot interpret any horizontal target motion in COAS.[14]

In summary, there are three sensors used by the pilot and crew during proximity operations. The COAS helps the pilot visually measure the line-of-sight angles and angle rates, while a laser measures the range and range rate to the Station. In addition, most pilots reference the Shuttle's inertial pitch and roll rates, which are provided by the Shuttle's IMU. These rates help a pilot estimate the amount of target motion across the COAS that can be attributed to the Shuttle's rotation.

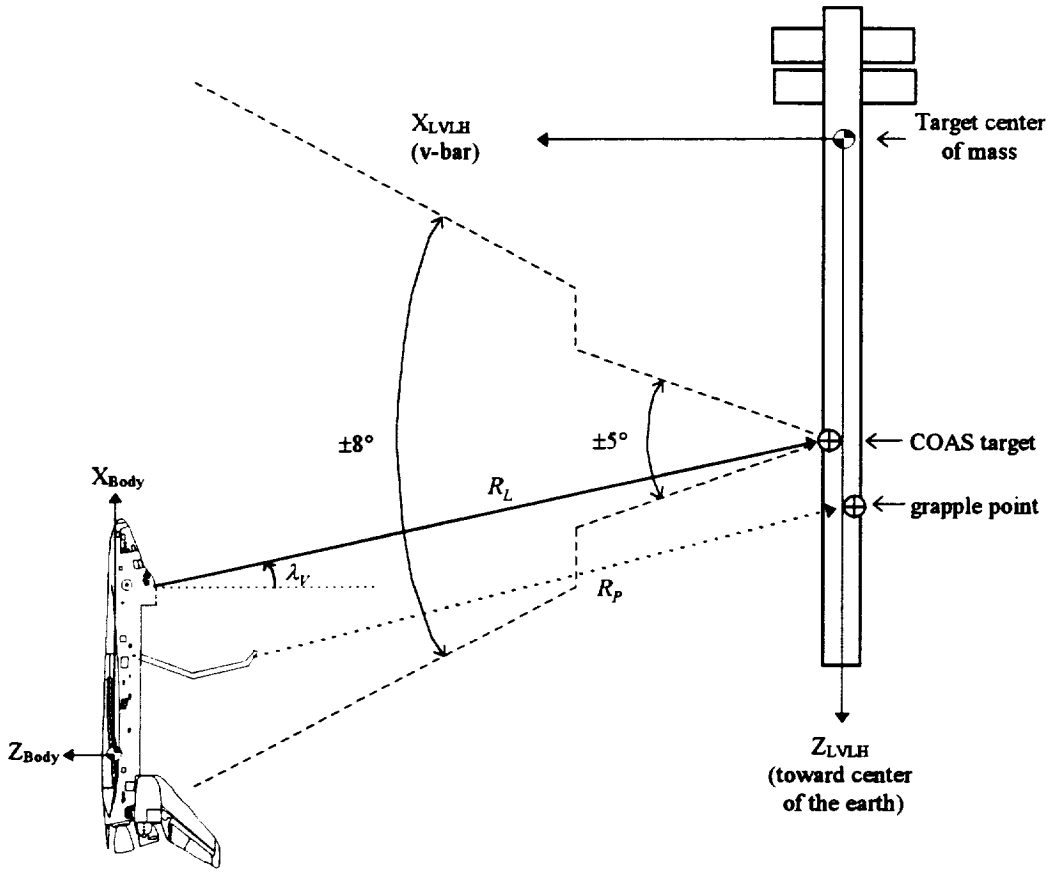

Figure 3-8 Profile view of the approach corridor in the orbital plane

3.6 PILOTING RULES

In an effort to standardize rendezvous and also minimize the Shuttle's jet plume effects on the Station, NASA imposes three simple rules on the pilots during the final portion of proximity operations. These rules define the approach corridor, limit the Shuttle's closure rate, and specify when a pilot may make "Low" and "Normal" Z translation burns.

The first rule requires a pilot to keep the COAS target within ± 8 in the COAS.[1] This restricts $|\lambda_V| \leq 8$ and $|\lambda_H| \leq 8$, and defines an approach corridor shaped like a right rectangular pyramid. When the range between docking ports is less than 25 feet, the approach corridor shrinks to ± 5 .[6] Figure 3-8 shows this approach corridor in the orbital plane.

The second proximity operations rule governs the Shuttle's closure rate. For $R_P \geq 100$ ft, this rule requires the range rate to be equal to the range divided by -1000, plus or minus $0.1 \frac{\text{ft}}{\text{sec}}$. Mathematically this is expressed as:

$$\frac{-R_L}{1000} - 0.1 \frac{\text{ft}}{\text{sec}} \leq \dot{R}_L \leq \frac{-R_L}{1000} + 0.1 \frac{\text{ft}}{\text{sec}} \tag{3-1}$$

In other words, when the Shuttle is 400 feet away its range rate should be no slower than $-.3 \frac{\text{ft}}{\text{sec}}$ and no faster than $-.5 \frac{\text{ft}}{\text{sec}}$. When the Shuttle is within 100 feet the range rate restriction is $0 \geq \dot{R}_L \geq -0.2 \frac{\text{ft}}{\text{sec}}$.[6]

The third and final piloting rule prohibits "Norm Z" jet firings between 1000 feet and 75 feet.[6] To prevent direct plume impingement on the Station's solar arrays, all $+Z_{Body}$ firings in this region are performed using "Low Z" burns. As explained previously, these jets provide an impulsive force in the $+Z_{Body}$ direction without firing directly at the Station. Instead, jets fire simultaneously at skewed angles off the nose and tail. This reduces the jet plume effects on the Station. However, Low Z burns are very fuel inefficient and less responsive than normal Z burns. For these reasons, braking burns inside 75 feet generally use normal +Z jets ("Norm Z"), which unfortunately fire directly at the Station along the $-Z_{Body}$ axis.

[1] Prior to 1993, COAS angles of ± 10° were allowed. The man-in-the-loop simulations presented in this thesis to SC-4 were generated using this less restrictive rule.[5]

Table 3-2 Summary of proximity operations piloting rules

PARAMETER	REQUIREMENT
COAS Angles:	
Port-to-port Range > 25 ft	$-8 \leq \lambda_V \leq 8$ and $-8 \leq \lambda_H \leq 8$ (± 10 for earlier runs to SC-4)
Port-to-port Range < 25 ft	$-5 \leq \lambda_V \leq 5$ and $-5 \leq \lambda_H \leq 5$
Range Rate:	
Port-to-port Range > 100 ft	$\frac{-R_L}{1000} - 0.1\frac{ft}{sec} \leq \dot{R}_L \leq \frac{-R_L}{1000} + 0.1\frac{ft}{sec}$
Port-to-port Range < 100 ft	$-0.2\frac{ft}{sec} \leq \dot{R}_L \leq 0\frac{ft}{sec}$
Low Z Restriction:	
Port-to-port Range > 75 ft	Low Z translation jets
Port-to-port Range < 75 ft	Normal Z translation jets

3.7 PILOTING TECHNIQUES

It is important to differentiate between piloting rules and piloting techniques. The rules, presented in the previous section, and summarized in Table 3-2, are common to all pilots. These rules are imposed by NASA. They limit a pilot's actions and define the specific requirements for proximity operations. Techniques, on the other hand, are the methods used by individual pilots to meet those requirements and often vary between different pilots. For example, it is perfectly acceptable if a pilot chooses to fly the full range of the COAS cone, from +8 to -8 when $R_P > 25$ ft. Another pilot may prefer to keep the COAS target centered in the COAS during the entire approach. These are two very

different techniques; both of which are acceptable and meet the requirements discussed in the previous section.

This section provides an overview of the techniques used by real pilots during proximity operations. It covers some basic control methods for determining the necessary THC commands. This includes deciding which axis requires a translation pulse, the size of the pulse (DAP A or DAP B), and the frequency of multiple commands if they are required. This section also discusses some specific techniques used to control the Shuttle's in-plane and out-of-plane motion. These techniques are the basis for the fuzzy sets and fuzzy rules presented in the following chapters.

3.7.1 Basic Piloting Techniques

Pilots use translation burns in the X, Y, and Z body axes to control λ_V, λ_H, and $\dot{R}_L$ respectively. These axes are controlled independently. For example, +X jets are used to increase the velocity in the $+X_{Body}$ direction, which causes the Shuttle to gain altitude and $\dot{\lambda}_V$ to decrease. Negative X_{Body} jets fire off the nose to push the Shuttle down and increase $\dot{\lambda}_V$. Likewise, pilots use $\pm Y_{Body}$ jets to control λ_H and $\dot{\lambda}_H$, and $\pm Z_{Body}$ jets to control $\dot{R}_L$. Positive Z burns slow the Shuttle's closure rate and make $\dot{R}_L$ less negative, while -Z commands increase the Shuttle's closure rate, making $\dot{R}_L$ more negative.

The size of these burns is determined by the current DAP setting. Pilots are free to switch between DAP A and B whenever they wish. However, they usually use DAP A (imparting about $.05\frac{ft}{sec}$) for large ranges and DAP B (imparting about $.02\frac{ft}{sec}$) for small ranges. This is because DAP A provides more command authority, and the ΔV necessary for a desired $\dot{\lambda}_V$ or $\dot{\lambda}_H$ is directly proportional to R_L. Consider Figure 3-9, depicting the Shuttle with a positive vertical COAS angle, λ_V, at a distance d from the centerline corresponding to $\lambda_V = 0$.

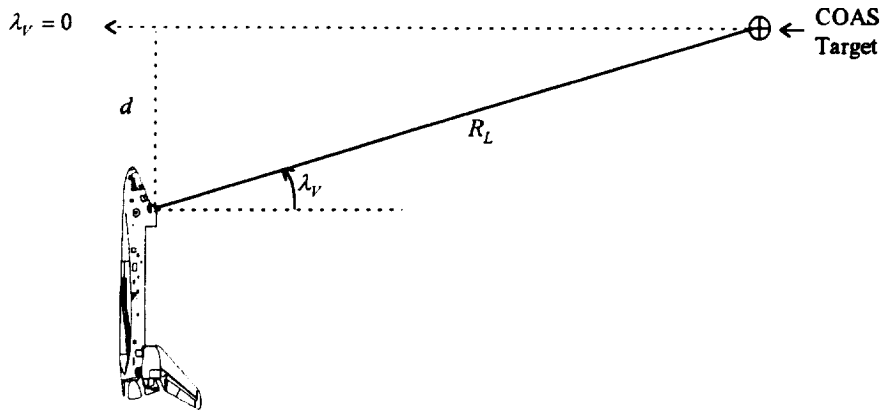

Figure 3-9 Shuttle with a positive λ_V

$$d = R_L \sin \lambda_V \qquad \dot{d} = \dot{R}_L \sin \lambda_V + R_L \dot{\lambda}_V \cos \lambda_V \tag{3-2}$$

For the small COAS angles encountered during proximity operations,

$$\dot{d} \approx R_L \dot{\lambda}_V \tag{3-3}$$

Obviously the same would be true for the horizontal angle. So for both X and Y firings, the velocity required for a desired $\dot{\lambda}_V$ or $\dot{\lambda}_H$ is directly proportional to R_L. For this reason, pilots generally use DAP A for large ranges and DAP B for small ranges. The DAP A/B transition point does vary between pilots and also between axes. However, pilots normally switch to DAP B about the same time they switch from "Low Z" to "Norm Z", when $R_P < 75$ ft (equivalent to $R_L < 100$ ft).

After a THC command, whether in DAP A or DAP B, a pilot waits a little while, and if needed makes another burn a few seconds later. It is extremely rare for a pilot to make two or more THC commands within two seconds. This general frequency characteristic appears to be common to all pilots.

3.7.2 In-Plane Piloting Techniques

As discussed in Section 3.3, motion in the orbital plane is coupled. Pilots must therefore account for orbital mechanics and compensate for this coupling as they make velocity corrections. This is accomplished using some specific techniques for controlling the Shuttle's in-plane motion.

The Shuttle's motion in the orbital plane is defined by x, z, $\dot{x}$, and $\dot{z}$ in the LVLH frame. This motion can best be understood by analyzing the solution to the Clohessy-Wiltshire equations, which was expressed in matrix form in Equation 3-1, on page 36. Consider a typical time between translation burns of four minutes, and a typical value for the Station's mean orbital motion, $\omega = 4\frac{\text{deg}}{\text{min}} = 0.00116\frac{rad}{\text{sec}}$. The first and third equations from 3-1, defining the Shuttle's in-plane position, are:

$$\begin{aligned} x &= x_0 + 0.0217z_0 + 227.5714\dot{x}_0 + 66.5862\dot{z}_0 \\ z &= 1.1162z_0 - 66.5862\dot{x}_0 + 236.8929\dot{z}_0 \end{aligned} \tag{3-4}$$

The Shuttle's distance below the v-bar is defined by z, while x defines its distance in front of the Station.

Looking at the second equation in 3-4, note $\dot{x}_0$ affects z. For the small COAS angles associated with Shuttle approaches to the Station, $\dot{x} \approx \dot{R}$, so Equations 3-4 can be approximated by:

$$\begin{aligned} x &\approx x_0 + 0.0217z_0 + 227.5714\dot{R}_0 + 66.5862\dot{z}_0 \\ z &\approx 1.1162z_0 - 66.5862\dot{R}_0 + 236.8929\dot{z}_0 \end{aligned} \tag{3-5}$$

Because $\dot{R}_0 < 0$, and its coefficient is negative, the Shuttle's closure rate causes z to increase. This means the Shuttle tends to "descend", and λ_t increases as the Shuttle approaches the Station.

To examine the change in λ_V due solely to $\dot{R}_0$, assume the Shuttle is near the v-bar with a small vertical velocity ($z_0 \approx 0$ and $\dot{z}_0 \approx 0$), and set $\dot{R}_0 = \frac{-R_0}{1000} \approx \frac{-x_0}{1000}$, corresponding to the piloting rule for range rate. Equations 3-5 become:

$$\begin{aligned} x &\approx x_0 + 227.5714\left(\frac{-x_0}{1000}\right) = 0.7724x_0 \\ z &\approx -66.5862\left(\frac{-x_0}{1000}\right) = 0.06659x_0 \end{aligned} \tag{3-6}$$

In other words, if the Shuttle coasts for four minutes, and the pilot obeys the rule for $\dot{R}$ exactly, the Shuttle will descend to $z = 0.06659x_0$ as it closes from $x = x_0$ to $x = 0.7724x_0$. This is a significant change of almost 5° in the vertical COAS angle.

$$\Delta\lambda_V = \tan^{-1}\left(\frac{0.06659x_0}{0.7724x_0}\right) = 4.9° \tag{3-7}$$

A pilot must repeatedly compensate for this effect $\dot{R}$ has on λ_V, which is one of the most dominant coupling effects during proximity operations.

Observing the second equation from 3-4, z is also affected by z_0, the Shuttle's initial position below the v-bar. Because this term has a coefficient greater than one, the contribution of z_0 to z increases with time. Therefore, if the Shuttle is initially below the Station, it tends to lose more altitude. For runs to SC-4, the Shuttle's center of mass is 35 feet below the end effector, and the target's center of mass is 56 feet above the grapple point. Therefore, z_0 has a nominal value of 91 feet. Consequently, the Shuttle tends to lose approximately 10 feet (0.1162×91) every four minutes, due to its position below v-bar.

Both the Shuttle's closure rate and its position below v-bar cause z (and λ_V) to increase. As a result, the Shuttle tends to approach the Station slightly below the grapple point. To compensate, pilots frequently have to impart an upward velocity with $+X_{Body}$ translation commands, which decrease $\dot{z}_0$ in the LVLH frame. As a result, +X commands

are the most common THC command during proximity operations. Also, due to these orbital trends, pilots have a negative bias for λ_{r_V} and $\dot{\lambda}_{r_V}$, meaning they would rather the Shuttle be "high" and increasing in altitude slightly than an equivalent distance "low" and slowly losing altitude. For example, if the Shuttle is high (λ_{r_V} is *Large Negative*) and is slowly gaining altitude ($\dot{\lambda}_{r_V}$ is *Small Negative*), there may be no need for a $-X_{Body}$ firing, because orbital mechanics will eventually cause the Shuttle to descend. However, if the Shuttle is an equivalent distance low (λ_{r_V} is *Large Positive*) and is slowly losing altitude ($\dot{\lambda}_{r_V}$ is *Small Positive*), a $+X_{Body}$ burn is necessary to overcome orbital mechanics. The degree to which a pilot has this bias for $\lambda_{r_V} < 0$ and $\dot{\lambda}_{r_V} < 0$ is determined by his/her definitions of "λ_{r_V} is a *Large Negative* number", "$\dot{\lambda}_{r_V}$ is a *Small Positive* number", etc.. These fuzzy definitions help define an individual pilot's technique. The fuzzy pilot model presented in this thesis captures these individual techniques for different human pilots.

3.7.3 Out-of-Plane Piloting Techniques

Motion perpendicular to the orbital plane is much easier for a pilot to control. As discussed in Section 3.3, the Shuttle's out-of-plane motion is uncoupled to the other two axes. Therefore, a pilot can control the Shuttle's distance out-of-plane using only ±Y burns, and does not need to consider the motion in the x or z directions. In addition, because the Shuttle's out-of-plane motion is an undamped sinusoid, it is symmetric about $\lambda_H = 0$ and $\dot{\lambda}_H = 0$. As a result, pilots do not have a bias for λ_H or $\dot{\lambda}_H$. Their decision process for controlling a *Large Positive* λ_H with a *Large Positive* $\dot{\lambda}_H$ is the same as it is for an equally *Large Negative* λ_H with a *Large Negative* $\dot{\lambda}_H$.

In addition, because the out-of-plane motion is a sinusoid, pilots rarely make a Y THC firing to reduce $|\lambda_H|$, if λ_H and $\dot{\lambda}_{r_V}$ have opposite signs (the Shuttle is correcting back to $\lambda_H = 0$). Although such a firing would quickly reduce $|\lambda_H|$, it would also increase the amplitude of the out-of-plane motion and would eventually require more Y burns. This is illustrated in Figure 3-10.

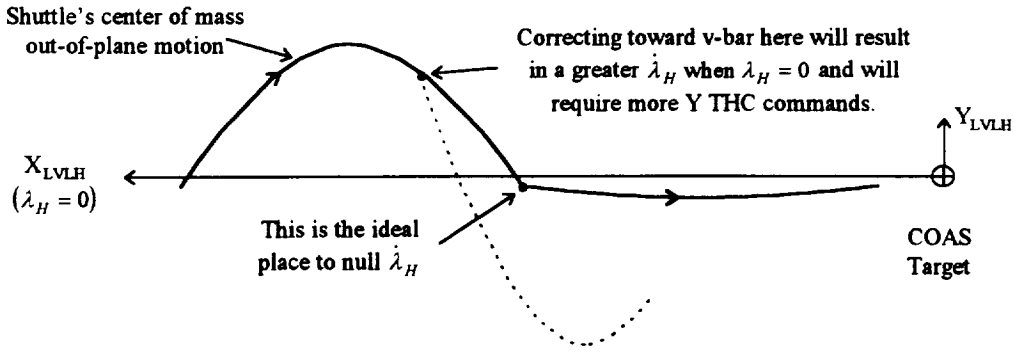

Figure 3-10 Out-of-plane motion of Shuttle's center of mass

Figure 3-10 also shows the best technique is to null the out-of-plane velocity. This would limit the amplitude of the sinusoid to the Shuttle's current distance from the orbital plane. Obviously, the best place to do this is when $\lambda_H \approx 0$.[1] Unfortunately, it is not quite this easy. Due to the Shuttle's attitude dynamics, it is difficult to accurately determine λ_H and $\dot{\lambda}_H$, and a pilot can only make discrete size burns. For these reasons, pilots usually only make Y firings to reduce $\left|\dot{\lambda}_H\right|$ when the range is relatively *Small*, and they make very few Y firings for *Large* ranges. The pilot model will incorporate these same techniques.

[1] This assumes the grapple position is located near the target's orbital plane, as it is for SC-2 and SC-4. For a few Station configurations the Shuttle's center of mass will be over 25 feet out-of-plane at the grapple point. In this case the sinusoidal motion is not symmetric about $\lambda_H = 0$.

3.7.4 Summary of Piloting Techniques

In summary, a number of piloting techniques have been identified based upon simple orbital analysis and an understanding of basic piloting methods. More importantly, analysis of over 90 man-in-the-loop runs confirms pilots use these basic techniques, which are summarized below:

1. Pilots control each axis independently: X_{Body} commands are used to control λ_V and $\dot{\lambda}_V$; Y_{Body} commands control λ_H and $\dot{\lambda}_H$; and Z_{Body} commands control $\dot{R}_L$.
2. The size of velocity corrections in the X and Y body axes is directly proportional R_L.
3. Pilots generally use DAP A for large ranges and DAP B for small ranges, transitioning to DAP B when R_L is approximately 100 feet.
4. Pilots seldom make two or more THC commands within two seconds of each other.
5. Due to orbital mechanics, the Shuttle continually loses altitude as it approaches the Station. As a result, pilot's tend to approach slightly below the grapple point, and they make many more +X burns than -X burns. In addition, pilots have a bias for $\lambda_V < 0$ and $\dot{\lambda}_V < 0$.
6. The decision process for controlling the horizontal COAS angle, λ_H, is symmetric about $\lambda_H = 0$ and $\dot{\lambda}_H = 0$. Pilots also rarely make a Y THC firing when $|\lambda_H|$ is decreasing or when R_L is *Large*.

Each of these techniques is incorporated in the fuzzy pilot model. Variations in individual pilot techniques are captured by changing the definitions of fuzzy terms such as *Large Positive*, *Small Positive*, *Fast*, and *Slow*.

Chapter 4 : Three Degree-of-Freedom Fuzzy Logic Pilot Model

4.1 INTRODUCTION

Having covered the basics of fuzzy logic and proximity operations; this chapter presents the architecture of the initial pilot model. This model is developed without considering the effects of Shuttle attitude motion on the pilot's ability to discern the need to make trajectory corrections. Any perceived target motion is attributed to the Shuttle's translation. This model is therefore referred to as a three degree-of-freedom (DOF) model.

Fuzzy logic was selected as a basis for this pilot model, because of its successful use in modeling the human decision process for control functions in other fields.[12,13,22] Human decisions are generally not based upon crisp thresholds, but involve general classification terms and gradual set transitions. Fuzzy logic can operate with these same imprecise definitions and goals, without introducing artificial randomness. Fuzzy logic is also able to combine a number of simple rules with conflicting conclusions. It can therefore easily model a pilot's ability to perform trade-offs between vague and opposing objectives. In addition, fuzzy logic uses a linguistic format, so it is relatively easy to

develop and modify. Different individual piloting techniques or new piloting rules can be captured simply by redefining fuzzy sets or adding additional fuzzy rules.

The fuzzy logic rules and set boundaries used by the pilot model are based upon the requirements and techniques identified in Chapter 3 and analysis of NASA's man-in-the-loop simulations. After explaining the model's decision logic, this chapter discusses two different simulation environments used to evaluate its performance. A brief discussion of the tests and results is provided as motivation for the enhancements developed in Chapter 5.

4.2 Overview of the Three Degree-of-Freedom Pilot Model

The fuzzy pilot model performs the two basic human pilot functions of navigation and guidance. The navigation portion of the model is concerned with determination of the relative geometry between the Shuttle and the Station. The guidance portion determines what actions, if any, are required to bring the two vehicles together along an acceptable trajectory. The block diagram in Figure 4-1 summarizes this process. The COAS model provides the pilot with the vertical and horizontal COAS angles, λ_V and λ_H, and the laser supplies range and range rate, R_L and $\dot{R}_L$. During the navigation process, the model estimates the COAS rates, $\dot{\lambda}_V$ and $\dot{\lambda}_H$, and filters the noisy $\dot{R}_L$. As part of the guidance function, the model determines the necessary Translation Hand Control (THC) commands for the X, Y, and Z body axes. The model also decides when to switch from DAP A to DAP B and from Low Z to Norm Z. These outputs from the fuzzy pilot are fed to the Shuttle flight software, which commands the specific jets to be fired. The simulator integrates the effects of these jet firings and other environment models and supplies the feedback to the COAS and laser.

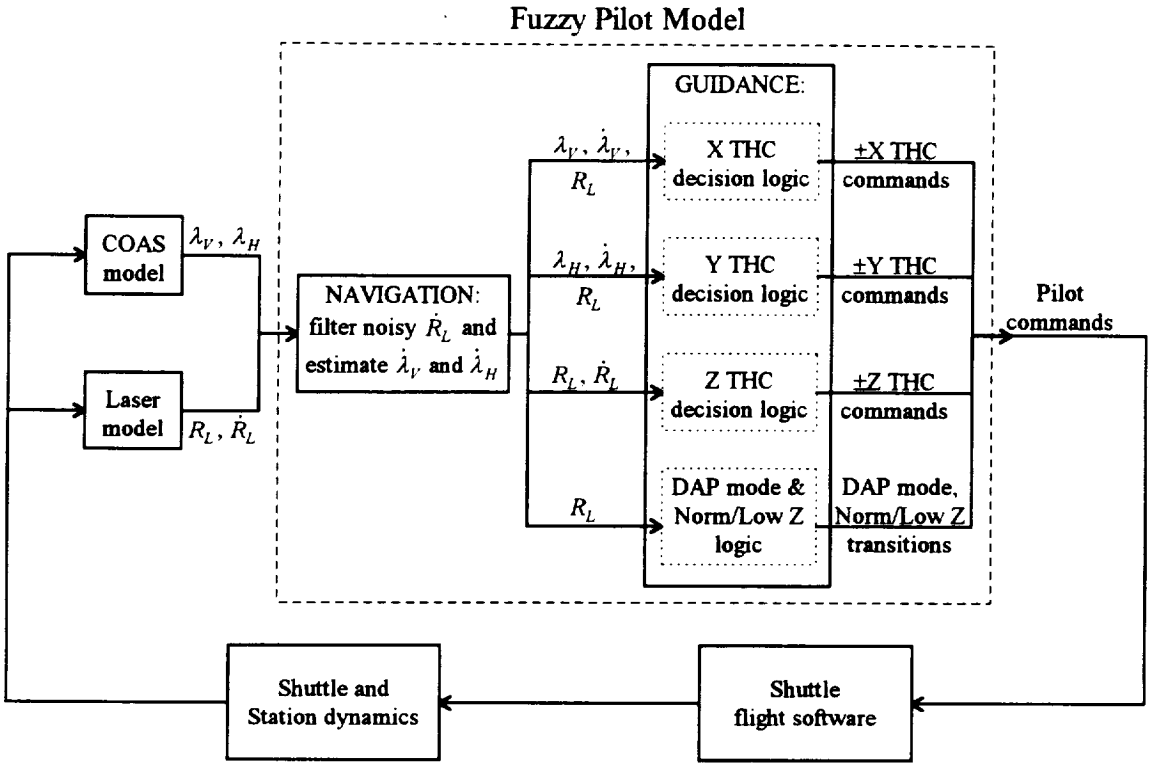

Figure 4-1 Block diagram for the three degree-of-freedom fuzzy pilot model

4.3 NAVIGATION

The navigation portion of the model is very simple. Using the same sensory information supplied to a human pilot, from the COAS and laser, the model estimates $\dot{\lambda}_V$ and $\dot{\lambda}_H$, and filters some of the laser's range rate noise.

There is no direct measure of the Shuttle's vertical or horizontal velocity. Instead, a pilot makes crude measurements of these velocities by estimating the COAS angle rates, $\dot{\lambda}_V$ and $\dot{\lambda}_H$, based upon how fast the target moves across the COAS. The pilot model uses a simple first order approximation to model this process. The last two data points,

which are 0.96 seconds apart, are back-differenced to estimate these rates.[1] The mathematical equations are:

$$\dot{\lambda}_V = \frac{\lambda_{V_n} - \lambda_{V_{n-1}}}{t_n - t_{n-1}} \qquad \dot{\lambda}_H = \frac{\lambda_{H_n} - \lambda_{H_{n-1}}}{t_n - t_{n-1}} \tag{4-1}$$

The subscript "n" indicates the present state, and "n-1" represents the previous data point.

The laser uses a digital display with a 0.96 second update rate, and has a one sigma random error of $0.01\frac{ft}{sec}$. Due to the instability of the right most digit, crewmembers filter $\dot{R}_L$ to estimate the Shuttle's true closure rate. To model this simple process the fuzzy pilot uses a low pass filter. With this filter, the model believes only 30% of any change in $\dot{R}_L$ from the previous reading. Mathematically, this is calculated by

$$\dot{R}_{L_n} = \dot{R}_{L_{n-1}} + 0.3\left(\dot{R}_{L_n} - \dot{R}_{L_{n-1}}\right) \tag{4-2}$$

At a 0.96 second cycle, this equates to believing 98% of a step input within 10.5 seconds.

4.4 GUIDANCE

The guidance portion of the pilot model uses fuzzy logic to implement the same decision process as a human pilot. It determines the required THC commands in each of the three axes. This constitutes the majority of the model and is the most difficult process. As with real pilots, the commands for each axis are computed independently. This portion of the model also determines when to switch from DAP A to DAP B and from Low Z to Norm Z.

[1] Real pilots almost never command a jet firing in the middle of a prior translation burn, and Low Z burns last at least 1.28 seconds. Therefore, the pilot model skips one cycle immediately following a THC burn; so in this case the back-difference is over 1.92 seconds.

The fuzzy logic rules, used in the guidance portion of the model, are based upon the piloting requirements and techniques identified in Chapter 3. The fuzzy sets were determined by analyzing NASA's man-in-the-loop database. This analysis consisted of reconstructing each simulation based upon the relative state between the two vehicles, and determining the pilot's sensory inputs and corresponding pilot commands.[9] This allowed identification of general piloting trends and fuzzy definitions for such terms as *Fast*, *Slow*, *Large*, and *Small*. Then through an iterative process these fuzzy sets were modified slightly to closely match a human pilot's performance.

4.4.1 X THC Decision Logic

Pilots control the Shuttle's vertical motion using $\pm X_{Body}$ burns based upon λ_V, $\dot{\lambda}_V$, and R_L. This process involves making some general, fuzzy observations about these variables, then determining the required burn size based upon these observations. A typical fuzzy rule used to model this process is of the form:

If (λ_V is *Large Negative* and $\dot{\lambda}_V$ is *Small Negative*) Then (Burn = Crisp number).

This crisp conclusion specifies the necessary number of minimum impulses needed. In this case, because the Shuttle is low (λ_V is *Large Negative*) and it is moving down slowly ($\dot{\lambda}_V$ is *Small Negative*) the burn would be a relatively large number. It would also be a positive X burn, which increases the Shuttle's vertical velocity.

However, before the model calculates the burn it must classify λ_V, $\dot{\lambda}_V$, and R_L by their membership values in the appropriate fuzzy sets. This process of converting crisp numbers into fuzzy variables is called "fuzzification". The fuzzy sets used for this purpose are shown in Figure 4-2. Notice, there are two membership functions for λ_V, one for *Large* ranges and one for *Small* ranges. This is because the membership function for λ_V is conditional upon range. As the range decreases, a real pilot's definitions for *Large* and *Small* $|\lambda_V|$ change. Therefore, for ranges that are somewhat *Large* and *Small*, the model

determines $\mu(\lambda_V)$ by interpolating between $\mu(\lambda_V|R_L \text{ is } Large)$ and $\mu(\lambda_V|R_L \text{ is } Small)$. This allows a gradual transition, adjusting for the smaller approach corridor as the range decreases. For example, the model defines an angle greater than 9° to be completely *Large Positive* for *Large* ranges. As the range decreases, this threshold will also decrease. Once $R_L \leq 40$ ft, the range is completely *Small*, and any angle greater than 2.5° is considered absolutely *Large Positive*.

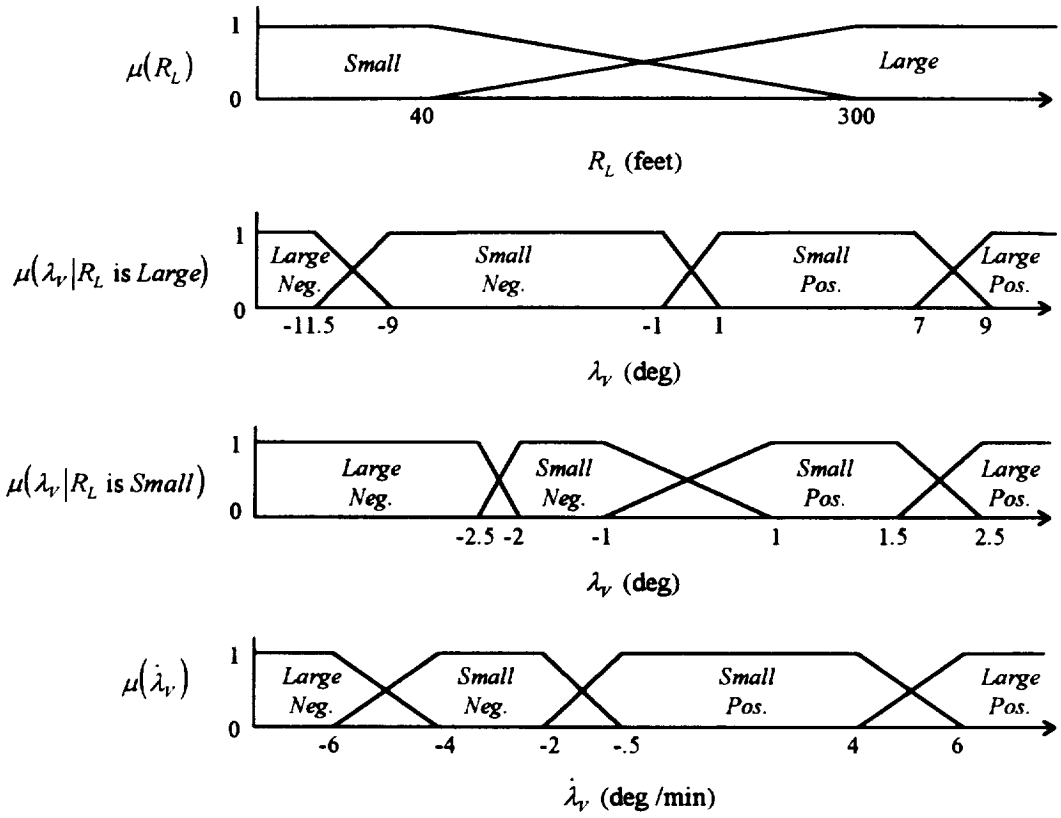

Figure 4-2 Fuzzy sets for R_L, λ_V, and $\dot{\lambda}_V$

Certainly, more fuzzy sets would have allowed the controller to distinguish finer differences in λ_V and $\dot{\lambda}_V$, and would have improved its performance. However, four is a conservative estimate of the number of sets a human can distinguish for the COAS angles and angle rates. For example, it is unlikely a human could accurately distinguish seven to ten different categories of $\dot{\lambda}_V$.

After determining the membership in these fuzzy sets, the controller calculates the necessary burn in the X_{Body} direction. This is based upon the sixteen fuzzy rules shown below. Each antecedent involves an intersection of the fuzzy sets for $\lambda_{r'}$ and $\dot{\lambda}_{r'}$, and the conclusion is a crisp number specifying the number of minimum impulses required.[1] These crisp conclusions are based upon the exact response from real pilots, determined from analyzing NASA's man-in-the-loop database. However, because of the iterative process used to closely match a human pilot's response, these numbers are not necessarily integers. Later, during the summation process, the output will be rounded to an integer number of THC commands.

1. If ($\lambda_{r'}$ is *Small Negative* and $\dot{\lambda}_{r'}$ is *Large Positive*) Then (Burn is 1.5 min. impulses).
2. If ($\lambda_{r'}$ is *Small Positive* and $\dot{\lambda}_{r'}$ is *Large Positive*) Then (Burn is 1.7 min. impulses).
3. If ($\lambda_{r'}$ is *Large Positive* and $\dot{\lambda}_{r'}$ is *Large Positive*) Then (Burn is 2.5 min. impulses).
4. If ($\lambda_{r'}$ is *Large Positive* and $\dot{\lambda}_{r'}$ is *Small Positive*) Then (Burn is 1.7 min. impulses).
5. If ($\lambda_{r'}$ is *Small Negative* and $\dot{\lambda}_{r'}$ is *Large Negative*) Then (Burn is -1.3 min. impulses).
6. If ($\lambda_{r'}$ is *Large Negative* and $\dot{\lambda}_{r'}$ is *Large Negative*) Then (Burn is -2.0 min. impulses).
7. If ($\lambda_{r'}$ is *Large Negative* and $\dot{\lambda}_{r'}$ is *Small Negative*) Then (Burn is -1.3 min. impulses).

8-16. All other intersections of $\lambda_{r'}$ and $\dot{\lambda}_{r'}$ result in "Burn is 0 minimum impulses".

Because these fuzzy rules determine the burn size based upon the intersection of fuzzy sets for $\lambda_{r'}$, and $\dot{\lambda}_{r'}$, they can easily be depicted by plotting $\dot{\lambda}_{r'}$ vs. $\lambda_{r'}$. This plot, shown in Figure 4-3, is called a vertical phase plane. It is divided into sixteen grids, corresponding to the fuzzy rules. The four fuzzy sets for $\lambda_{r'}$ are indicated on the x axis, and the y axis shows the four sets for $\dot{\lambda}_{r'}$. Each grid represents the intersection of two

[1] As explained in Chapter 3, for a typical Shuttle mass each minimum impulse imparts slightly less than $.02\frac{ft}{sec}$. For the X and Y axes, DAP A burns impart three minimum impulses, and DAP B burns impart one minimum impulse.

sets. The number in the grid is the resulting conclusion, specifying the number of minimum impulses in the X axis.

$\dot{\lambda}_V$	λ_V is *Large Neg* (Shuttle is "high")	λ_V is *Small Neg*	λ_V is *Small Pos*	λ_V is *Large Pos* (Shuttle is "low")
$\dot{\lambda}_V$ is *Large Pos* (Shuttle moving "down" fast)	Burn = 0	Burn = 1.5 (rule 1)	Burn = 1.7 (rule 2)	Burn = 2.5 (rule 3)
$\dot{\lambda}_V$ is *Small Pos*	Burn = 0	Burn = 0	Burn = 0	Burn = 1.7 (rule 4)
$\dot{\lambda}_V$ is *Small Neg*	Burn = -1.3 (rule 7)	Burn = 0	Burn = 0	Burn = 0
$\dot{\lambda}_V$ is *Large Neg* (Shuttle moving "up" fast)	Burn = -2 (rule 6)	Burn = -1.3 (rule 5)	Burn = 0	Burn = 0

Figure 4-3 X THC burn size depicted on a vertical COAS phase plane

Figure 4-3 is an easy way to express the sixteen rules that specify the X burn size. However, because the sets for λ_V, and $\dot{\lambda}_V$ are fuzzy variables, it is slightly misleading. The transitions between grids are not "crisp" as shown. Instead, there is actually a gray area between each grid, where the fuzzy sets overlap and blend together. This more correct, fuzzy phase plane, is shown in Figure 4-4. The fuzzy boundaries depicted are for *Large* ranges ($R_L \geq 300\text{ft}$). As the range decreases, the membership function for λ_V shrinks. Eventually, when the range is completely *Small* ($R_L \leq 40\text{ft}$), the fuzzy phase plane looks like Figure 4-5.

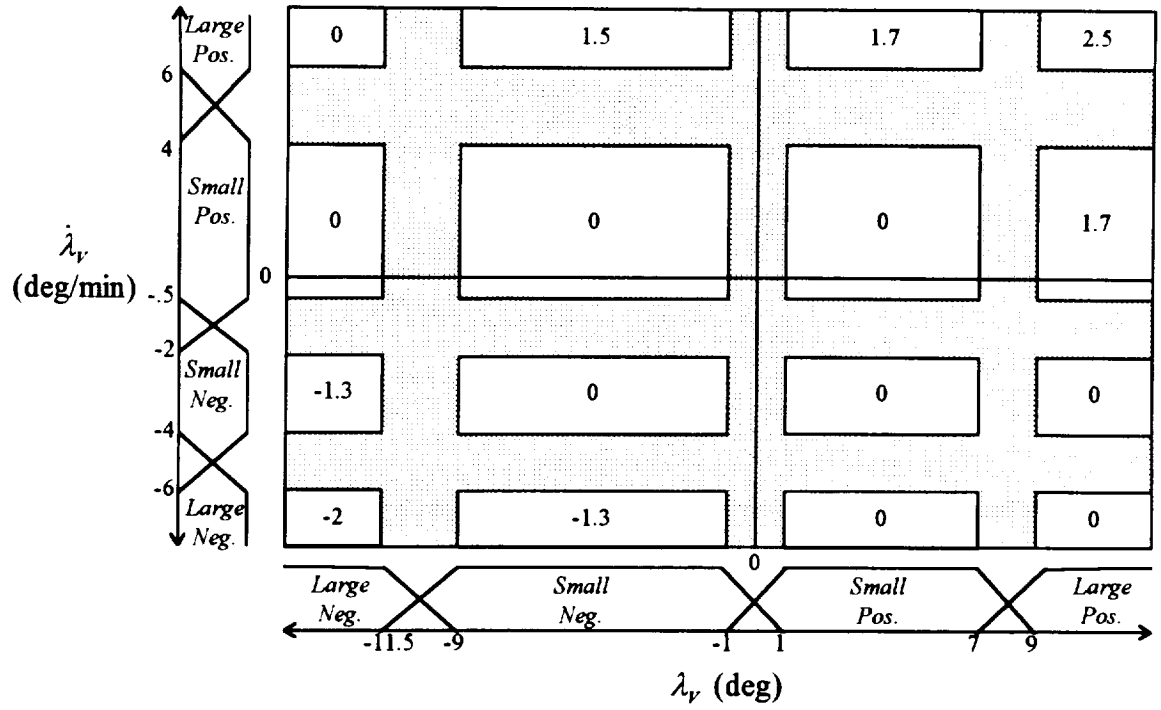

Figure 4-4 X THC burn size for *Large* ranges

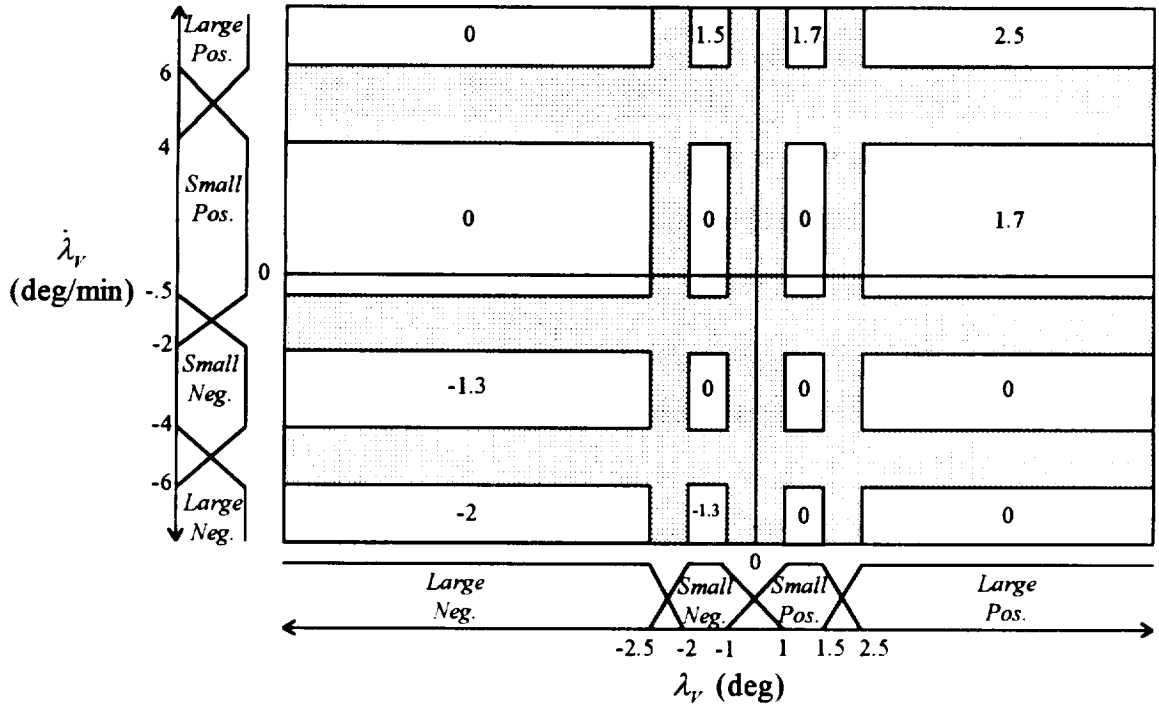

Figure 4-5 X THC burn size for *Small* Ranges

In each grid that is not shaded, only one rule is completely true, and all other rules are completely false. In the gray areas between the grids, the fuzzy sets overlap, and the antecedent from two or more rules is partially true. In this case the conclusions must be combined. This is accomplished with the equation

$$\text{Aggregate output} = \frac{\sum_{n=1}^{N} \mu_n * \text{conclusion}_n}{\sum_{n=1}^{N} \mu_n} \tag{4-3}$$

where μ_n is the truth value of the antecedent from the nth rule, and N is the total number of rules combined.

Pilots make larger velocity corrections at larger ranges. Therefore, the aggregate output for burn size is multiplied by a scale factor, K_X, which is a function of range. This scale factor is determined by combining the conclusions from rules 17 and 18.

17. If (R_L is *Large*) Then (K_X is 3).
18. If (R_L is *Small*) Then (K_X is 1).

This insures the final burn size is directly proportional to range, which is one of the basic piloting techniques identified in Chapter 3.

As shown by the block diagram in Figure 4-6, the product of K_X and the aggregate output from rules 1 through 16 gives the required number of minimum impulses in the X body direction. This number is quantized into pulses based upon the current DAP mode. If the Shuttle is in DAP B mode, each pulse imparts one minimum impulse, which is slightly less than $.02\frac{ft}{sec}$. If the Shuttle is in DAP A mode, each pulse imparts three minimum impulses, or approximately $.05\frac{ft}{sec}$.

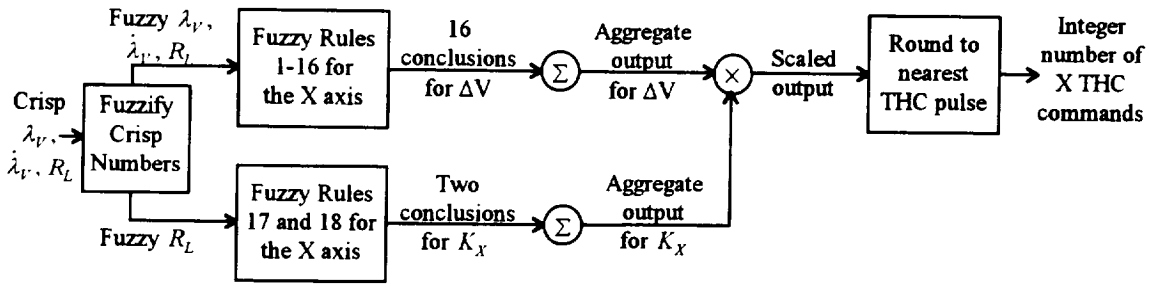

Figure 4-6 Three degree-of-freedom, X THC decision logic

Using this logic and the corresponding fuzzy sets, the pilot model incorporates all the piloting techniques identified in Chapter 3 for the X_{Body} axis. First, the burn sizes are directly proportional to range, resulting in larger velocity changes for large ranges. Also, the vertical COAS phase planes in Figure 4-4 and Figure 4-5 are not symmetric, reflecting a human pilot's bias for $\lambda_V < 0$ and $\dot{\lambda}_V < 0$. As a result, the model does not make a burn if λ_V is *Large Negative* (the Shuttle is "high") and $\dot{\lambda}_V \approx -0.25 \frac{\text{deg}}{\text{min}}$ (the Shuttle is moving "up" slowly). This reflects a pilot's knowledge of orbital mechanics, which will eventually cause the Shuttle to descend, reversing $\dot{\lambda}_V$ without any THC commands. However, when λ_V is *Large Positive* (the Shuttle is "low") and $\dot{\lambda}_V \geq 0$ (the Shuttle is moving "down") the model continues commanding +X THC pulses until $\dot{\lambda}_V$ is negative.

In addition, the pilot model rarely determines the current geometry requires more than one THC command, which is consistent with the general frequency response from the man-in-the-loop data. Theoretically, it is possible to have a maximum burn size of 7.5 minimum impulses if $\mu_{Large}(R_L) = 1$, $\mu_{Large\,Pos}(\lambda_V) = 1$, and $\mu_{Large\,Pos}(\dot{\lambda}_V) = 1$. This corresponds to the upper right grid of Figure 4-4 with $K_X = 3$, and would be rounded to three DAP A commands, imparting nine minimum impulses. However, this state is very unlikely in the Shuttle's normal operating environment. Instead, the model would make a few individual THC pulses as λ_V and $\dot{\lambda}_V$ increased and the operating point passed through the other cells or the gray regions on the phase plane. These burns would be +1 or +3

minimum impulses depending upon the current DAP setting. Therefore, the model will almost never command two or more THC burns within its 0.96 second cycle. This behavior, incorporated in the pilot model, is also observed in NASA's man-in-the-loop data.

4.4.2 Y THC Decision Logic

The decision logic for controlling λ_H with Y burns is identical to method for controlling λ_V with X burns. The only difference is the fuzzy sets and conclusions are slightly different to reflect the unique piloting techniques for the Shuttle's out-of-plane motion.

The model first fuzzifies the crisp values for λ_H, $\dot{\lambda}_H$, and R_P. Then based upon the intersection of the fuzzy sets for λ_H and $\dot{\lambda}_H$, it determines the burn size from sixteen fuzzy rules. These rules, shown below, specify a crisp conclusion for the number of minimum impulses required in the Y_{Body} axis.

1. If (λ_H is *Small Positive* and $\dot{\lambda}_H$ is *Large Positive*) Then (Burn is 1.3 min. impulses).
2. If (λ_H is *Large Positive* and $\dot{\lambda}_H$ is *Large Positive*) Then (Burn is 2.0 min. impulses).
3. If (λ_H is *Large Positive* and $\dot{\lambda}_H$ is *Small Positive*) Then (Burn is 1.5 min. impulses).
4. If (λ_H is *Small Negative* and $\dot{\lambda}_H$ is *Large Negative*) Then (Burn is -1.3 min. impulses).
5. If (λ_H is *Large Negative* and $\dot{\lambda}_H$ is *Large Negative*) Then (Burn is -2.0 min. impulses).
6. If (λ_H is *Large Negative* and $\dot{\lambda}_H$ is *Small Negative*) Then (Burn is -1.5 min. impulses).

7-16. All other intersections of λ_H and $\dot{\lambda}_H$ result in "Burn is 0 minimum impulses".

Similar to the X axis, these rules can best be depicted by representing the intersection of the fuzzy sets for $\dot{\lambda}_H$ and λ_H on a fuzzy horizontal COAS phase plane. There are two membership functions for λ_H, one for *Large* ranges, and one for *Small* ranges. The phase plane for each is shown in Figure 4-7 and Figure 4-8. As with the X axis, the burn size for each rule is shown in the appropriate grid.

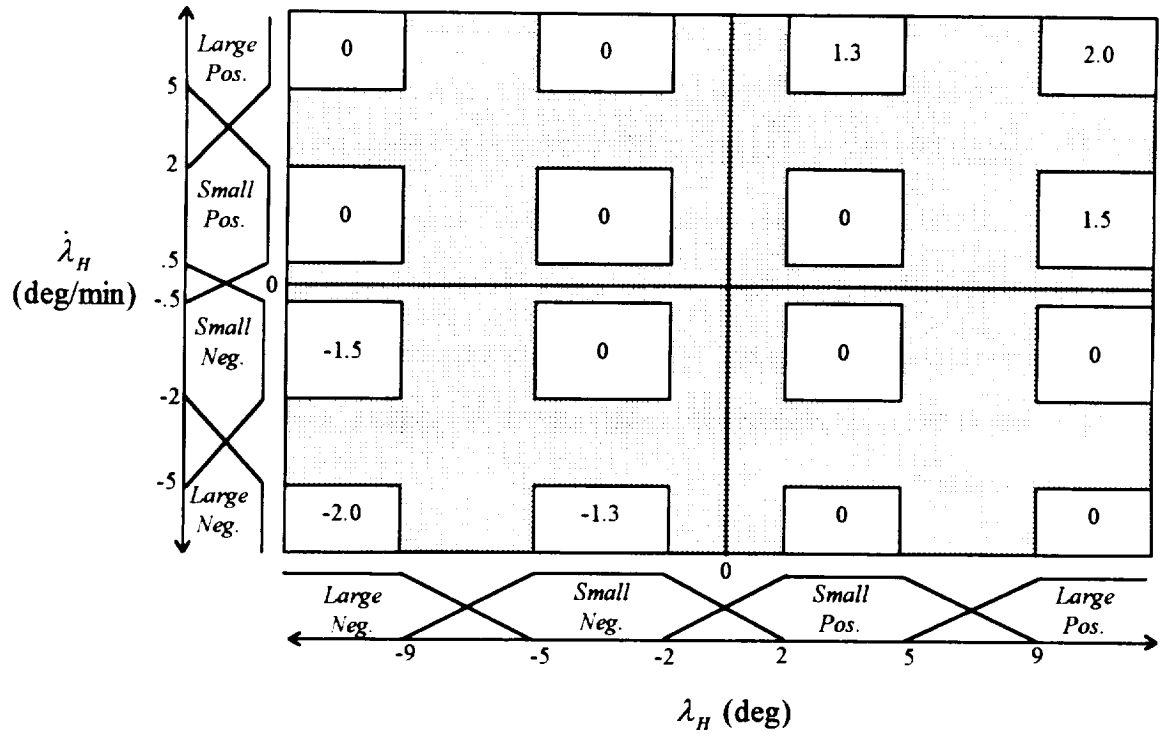

Figure 4-7 Y THC burn size for *Large* ranges

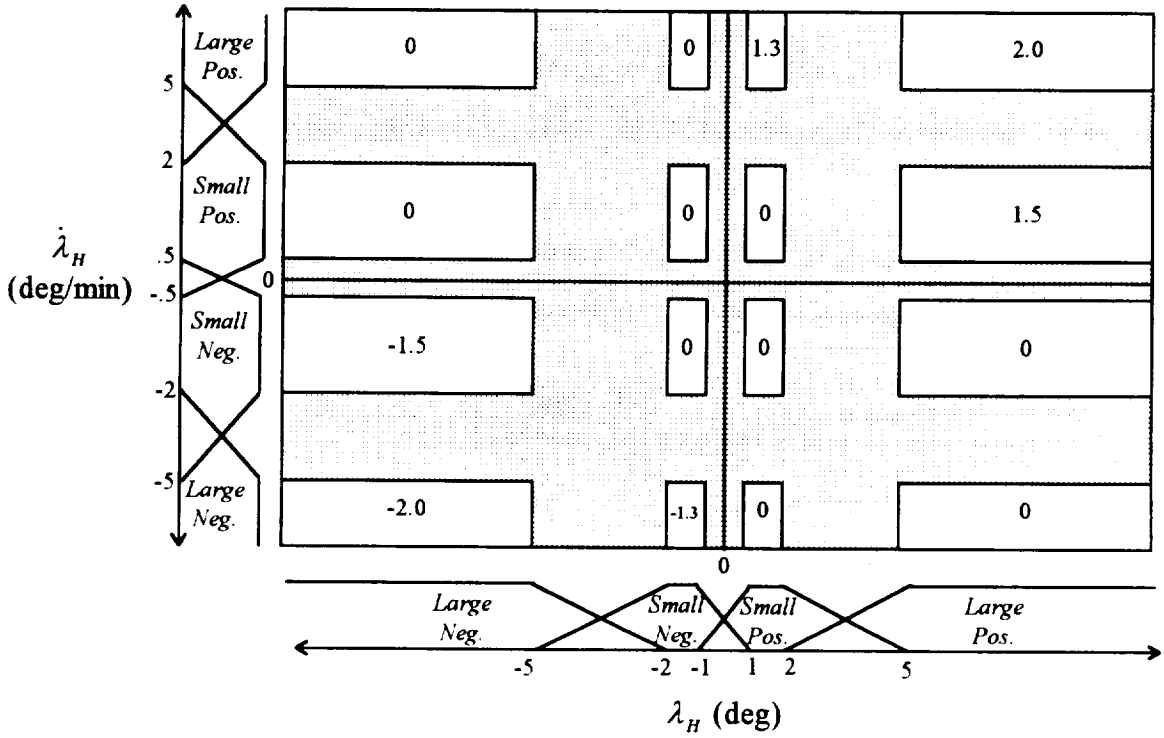

Figure 4-8 Y THC burn size for *Small* ranges

These figures illustrate some significant differences between the X and Y axes. Notice, the control logic for the Y axis is symmetric. As a result, the model does not have a bias for λ_H or $\dot{\lambda}_H$. Also, the model will not make a Y firing when λ_H and $\dot{\lambda}_H$ have opposite signs. These techniques, which were identified in Chapter 3, are unique to the Y axis and are used by human pilots.

The sixteen conclusions for Y burn size are combined using Equation 4-3. This aggregate output is then multiplied by a scale factor, K_Y, which is determined by rules 17 and 18 for the Y axis.

17. If (R_L is *Large*) Then (K_Y is 2).
18. If (R_L is *Small*) Then (K_Y is 1).

This allows the Y burn size to be directly proportional to range, as it was for the X axis. However, for *Large* ranges $K_Y = 2$, while $K_X = 3$. This smaller scale factor for the Y axis accounts for the fact that pilots make far fewer Y burns than X burns at *Large* ranges.

To summarize, the eighteen fuzzy rules for the Y_{Body} axis are combined in the same manner as the rules for the X_{Body} axis. This decision logic is illustrated in Figure 4-9.

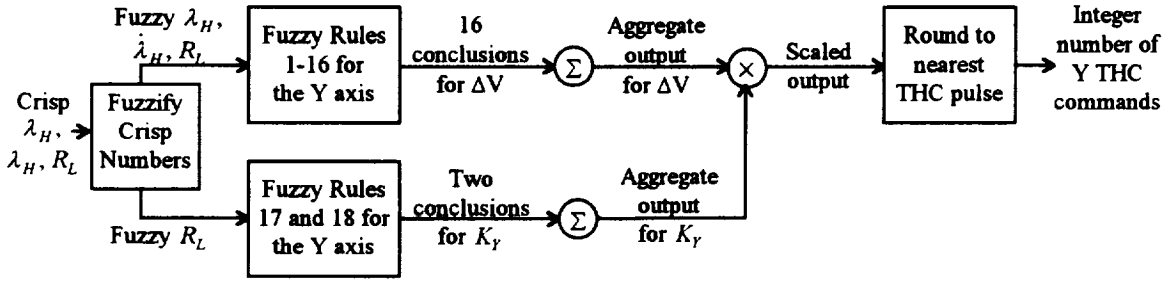

Figure 4-9 Three degree-of-freedom, Y THC decision logic

4.4.3 Z THC Decision Logic

The control logic for the Z_{Body} axis is relatively simple. Based on the laser's range and its filtered range rate, the model determines if the Shuttle is closing *Fast* or *Slow*, then decides if any Z THC commands are needed.

As discussed in Chapter 3, the desired $\dot{R}_L$ varies with range; so a pilot's definition of *Fast* and *Slow* will also vary with range. Therefore, the membership function for $\dot{R}_L$ is conditional upon R_L. All four membership functions for the Z axis are depicted in Figure 4-10. Notice, unlike the X and Y axes, which defined only two sets for R_L, the Z axis uses three different sets for range. There are also three different membership functions for $\dot{R}_L$ corresponding with the three sets for R_L.

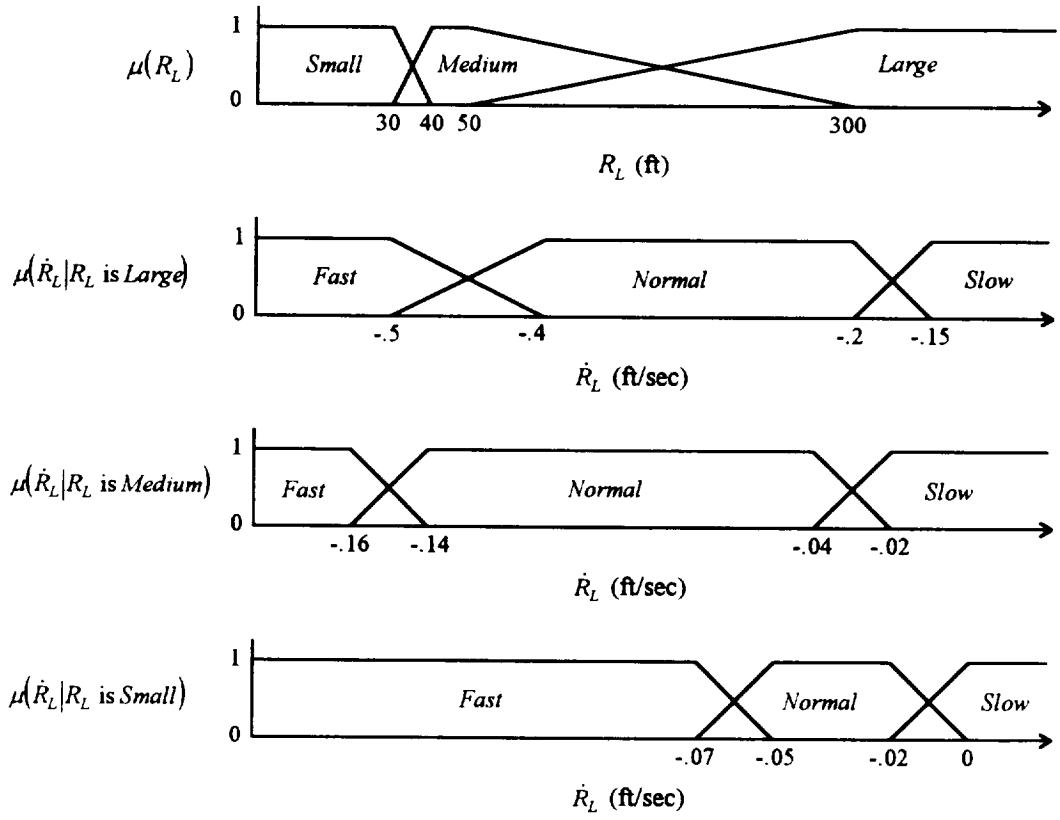

Figure 4-10 Fuzzy sets for R_L, and $\dot{R}_L$

After deciding if $\dot{R}_L$ is *Fast*, *Slow*, *Normal*, or some combination of these fuzzy terms, the model determines what, if any, Z THC command is required. This is a very simple task that only involves three fuzzy rules, each yielding a crisp conclusion for the number of Z THC commands.

1. If ($\dot{R}_L$ is *Fast*) Then (Burn is +1 THC).
2. If ($\dot{R}_L$ is *Slow*) Then (Burn is -1 THC).
3. If ($\dot{R}_L$ is *Normal*) Then (Burn is 0 THC).

The rules for the Z axis specify the number of THC commands, while the rules for the X and Y axes determine the number of minimum impulses required. This difference is due to analysis that indicates pilots' decision process for the Z_{Body} axis is independent of the current DAP mode. Pilots make a +Z THC command when $\dot{R}_L$ is *Fast* and a -Z command when $\dot{R}_L$ is *Slow* regardless of the current DAP setting.

These three conclusions are combined using Equation 4-3, then rounded to the nearest integer, which will always be 1,-1, or 0. This process is illustrated in Figure 4-11.

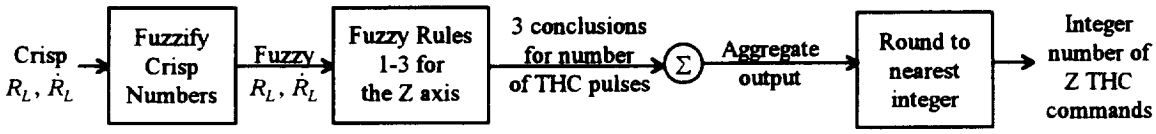

Figure 4-11 Z THC decision logic

Because the three fuzzy rules have crisp conclusions of 1, -1, and 0, and are all a function of $\dot{R}_L$, the crossover points for $\mu(\dot{R}_L)$ determine when the model makes a THC command. Due to numerical rounding, the pilot model commands a +Z burn when $\mu_{Fast}(\dot{R}_L) \geq 0.5$, and a -Z burn when $\mu_{Slow}(\dot{R}_L) \geq 0.5$. For ranges that are completely *Large*, the second function in Figure 4-10 determines when a Z firing is commanded. At these ranges a positive burn is made when $\dot{R}_L \leq -0.45$, and a -Z firing is made when

$\dot{R}_L \geq -0.175$. As the range decreases and becomes somewhat *Medium*, these thresholds slowly increase. When $40 \leq R_L \leq 50$, the range is completely *Medium*. For this range, the third function in Figure 4-10 results in a +Z braking burn when $\dot{R}_L \leq -0.15$, and a -Z burn if $\dot{R}_L \geq -0.03$. Inside 40 ft, these thresholds increase again until $R_L \leq 30$ (equivalent to $R_P \leq 5$). During these last five feet, the range is completely *Small*, and the model commands a +Z burn to slow the Shuttle when $R_L \leq -0.06$, and a -Z burn if $\dot{R}_L \geq -0.01$.

This simple logic results in a well-defined corridor outside which the model will make a corrective Z THC command. This is depicted on the range rate vs. range graph in Figure 4-12. For this plot the *x* axis shows the negative of R_L. This allows the corridor to begin on the left and end on the right, which is consistent with a v-bar approach and with all of the trajectory plots shown later. This corridor was selected based upon analysis of man-in-the-loop data. It does differ slightly from the corridor defined by the piloting rules for range rate, which is shown in Figure 4-13. From 350 ft to approximately 125 ft, pilots fly slightly faster than the maximum closure rate defined by $\frac{-R_L}{1000} - 0.1 \frac{\text{ft}}{\text{sec}}$. Once $R_L < 125$ ft (equivalent to $R_P < 100$ ft), they fly much slower than the maximum allowed closure rate of $\dot{R}_L \geq -0.2 \frac{\text{ft}}{\text{sec}}$. Because the fuzzy pilot model is designed to duplicate a human's performance, it will also deviate slightly from these piloting rules.

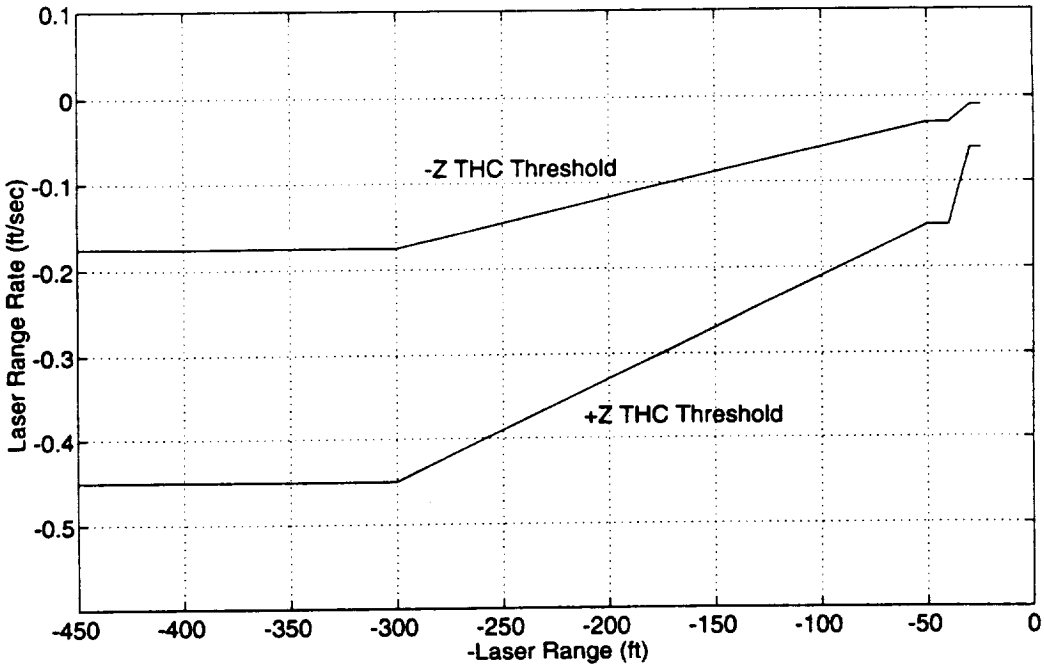

Figure 4-12 Range rate vs. range corridor defined by the fuzzy rules

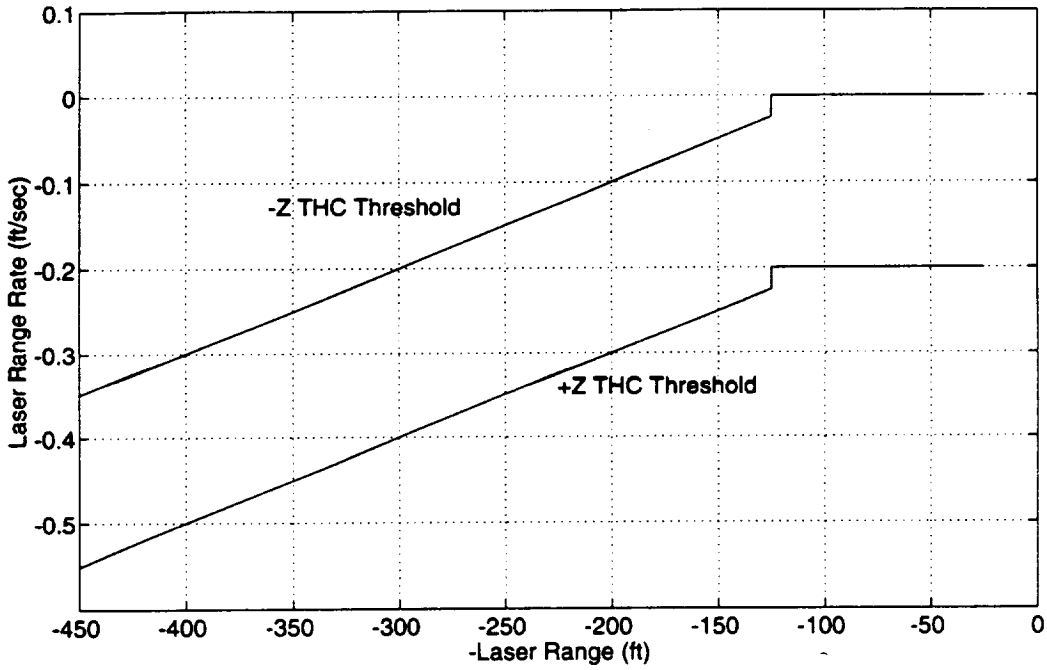

Figure 4-13 Range rate vs. range corridor defined by the piloting rules[1]

[1] The discontinuity at 125 ft is a result of a strict interpretation of the piloting rules. R_L is used to compute $\dot{R}_L$ "outside 100 ft", yet R_P is used to determine when to transition to new rule of $\dot{R}_L \geq -0.2 \frac{\text{ft}}{\text{sec}}$ for "inside 100 ft".

4.4.4 Selection of DAP mode and Low Z/Norm Z Transition

In addition to determining the required translation burns along each axis, the pilot model also decides when to switch from Low Z to Norm Z and selects the DAP mode. The Low Z to Norm Z transition is easy to determine. The piloting rules specify the crew should switch to Norm Z when the range is 75 feet. Because this "range" refers to the port-to-port distance, and for SC-2 and SC-4 $R_L = R_P + 25$ ft, pilots select Norm Z when the laser reads approximately 100 ft. The man-in-the-loop data indicates pilots follow this rule very closely. Therefore, the pilot model switches from Low Z to Norm Z once inside $R_L = 100$ ft.

The selection of DAP A or DAP B is a more difficult problem. It seems logical for the model to use DAP A whenever a burn of three or more minimum impulses is required, and use DAP B for small velocity changes of one or two minimum impulses. However, this would result in the model flying almost the entire approach in DAP B mode. As the need for a correction increased, the model would decide to implement a relatively small DAP B pulse, rather than waiting until a DAP A pulse was required. This would be inconsistent with real pilots, who generally use DAP A for the first half of the run, then transition to predominantly DAP B burns inside $R_L \approx 100$ ft. Therefore, the pilot model switches from DAP A to DAP B at the same time it transitions from Low Z to Norm Z. This gives similar results to the man-in-the-loop data. However, it is not identical because real pilots occasionally switch back and forth between DAP modes, and the pilot model only switches modes once each run. This slight difference will be addressed later.

4.5 RESULTS

The three degree-of-freedom pilot model was evaluated using two different software simulators. The first simulator assessed the model's performance flying a simple three-

degree-of-freedom Shuttle. The second evaluation used Draper Laboratory's high fidelity On-orbit Functional Simulator (OFS), which accurately models the Shuttle's dynamics. This allowed an assessment of the three DOF model's performance flying a six DOF vehicle. Using both of these simulators, the three DOF fuzzy model's results were compared with four man-in-the-loop simulations from the same initial condition to Station Configuration 4.

4.5.1 Introduce the Four Man-in-the-Loop Runs

The man-in-the-loop data consisted of four runs: two runs by Pilot 1 and two runs by Pilot 2. These four runs are referred to as 1-A, 1-B, 2-A, and 2-B; the number designating the individual pilot, and the letter specifying which of the two runs. Their in-plane trajectories are shown in Figure 4-14.

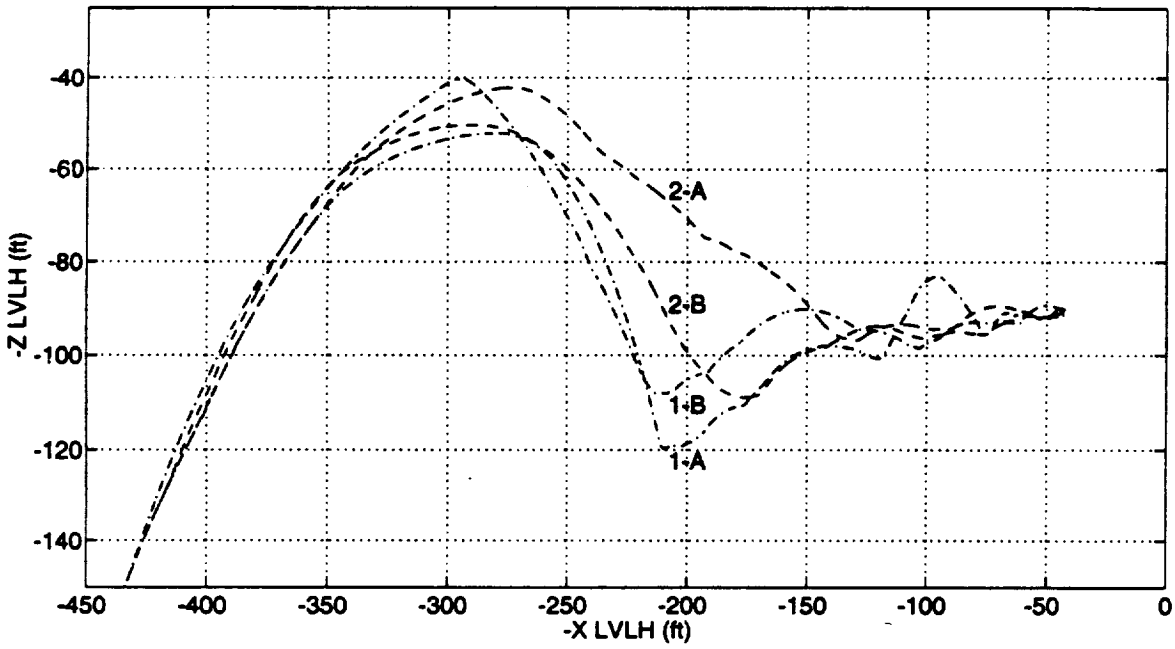

Figure 4-14 Man-in-the-loop, center of mass, in-plane trajectories to SC-4

Notice all of the runs have the same general shape. They begin with one big hop. Then through a series of smaller hops, the Shuttle approaches the Station. At the grapple

point the Shuttle's center of mass is about 91 ft below v-bar. Despite these similarities, neither pilot duplicates their first run. There are slight differences between runs 1-A and 1-B and between 2-A and 2-B. This is probably a result of slight variations with each pilot. Also notice, the two pilots have different individual techniques. Pilot 1 consistently flies a lower approach trajectory than Pilot 2. This is most likely due to different individual definitions for "$\lambda_{\dot{r}}$ is *Large Positive*", "$\dot{\lambda}_{\dot{r}}$ is *Large Negative*", etc.. These different definitions define their techniques. Later, Chapter 6 shows the fuzzy pilot model can be adjusted to match the extreme techniques from run 1-A and 2-A. However, for now the goal is to fly an "average" approach, down the middle of these four trajectories.

4.5.2 Three Degree-of-Freedom Model Flying a Three Degree-of-Freedom Shuttle

The first evaluation of the three DOF model was a comparison of the four trajectories in Figure 4-14 with model's results flying a simple simulator developed on a graphic workstation. This simulator makes a number of assumptions including: a three DOF Shuttle, a spherical earth, no aerodynamic or plume forces, a perfect laser, and impulsive jet firings. These assumptions allowed a proof of the fuzzy logic concept before progressing to a more accurate simulator. The workstation's graphic environment also provided immediate visual feedback. As a result it was easy to quickly modify the pilot model during the iterative process used to determine the fuzzy set boundaries.

Figure 4-15 shows the comparison of this model with the four man-in-the-loop runs, depicting their center of mass, in-plane trajectories. These in-plane trajectories are fairly similar. Comparisons were also made of the out-of-plane trajectories, the range rate vs. range profiles, the view through the COAS, and the location of THC commands. All of these comparisons indicated the fuzzy pilot model was a suitable method for duplicating a human's performance during proximity operations. However, these results were generated using a simplified simulator. Because the man-in-the-loop runs were generated

using a much more accurate simulator, these comparisons are not entirely valid. They serve only to demonstrate the potential for a fuzzy logic pilot model.

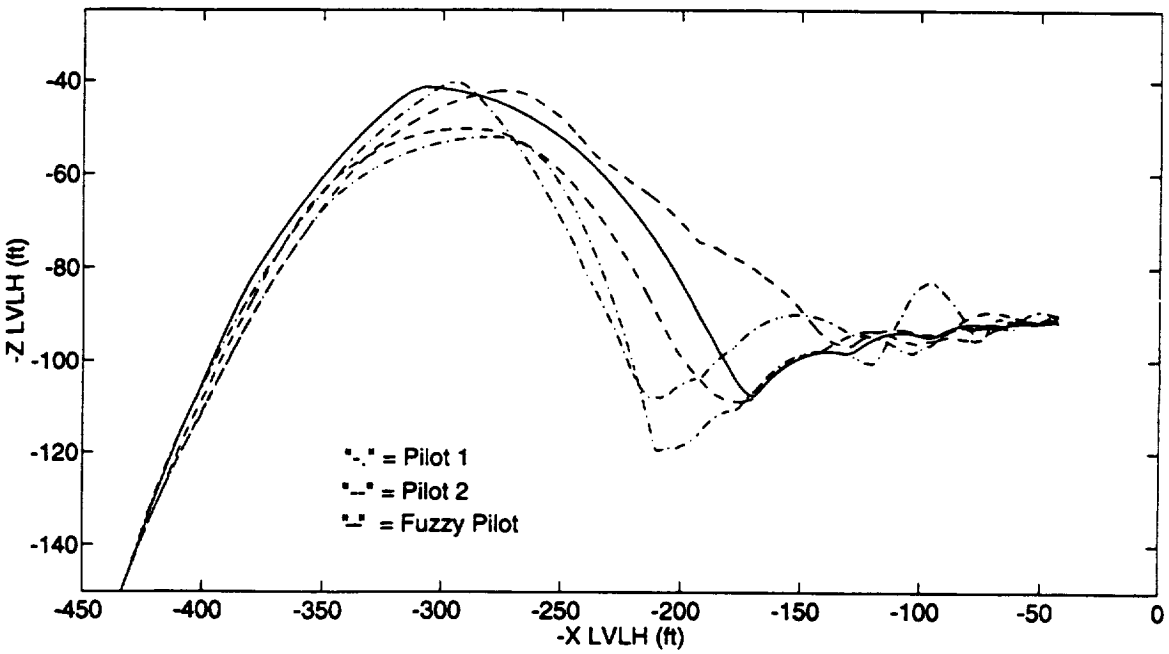

Figure 4-15 Evaluating the three DOF model using a three DOF simulator

4.5.3 Three Degree-of-Freedom Model Flying a Six Degree-of-Freedom Shuttle

The next step evaluated the three DOF model's performance flying a realistic simulator that accounts for the Shuttle's six DOF dynamics. This was accomplished using Draper Laboratory's OFS, which accurately models the Shuttle's six degree-of-freedom dynamics. After transferring the fuzzy model to this simulator, a few set boundaries were changed slightly to better match the human's performance. This resulted in the fuzzy sets presented in Section 4.4.

The pilot model performed reasonably well on this simulator. Figure 4-16 shows a sample of these results, with the center of mass, in-plane trajectories for the fuzzy pilot model and the man-in-the-loop runs. It also shows the location of each ±X burn by the pilot model. The fuzzy pilot made three $-X_{Body}$ burns near the top of the first hop to push

the Shuttle "down" and increase λ_V. For the rest of the run, numerous +X burns were applied to compensate for the effects of orbital mechanics that cause the Shuttle to lose altitude as it approaches the Station.

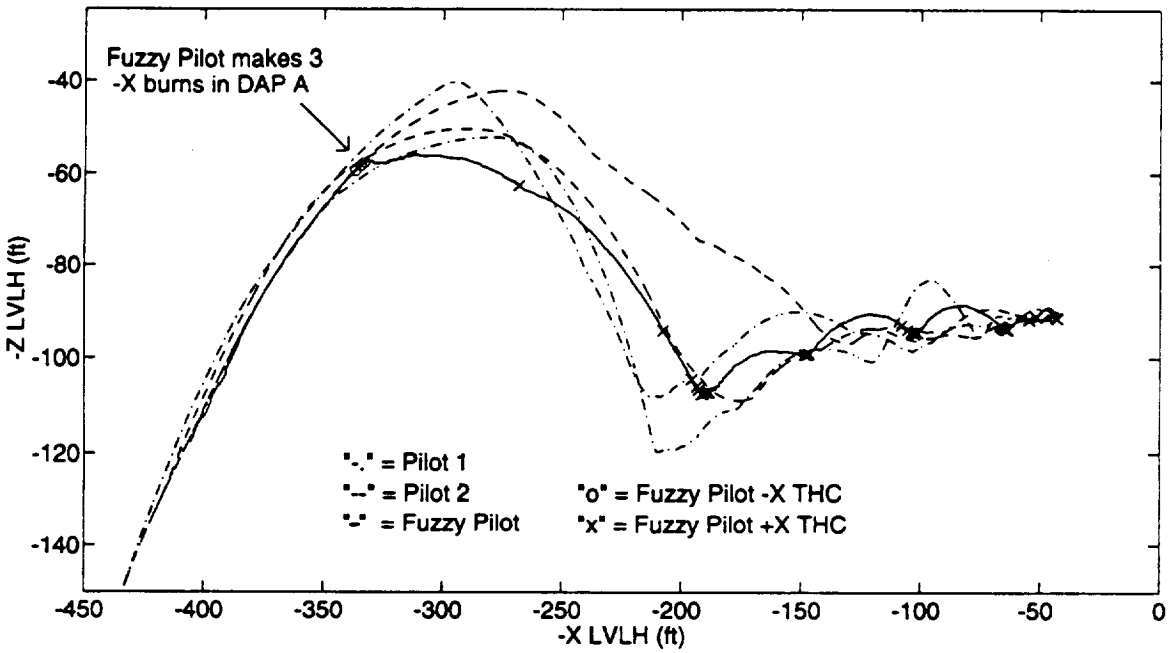

Figure 4-16 Evaluating the three DOF model using a six DOF simulator

This trajectory is fairly similar to the man-in-the-loop results, with one exception. The model overcontrols with three successive -X burns in DAP A at the top of the first hop. None of the human pilots make such a big correction in this area.

This problem is a result of the three DOF model ignoring the Shuttle's attitude motion. Any perceived movement of the target through the COAS is attributed to the Shuttle's translation. However, in reality the Shuttle's attitude motion also causes the target to appear to move through the COAS. When the -X jets fire, they not only apply a force in the $-X_{Body}$ direction, they also add a negative pitch rate to the Shuttle. As the Shuttle pitches back, the target moves down through the COAS, giving the appearance that the Shuttle is continuing to gain altitude. As a result, the model applies another -X

THC burn. This process could continue until the DAP commands attitude jets to slow the Shuttle's body rate.

For example, immediately before the model's first -X burn in Figure 4-16, $\dot{\lambda}_V$ was estimated to be $-4.95\frac{\text{deg}}{\text{min}}$. As a result the model commanded a -X burn to "push" the Shuttle down and reduce $\left|\dot{\lambda}_V\right|$. Less than five seconds later, due to the attitude motion created by the -X burn, the model estimated $\dot{\lambda}_V$ to be $-5.97\frac{\text{deg}}{\text{min}}$, indicating the Shuttle was actually moving "up" even faster. This resulted in the second -X burn. Four seconds later, $\dot{\lambda}_V$ was estimated to be $-6.98\frac{\text{deg}}{\text{sec}}$. Again, due to attitude motion, the pilot model mistakenly thought the Shuttle was gaining altitude at an increasing rate, resulting in the third -X burn. Finally, a half of second later the DAP commanded some jets to reduce the attitude motion, and $\dot{\lambda}_V$ was estimated to be a more realistic $+1.67\frac{\text{deg}}{\text{min}}$. The model finally believed the Shuttle was losing altitude. If the pilot model had been able to back out attitude motion perfectly, only one of these three -X burns would have been commanded. Instead, the three DOF model mistakenly assumed all of the target's movement through the COAS was due to the Shuttle's translation, and three -X burns were commanded.

Adjusting the set boundaries could not prevent this problem. In some cases, it actually made the problem worse, resulting in the model overcontrolling with +X and ±Y burns as well. One attempt to solve this problem, with slightly different fuzzy sets, resulted in the model applying six successive -X burns, when one would have been sufficient. This tendency of overcontrolling with X and Y burns is the only noteworthy difference between the three degree-of-freedom pilot model and the man-in-the-loop runs.

4.6 CONCLUSIONS

This chapter demonstrates fuzzy logic is a viable means of duplicating a human's performance during proximity operations. It accurately models a pilot's ability to perform trade-offs between vague goals and conflicting constraints.

However, the model's performance using a six DOF simulator does not accurately match the man-in-the-loop data. Additional logic is needed to account for the Shuttle's attitude motion. Without such logic, the model will make unnecessary burns, usually in the form of multiple THC commands. Negative X firings are especially prone to this problem because their jet axes are offset farther from the Shuttle's center of mass, resulting in more attitude coupling.[20] However, the problem can also occur in the +X and ±Y axes. It is possible the Shuttle could reach its maximum pitch or roll rate of $\pm 0.1 \frac{\text{deg}}{\text{sec}}$ before any attitude jets fire. This would cause the target to move through the COAS at a rate of $\pm 6 \frac{\text{deg}}{\text{min}}$, while the Shuttle center of mass was stationary. This maximum rate could be maintained for up to 20 seconds, as the Shuttle moves through its ±1° attitude deadband. As seen from the phase planes in Section 4.4, this large of an error in estimating $\dot{\lambda}_V$ or $\dot{\lambda}_H$ would result in erratic control responses.

A reasonable solution to this problem is to incorporate Shuttle attitude information in the fuzzy logic decision process. This is a relatively easy modification. Because fuzzy logic allows the combination of a number of conclusions, additional rules can be added without changing the existing rules used by the three DOF pilot model. This evolutionary development process, used to create a six degree-of-freedom pilot model, is presented in the next chapter.

Chapter 5 : Six Degree-of-Freedom Fuzzy Logic Pilot Model

This chapter discusses the additional fuzzy rules that enhance the pilot model and account for the Shuttle's attitude motion, creating a six degree-of-freedom model. After explaining this logic, the new model is compared with man-in-the-loop simulations and with another pilot model that uses similar rules based upon "crisp" logic. This demonstrates the fuzzy model's ability to match an average human pilot's performance. It also shows some of the benefits of fuzzy logic when compared with traditional, Boolean logic.

5.1 Additional Fuzzy Logic

To correct the problems with the three DOF model, additional logic is required to limit the pilot's actions in the X and Y axes when the Shuttle's attitude rates are relatively *High*. Real pilots do this by referencing the cockpit universal pointing display, which provides the Shuttle's inertial body rates. When the Shuttle's pitch rate is *High*, pilots know a large portion of the target's vertical movement in the COAS is likely due to attitude motion. Therefore, they do not make any X THC commands and wait to reevaluate the sensory information when the pitch rate is *Low*. Pilots use the roll rate in the same way to inhibit

Y THC commands.[14] This technique, of inhibiting X and Y burns when the body rates are *High,* can be captured using fuzzy logic.

The fuzzy definitions used by the model for *High* and *Low* pitch rates are fairly simple. The pitch rate, $\dot{\theta}$, is defined to be completely *Low* if it is within $0.025\frac{deg}{sec}$ of the rotating LVLH frame. It is completely *High,* if it is outside $0.075\frac{deg}{sec}$. These numbers, shown in Figure 5-1. They equate to $.5\frac{deg}{min}$ and $4.5\frac{deg}{min}$, which are 25% and 75% of the Shuttle's attitude rate limits.

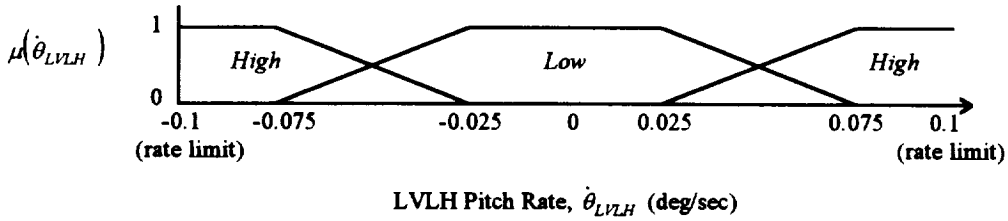

Figure 5-1 Fuzzy sets for LVLH pitch rate

Unfortunately, the universal pointing display does not provide LVLH attitude rates, but displays the Shuttle's inertial body rates. Because the Shuttle must pitch approximately $-4\frac{deg}{min}$ to maintain a perfect LVLH attitude, the pitch rate display has a bias of $-0.067\frac{deg}{sec}$. Therefore, pilots estimate the LVLH pitch rate by the display's deviation from this nominal value.[14] Figure 5-2 shows the membership function used by the pilot model, which accounts for this bias.

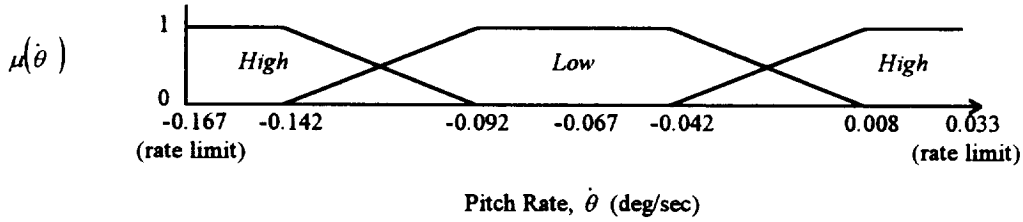

Figure 5-2 Fuzzy sets for inertial pitch rate

After determining if the pitch rate is *High, Low*, or some combination of both, the model calculates a scale factor, $K_{\dot{\theta}}$, ranging between 0 and 1. This scale factor is determined by combining the conclusions from two additional fuzzy rules for the X axis that are shown below.[1]

19. If $\dot{\theta}$ is *Low* Then $K_{\dot{\theta}}$ is 1.
20. If $\dot{\theta}$ is *High* Then $K_{\dot{\theta}}$ is 0.

The scale factor, $K_{\dot{\theta}}$, accounts for attitude motion by weighting the output from the three DOF pilot model. As shown in Figure 5-3, when $K_{\dot{\theta}} = 0$ the logic does not allow any X burns, because the pitch rate is completely *High*. If $K_{\dot{\theta}} = 1$ the model is not inhibited at all by the attitude motion, because the pitch rate is completely *Low*. If the pitch rate is neither completely *High* nor *Low*, but is a combination of both, then $0 < K_{\dot{\theta}} < 1$. In this case, the model will be inhibited to a degree. For example, if the pitch rate is equally *High* and *Low* the model assumes half of the perceived motion is due to translation and half due to rotation, and $K_{\dot{\theta}} = 0.5$. As a result, the six DOF pilot model commands half of the three DOF model's output.

This is a realistic method of including attitude information in the pilot model. It is based upon the same sensory data and techniques used by real pilots. This new logic does not prevent the model from being fooled by attitude motion, but it does reduce the possibility. This is reasonable because real pilots do occasionally mistake some attitude motion for translation, resulting in a few unnecessary burns.

---

[1] Notice, because these two rules have conclusions of 1 and 0, their combination, which defines $K_{\dot{\theta}}$, will always be equal to $\mu_{Low}(\dot{\theta})$. Therefore, only rule 19 is required. Two rules were used in the event the conclusions had to be changed during the iterative process, or additional logic was added later.

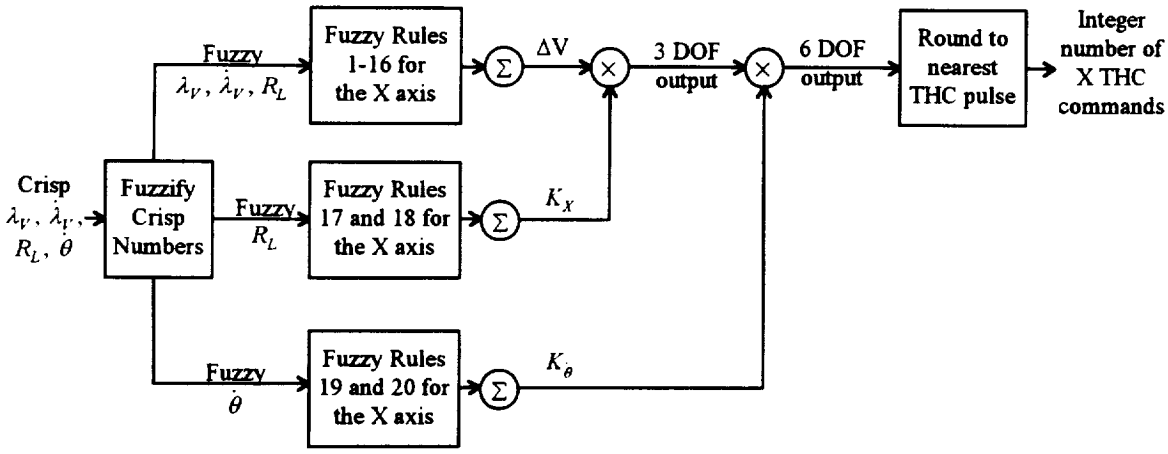

Figure 5-3 Six degree-of-freedom, X THC decision logic

The Y axis uses the same logic to inhibit Y burns when the roll rate ($\dot{\phi}$) is *High*. The fuzzy sets for $\dot{\phi}$, shown in Figure 5-4, are identical to the sets for $\dot{\theta}$, with the exception that roll rate does not have a bias. Because the LVLH frame does not rotate out-of-plane, the inertial roll rate is identical to the LVLH rate. Therefore, the membership function for roll rate is symmetric about zero.

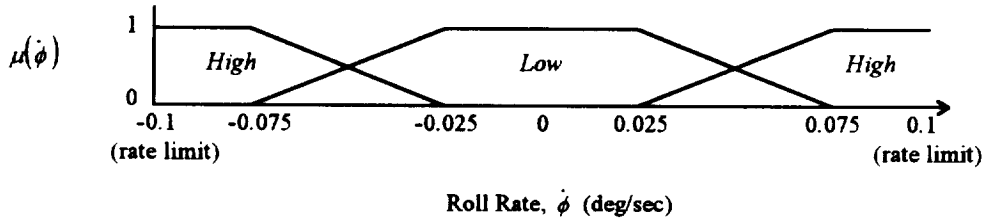

Figure 5-4 Fuzzy sets for inertial roll rate

After determining $\dot{\phi}$'s membership in *High* and *Low*, the model calculates the scale factor $K_{\dot{\phi}}$ by combining the conclusions from two additional fuzzy rules for the Y axis.

19. If $\dot{\phi}$ is *Low* Then $K_{\dot{\phi}}$ is 1.
20. If $\dot{\phi}$ is *High* Then $K_{\dot{\phi}}$ is 0.

Just like the X axis, this scale factor is multiplied by the three DOF pilot model's output. As depicted in Figure 5-5, no Y burns are made if the roll rate is completely *High*. When the roll rate is completely *Low* the output from the six DOF pilot model is identical to the three DOF model's output. If the roll rate is partially *High* and *Low*, the model is inhibited to a degree corresponding to the roll rate's membership in *High*.

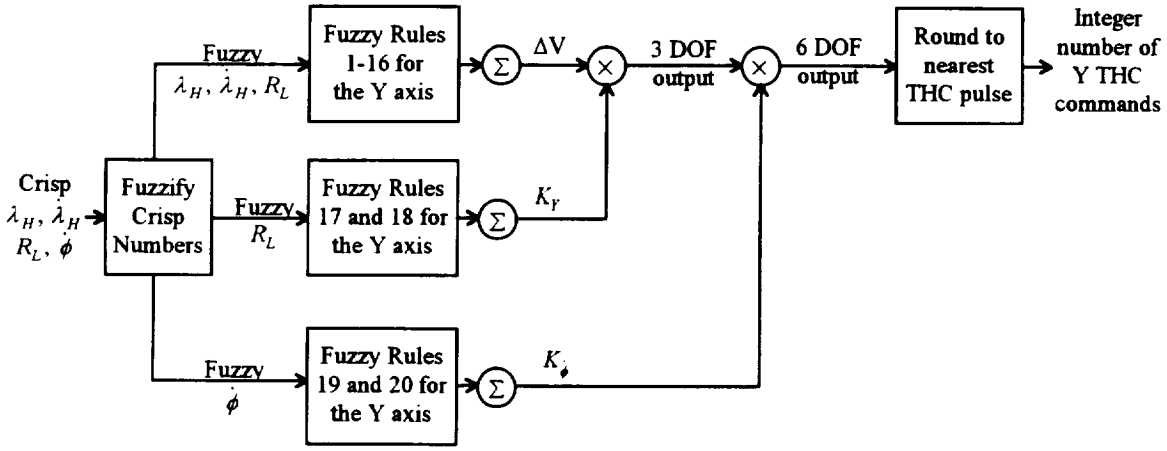

Figure 5-5 Six degree-of-freedom, Y THC decision logic

This concludes all of the additional logic necessary to model a human pilot's technique of accounting for the Shuttle's attitude motion. This enhancement required only four additional fuzzy rules: two for the X axis and two for the Y axis. No changes were necessary for the Z axis, and all of the rules used by the three DOF pilot model are incorporated in the six DOF model.

5.2 RESULTS

The section presents the results of the six DOF fuzzy pilot model. These results are compared with the four man-in-the-loop runs introduced in Chapter 4, and with another pilot model using similar rules with traditional, "crisp", logic.[4] Both pilot models were

evaluated using Draper Laboratory's On-orbit Functional Simulator (OFS), and all of the simulations used the same initial conditions. Comparisons are made in four general areas:

1. Trajectories and pilot sensory data
2. Location of THC commands
3. Total time, fuel consumed, and THC activity
4. Adherence to the piloting rules and final miss distance

5.2.1 Trajectories and Pilot Sensory Data

Four types of plots are used to compare the trajectories and sensory data. The first plots show the Shuttle's in-plane and out-of-plane trajectories. This allows a comparison of the Shuttle's vertical and horizontal motion during each simulation. The next two plots compare the sensory information displayed to the pilot. The laser's range rate vs. range profile compares the Shuttle's closure rate for each run. The final plot compares the COAS angles, depicting λ_V and λ_H as a function of range. These last two plots of the sensory data are not available for the crisp pilot model. However, this does not detract significantly from the overall comparison.

Figure 5-6 shows the six DOF fuzzy pilot's in-plane trajectory compared with the four man-in-the-loop runs. Because this model compensates for attitude motion, it has much better results than the three DOF model presented in the previous chapter. Instead of three -X burns near the top of the first hop, this enhanced model only commands two burns. This enhanced fuzzy pilot model flies a very average approach compared with the four man-in-the-loop runs. In contrast, the crisp pilot model, shown in Figure 5-7, is not as representative of the man-in- the-loop results. It does not travel as "high" on the first hop, and never drops as "low" as the other runs. It also has a more abrupt control response than the human pilots. This is a result of the limitations associated with "crisp"

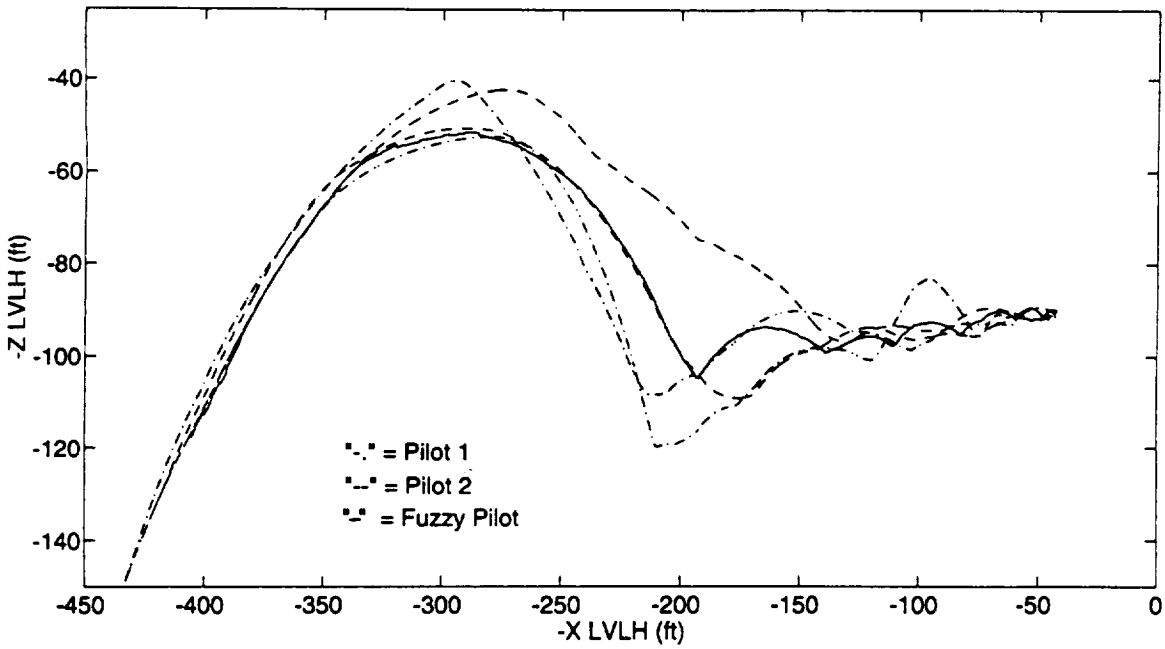

Figure 5-6 Comparison of the six DOF fuzzy model and man-in-the-loop in-plane trajectories

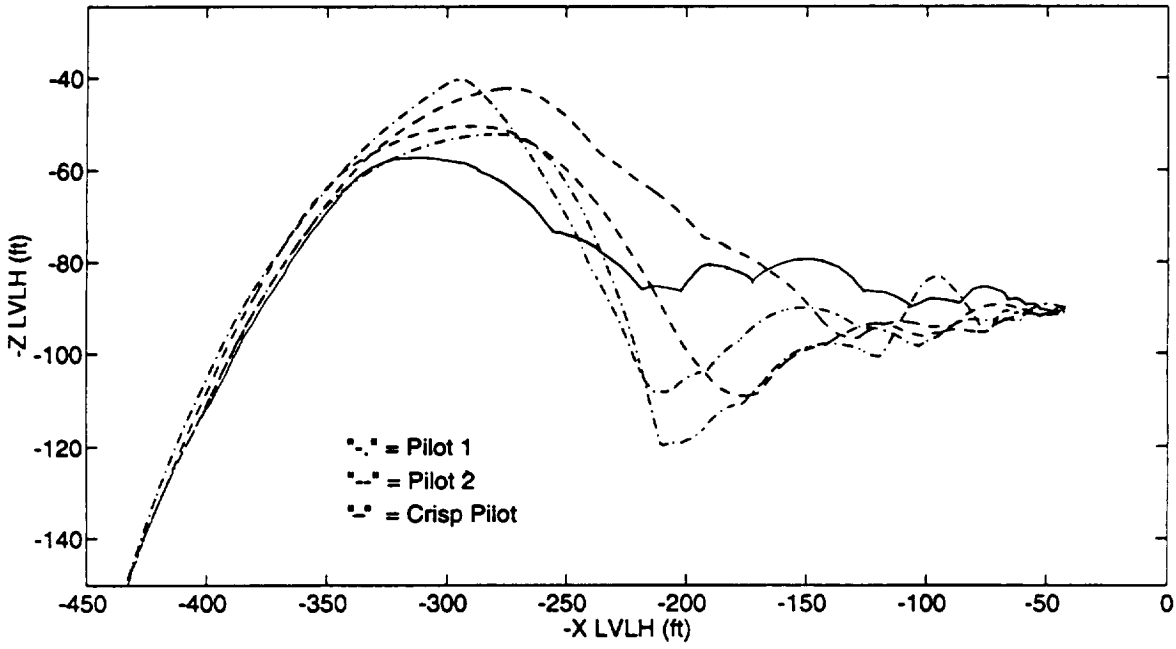

Figure 5-7 Comparison of the crisp model and man-in-the-loop in-plane trajectories

logic. Traditional logic cannot easily combine the conclusions from a number of rules. Therefore, it does not allow a gradual transition between the model's decision to not make a burn and the decision to make a burn. As a result, the crisp model does not fly a smooth approach. Because fuzzy logic can easily combine several rules, with conflicting conclusions, it has a more gradual control response, which is very similar to a human pilot.

Figure 5-8 shows the fuzzy pilot model's out-of-plane trajectory compared with the four man-in-the-loop runs. This motion is depicted using the Shuttle's x and y LVLH vectors, providing a view looking down toward the center of the earth with the Shuttle approaching from the left. Again, the fuzzy pilot's performance is very similar to the man-in-the-loop runs. Figure 5-9 shows the same plot for the crisp pilot model. In this case the crisp model is also representative of the humans' performance. It does not have the abrupt control response seen in the in-plane trajectory. However, it does deviate from the other runs by about three or four feet just before the grapple point, around $x = 50$ ft. This is a small difference, but at this close of a range it results in the crisp pilot exceeding the limit for $|\lambda_H| \leq 5°$ when $R_P < 25$ ft. This difference will be covered later, when comparing the pilots' ability to adhere to the proximity operations rules.

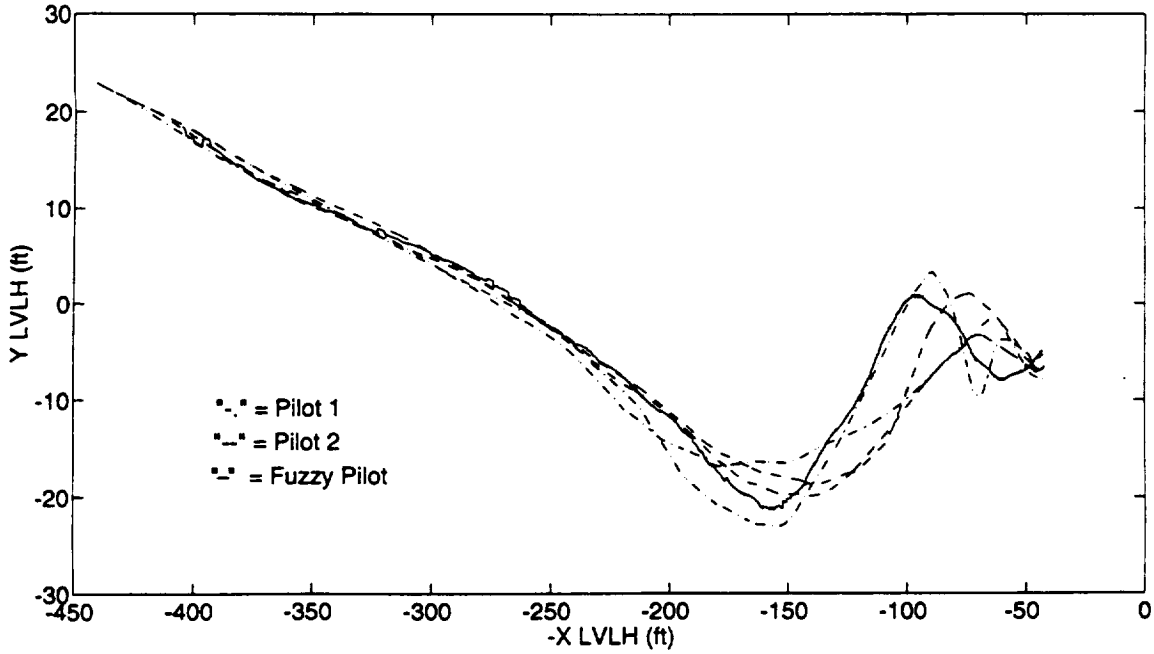

Figure 5-8 Comparison of the six DOF fuzzy model and man-in-the-loop out-of-plane trajectories

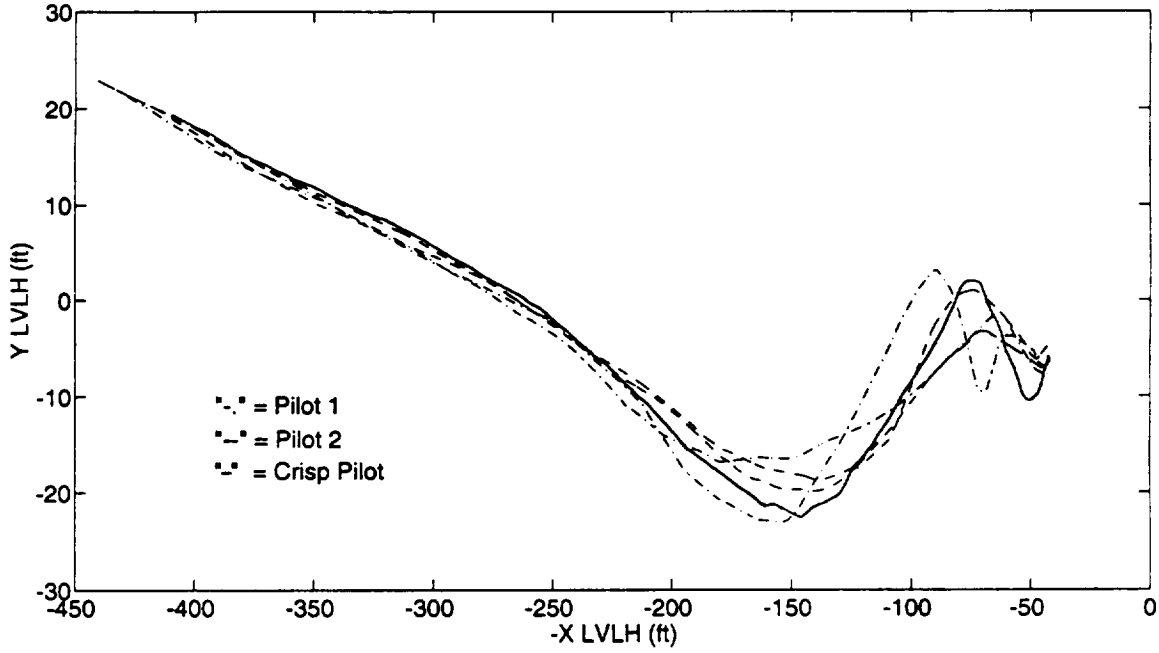

Figure 5-9 Comparison of the crisp model and man-in-the-loop out-of-plane trajectories

The in-plane and out-of-plane trajectories give a graphical representation of the pilots' ability to control the Shuttle's vertical and horizontal motion. In the same way, the best representation of the pilots' ability to control $\dot{R}_L$ is a plot of range rate as a function of range. This is shown in Figure 5-10 for the fuzzy pilot model and the four man-in-the-loop runs. Because each simulator stored slightly different data, there is a small difference in the plots. For the man-in-the-loop run's, the noisy range rate was not saved. Therefore, the $\dot{R}_L$ shown is the exact distance between the laser and the reflector on the Station, without any noise. This equivalent number was not available for the fuzzy pilot model. Instead, the range rate shown for the fuzzy model, is the filtered $\dot{R}_L$; which still has a little noise. Despite this minor difference, it is obvious the fuzzy pilot model flies an average profile. It is consistently somewhere between the fastest and the slowest man-in-the-loop simulation.

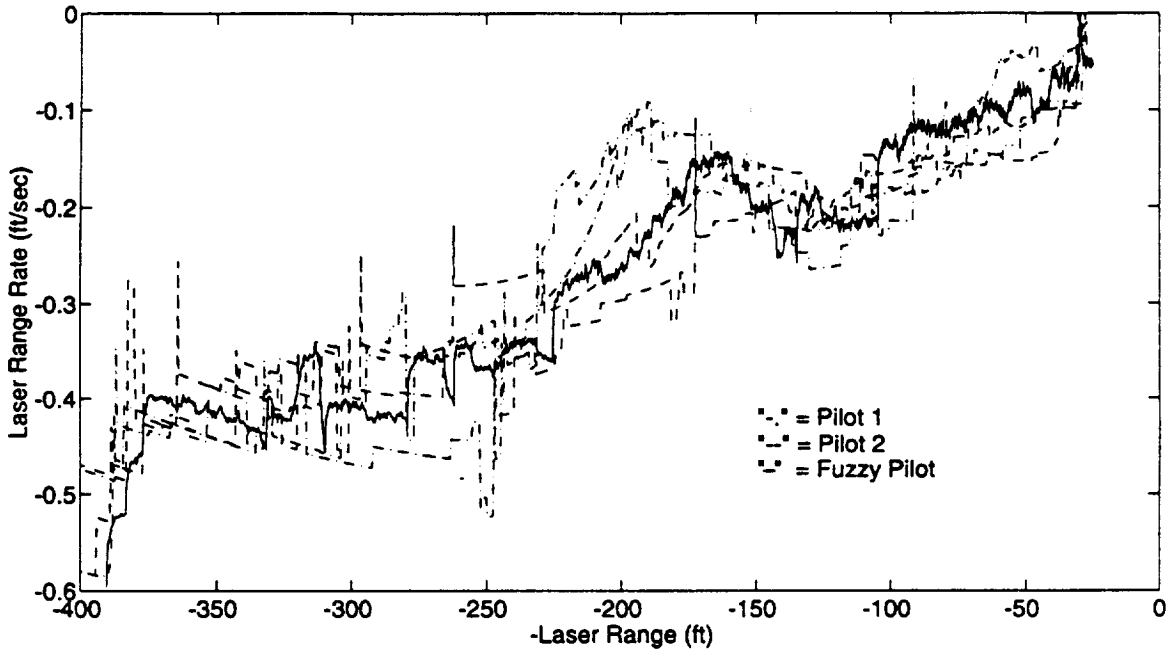

Figure 5-10 Comparison of the six DOF fuzzy model and man-in-the loop range rate vs. range profiles

Figure 5-11 compares the COAS angles from the fuzzy pilot model's simulation and the man-in-the-loop runs. These two plots show the horizontal and vertical COAS angles as a function of $-R_L$. As with many plots in this thesis, the negative value along the x axis allows the plot to begin on the left and end on the right, which is consistent with a v-bar approach. Notice, the graphs in Figure 5-11, are not as smooth as the center of mass trajectory plots shown earlier. Because these plots show the actual COAS angles, viewed through the window, they could vary by up to ±1° due to the Shuttle's attitude motion.

As with the other comparisons, these graphs indicate the fuzzy pilot model successfully matched the average of the four man-in-the-loop runs. This is especially evident from observing the vertical angle plot. All four man-in-the-loop runs vary significantly between 250 and 125 feet. However, the fuzzy model was right in the middle of these runs during the entire simulation.

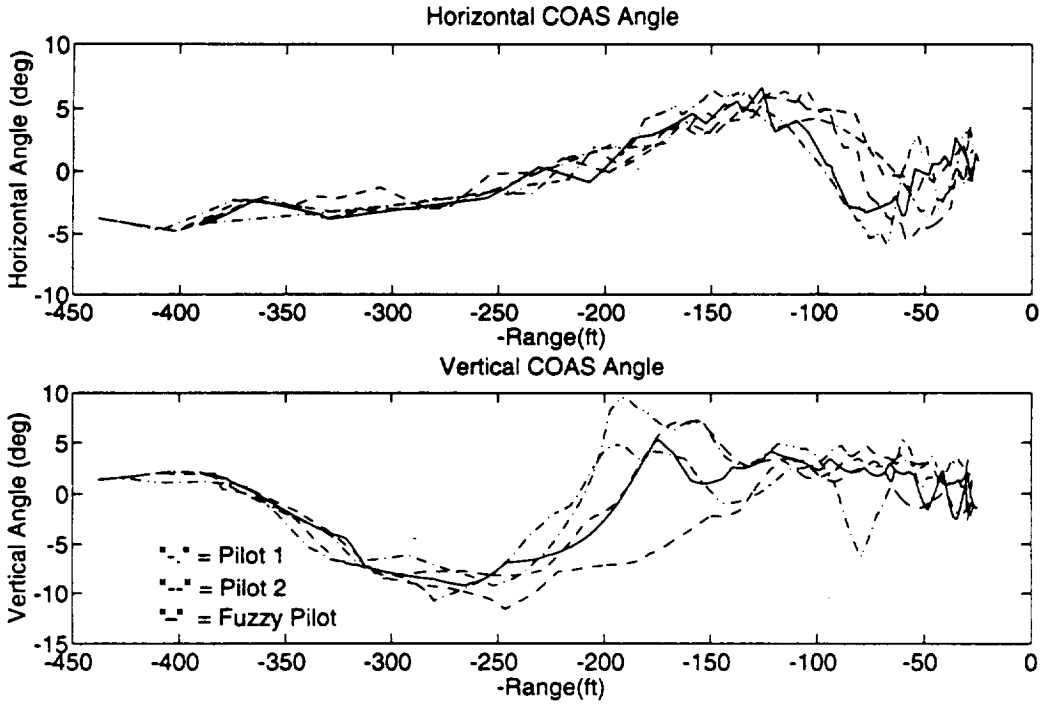

Figure 5-11 Comparison of the six DOF fuzzy model and man-in-the loop COAS angles

5.2.2 Location of THC Commands

In addition to producing similar trajectories, it is also important for the pilot model to make THC commands in the same general location as a human pilot. This allows the model to produce equivalent plume forces on the Station.

The next three plots compare the location of the THC commands for the fuzzy pilot model, the crisp model, and the man-in-the-loop runs. One plot is devoted to comparing the ±X burns; one for the ±Y burns; and the last for the ±Z burns. In each plot, all four man-in-the-loop runs are grouped together. Their burns are indicated by an "o"; the fuzzy pilot's commands are indicated by an "x", and the crisp model's burns are indicated by a "+". As a point of reference, the fuzzy pilot's trajectory is shown as a dashed line.

Figure 5-12 shows the location of the X THC commands for each simulation. The fuzzy model does a very good job of matching the human runs, placing all of its X burns in almost identical locations. On the other hand, inside 250 feet the crisp model makes a number of X burns at a higher altitude than the human pilots. It also never makes a burn below 95 feet on the Z_{LVLH} axis, which is where the majority of the human burns were located.

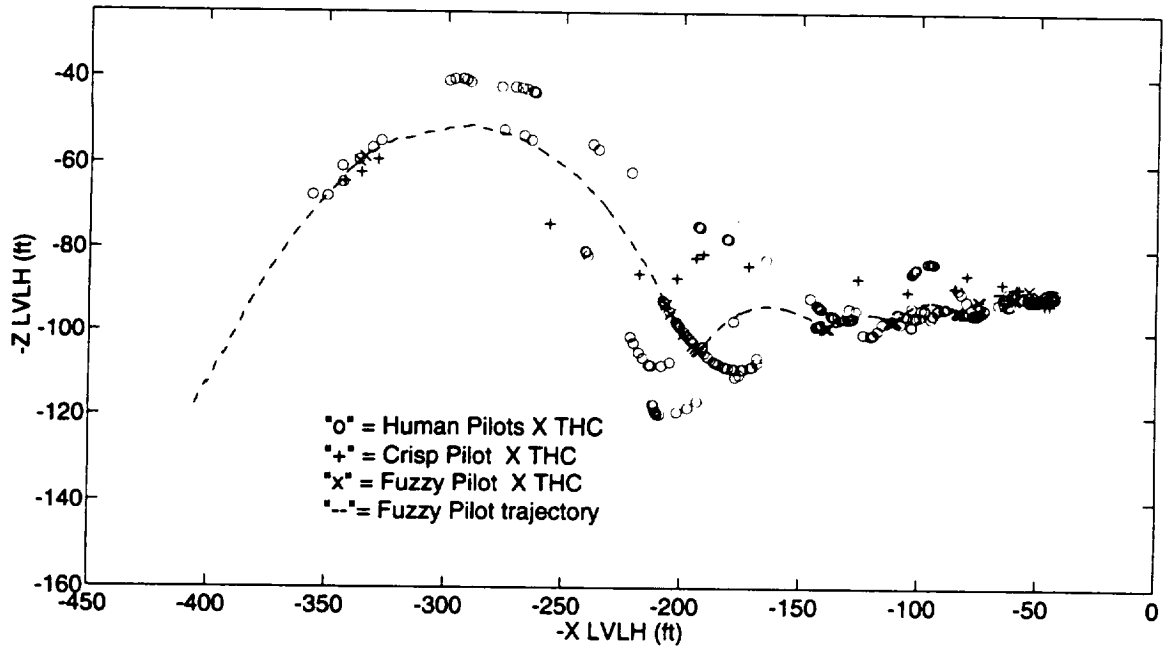

Figure 5-12 Location of the X THC commands

Figure 5-13 and Figure 5-14 show the location of the Y and Z THC commands respectively. For these axes, both models do a fairly good job of matching the human pilots.

This page is intentionally left blank.

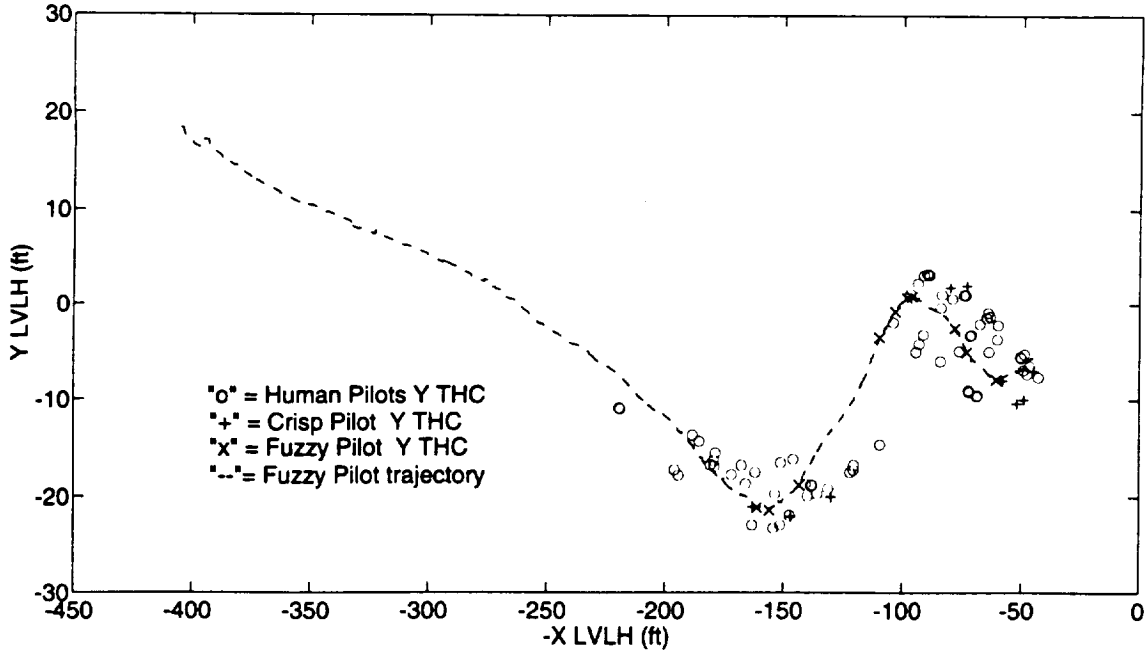

Figure 5-13 Location of the Y THC commands

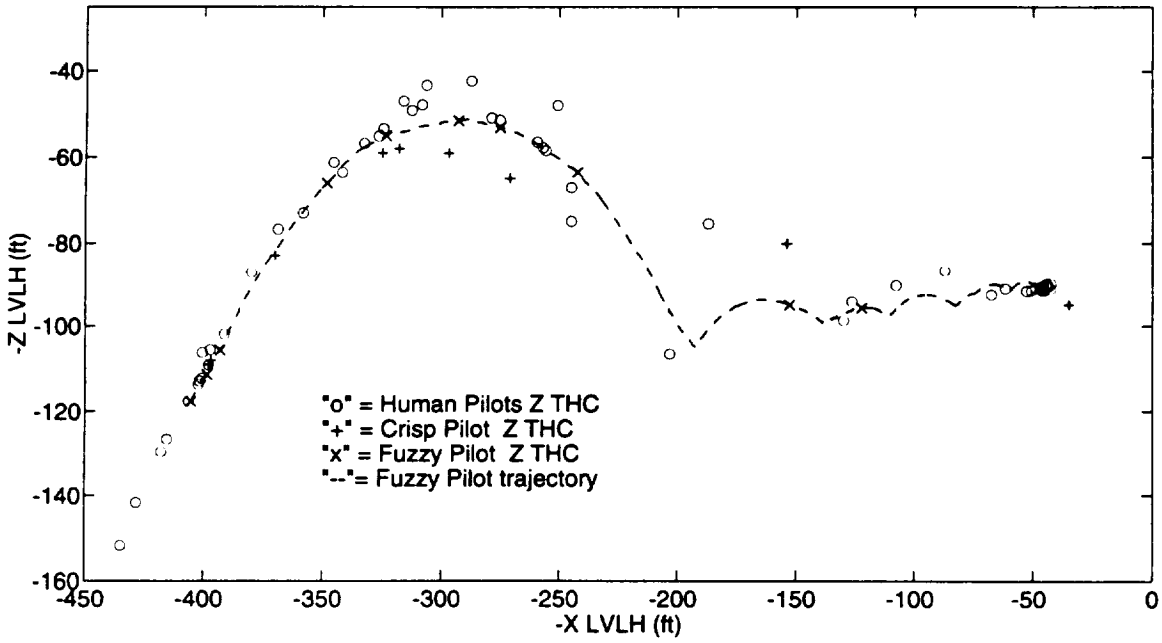

Figure 5-14 Location of the Z THC commands

5.2.3 Total Time, Fuel, and THC Activity

The next evaluation of the pilot models compares their overall performance, in terms of total simulation time, fuel, and THC jet activity, with the average man-in-the-loop values.

The first row of Table 5-1 provides a comparison of the total simulation time for each run, defined as the time to transition from the initial condition to the grapple point at the end of the run. This row shows the four man-in-the-loop runs lasted an average of 1,975 seconds, and had a standard deviation of 254 seconds. The crisp model was 0.6σ below this mean. (This is shown in the $\pm\sigma$ column, which designates the number of man-in-the-loop σ's from the average.) The fuzzy model was only 0.04σ below average.

The second row compares the total fuel consumed, including the firings by both the attitude and translation jets. The crisp model required 13.8 lb. less than the average man-in-the-loop run, which equates to 0.5σ. The fuzzy model, however, was only 2.2 lb. less than average, equating to 0.1σ below the mean.

The third row of Table 5-1 provides a comparison of the total THC activity for each run, measured in seconds of jet on time. This includes only the translation jets. Because the attitude jets are not included, this allows a comparison of the pilots' control activity. These numbers were computed using the jet on times summarized in Table 3-1, which provides a common means for summing Low Z and Norm Z burns, as well as DAP A and DAP B commands from each axis. Once again the fuzzy model is extremely close to the average man-in-the-loop run, only 0.2σ below the mean. However, the crisp pilot was 1.3σ below average, and required less THC jet time than any other run.

The remaining rows in Table 5-1 compare the jet on times and number of different THC burns for each axis. These numbers indicate the fuzzy model is representative of the average human pilot. However, the crisp model differs significantly in the Z axis. It made only 8 +Z commands, and required less Z jet on time than any human pilot. This can explain why the crisp model used considerably less fuel than the average human pilot.

Table 5-1 Comparison of total time, fuel, and THC activity

	Man-in-the-Loop						Crisp Pilot		Fuzzy Pilot	
	1-A	1-B	2-A	2-B	**AVE**	σ	value	±σ	value	±σ
Total Numbers										
Total Time (sec)	2,343	1,838	1,782	1,938	**1,975**	254	1,830	**-.6**	1,966	**-.04**
Total Fuel Consumed (lb.)	286	231	229	245	**247.8**	26.47	234	**-0.5**	245.6	**-.1**
Total THC Jet on Time (sec)	76.64	64.16	62.48	62.72	**66.50**	6.80	57.92	**-1.3**	65.04	**-.2**
X THC PULSES:										
±X THC Jet on Time (sec)	19.36	14.08	12.00	12.48	**14.48**	3.37	13.6	**-0.3**	10.56	**-1.2**
Number of ±X THC Pulses	69	32	63	70	**58.50**	17.93	37	-1.2	40	-1.0
Number of +X THC	52	27	53	67	**49.75**	16.64	30	-1.2	37	-.8
DAP A +X	21	23	6	2	**13.00**	10.55	18	-.5	11	-.2
DAP B +X	31	4	47	65	**36.75**	25.87	12	-1.0	26	-.4
Number of -X THC	17	5	10	3	**8.75**	6.24	7	-.3	3	-.9
DAP A -X	5	5	0	2	**3.00**	2.45	6	1.2	2	-.4
DAP B -X	12	0	10	1	**5.75**	6.13	1	-.8	1	-.8
Y THC PULSES:										
±Y THC Jet on Time (sec)	4.64	2.08	3.68	1.76	**3.04**	1.36	3.36	**0.2**	2.56	**-.3**
Number of ±Y THC Pulses	23	13	21	11	**17.00**	5.89	13	-0.7	10	-1.2
Number of +Y THC	12	9	13	8	**10.50**	2.38	9	-0.6	5	-2.3
DAP A +Y	3	0	1	0	**1.00**	1.41	3	1.4	3	1.4
DAP B +Y	9	9	12	8	**9.50**	1.73	6	-2.0	2	-4.3
Number of -Y THC	11	4	8	3	**6.50**	3.70	4	-.7	5	-.4
DAP A -Y	0	0	0	0	**0**	0	1	N/A	0	0
DAP B -Y	11	4	8	3	**6.50**	3.70	3	-.9	5	-.4
Z THC PULSES:										
±Z THC Jet on Time (sec)	52.64	48.00	46.80	48.48	**48.98**	2.54	**40.96**	**-3.2**	51.92	**1.2**
Number of ±Z THC Pulses	14	14	12	16	**14.00**	1.63	8	-3.7	12	-1.2
Number of +Z THC	12	13	12	13	**12.50**	0.58	**8**	**-7.8**	11	-2.6
Low Z										
DAP A	10	9	9	9	**9.25**	0.50	8	-2.5	10	1.5
DAP B	0	0	0	0	**0**	0	0	0	0	0
Norm Z										
DAP A	0	0	0	0	**0**	0	0	0	0	0
DAP B	2	4	3	4	**3.25**	0.96	0	-3.4	1	-2.3
Number of -Z THC	2	1	0	3	**1.50**	1.29	0	-1.2	1	-.4
DAP A -Z	0	1	0	0	**0.25**	0.50	0	-0.5	0	-.5
DAP B -Z	2	0	0	3	**1.25**	1.50	0	-0.8	1	-.2

5.2.4 Adherence to Piloting Rules and Miss Distance

The last comparison of the different simulations evaluates their adherence to the piloting rules and shows their final miss distance. Each requirement for controlling λ_V, λ_H, and $\dot{R}_L$ is compared in the top two sections of Table 5-2, and the miss distance is compared in the bottom section of this table. There is not a piloting rule for miss distance, but it is measure of performance worthy of comparison, and is therefore included in this table.

The first two sections of Table 5-2 compare the ability of the crisp and fuzzy models to obey the piloting rules with the average human's adherence to the same requirement. All of the runs had fairly similar results relative to the range rate rules. However, when comparing the pilots' adherence to the COAS angle requirements, the crisp model deviated by over 2σ for five of the eight parameters. The worst comparison was a 5σ deviation for the maximum λ_H inside 25 ft. This large difference can be seen on the out-of-plane trajectory plot in Figure 5-9, on page 89. In contrast, the fuzzy pilot was very similar to the man-in-the-loop runs. For two parameters, it deviated 1.5σ from the mean, but for all of the other parameters it was within 0.8σ or less of the average human.

Comparing the pilots' miss distance is slightly more difficult. This distance is defined as the range between the RMS end effector and the grapple point on the Station at the conclusion of the run. For the two software pilot models, the simulation ends when the Shuttle's RMS crosses the plane defined by the Y_{LVLH} and Z_{LVLH} axes. Therefore, both pilot models have 0 miss distance in the X_{LVLH} direction. Unfortunately, the man-in-the-loop runs do not have a well-defined end condition. The human operator simply decides when the Shuttle is close enough, then allows it to drift for approximately three minutes without any jet firings. For all four man-in-the-loop runs, the RMS arm never crosses the YZ plane. There was, therefore, no well-defined end condition based upon time or position. Therefore, the "miss distance" for these runs was taken to be the minimum port-

to-port distance during the entire simulation. Despite these slightly different definitions, both pilot models missed by the about the same distance as a typical human.

Table 5-2 Comparison of adherence to piloting rules and final miss distance

PARAMETER	Rule or Ideal	Man-in-the-loop 1-A	1-B	2-A	2-B	AVE	σ	Crisp Pilot value	±σ	Fuzzy Pilot value	±σ
COAS ANGLES:											
Port-to-Port Range > 25											
Minimum λ_V (deg)	-10	-9.3	-10.8	-11.5	-8.2	**10.0**	1.5	-7	2.0	-9.2	.5
Maximum λ_V (deg)	10	9.6	4.8	3.5	7.2	**6.3**	2.7	-1	-2.6	5.3	-.4
Minimum λ_H (deg)	-10	-5.9	-4.7	-5.6	-4.7	**-5.2**	.6	-8	-4.5	-4.3	1.5
Maximum λ_H (deg)	10	6.4	4.9	6.5	6.4	**6.0**	.8	8	2.5	6.7	.8
Port-to-Port Range < 25											
Minimum λ_V (deg)	-5	.8	-2	-2.2	.9	**-.6**	1.7	-3	-1.4	-1.9	-.7
Maximum λ_V (deg)	5	3.4	3.7	1.4	3.0	**2.9**	1.0	2.5	-.4	2.2	-.7
Minimum λ_H (deg)	-5	-2.3	-3.8	-4.6	-.8	**-2.9**	1.7	-6	-1.9	-.3	1.5
Maximum λ_H (deg)	5	2.2	3.1	.2	2.1	**1.9**	1.2	8	**5.0**	1.5	-.3
RANGE RATE:											
Port-to-Port Range > 100 ft:											
Max neg. deviation from $\frac{-R_L}{1000}$ ($\frac{ft}{sec}$)	-.1	-.27	-.17	-.18	-.13	**-.17**	.03	-.11	1.3	-.15	.6
Max pos. deviation from $\frac{-R_L}{1000}$ ($\frac{ft}{sec}$)	.1	.09	.09	-.04	0	**.04**	.07	.02	-.2	.02	-.2
Port-to-Port Range < 100 ft:											
Min $\dot{R}_L$ (max closure rate) ($\frac{ft}{sec}$)	-.2	-.22	-.2	-.19	-.2	**-.2**	.01	-.2	.6	-.21	-.3
MISS DISTANCE:											
X_{LVLH} (ft)	0	.7	.6	.7	.2	**.6**	.2	0	-2.3	0	-2.3
Y_{LVLH} (ft)	0	-.8	-.9	-.1	-1.5	**-.8**	.6	.7	2.7	-.7	.2
Z_{LVLH} (ft)	0	.5	.5	.2	-.1	**.3**	.3	.2	-.3	.4	.3
Total (RMS) Miss Distance (ft)	0	1.2	1.2	.7	1.5	**1.2**	.3	.7	-1.4	0.8	-1.1

5.3 CONCLUSIONS

In summary, the six degree-of-freedom fuzzy pilot was created by adding additional logic to the three DOF model. This new logic was based upon a simple technique used by human pilots. The model does not make X burns when the Shuttle's pitch rate is *High*, and it does not make Y burns when the roll rate is *High*.

The resulting fuzzy pilot model performs very well. It no longer overcontrols with X or Y THC commands. As a result, the fuzzy model flew a very average trajectory when compared with the four man-in-the-loop runs from the same initial condition. The locations of the THC commands were also similar to the human pilots' results. In addition, the fuzzy model's overall approach time, fuel, and THC activity was extremely close to the average values for the man-in-the-loop runs. Finally, the fuzzy model and man-in-the-loop runs were very similar when comparing their adherence to the piloting rules, and their final miss distance. These comparisons demonstrate the fuzzy model's ability to match an "average" human pilot.

On the other hand, the crisp pilot model is not as "average" and has more abrupt control responses than a human pilot. This abrupt control is a result of the sudden transitions between $\mu = 0$ and $\mu = 1$ inherent with crisp logic. As a result, the crisp model suddenly transitions from a state that does not require a THC burn, to one that does. In contrast, because the fuzzy pilot model can easily combine conflicting conclusions from several rules, it has a very gradual transition between the pilot's actions and inactions. This is much more similar to a human pilot, and demonstrates one of the benefits of fuzzy logic.

Chapter 6 : Modeling Different Piloting Techniques

6.1 Overview

It is not sufficient that a pilot model is able to duplicate an "average" human's performance. It should also be capable to matching extreme pilots whose performance deviates significantly from the norm. These are the individuals that define the spectrum of potential pilots, and will likely create the greatest plume forces on the Station. Therefore, the fuzzy model should allow the *Average* pilot to be adjusted slightly, so it can model different, individual techniques.

This chapter demonstrates the fuzzy model's ability to mimic different piloting techniques. These techniques are not the result of a unique decision process, but are due to different individual definitions for "λ_r is *Large Positive*", "$\dot{\lambda}_r$ is *Small Positive*", etc.. Therefore, the pilot model can adjust these fuzzy sets to capture different techniques without adding any additional logic. To demonstrate this ability, two extreme techniques are modeled by varying the membership functions for $\dot{\lambda}_r$ and λ_r. For each technique, the new fuzzy sets are explained, and the resulting trajectory is compared with the appropriate man-in-the-loop run.

6.2 Modeling Two Extreme Piloting Techniques

6.2.1 Identifying Extreme Piloting Techniques

The most significant difference among the four man-in-the-loop runs is evident by the plots of their center of mass, in-plane trajectories and their vertical COAS angles. Pilot number 2 flies the two "highest" approaches, while Pilot 1 allows the Shuttle to drop considerably "lower". These different approaches are shown again in Figure 6-1 and Figure 6-2. Run 2-A and 1-A represent the two extreme techniques that are captured by the fuzzy pilot model. They will be referred to as the *High* technique and the *Low* technique.

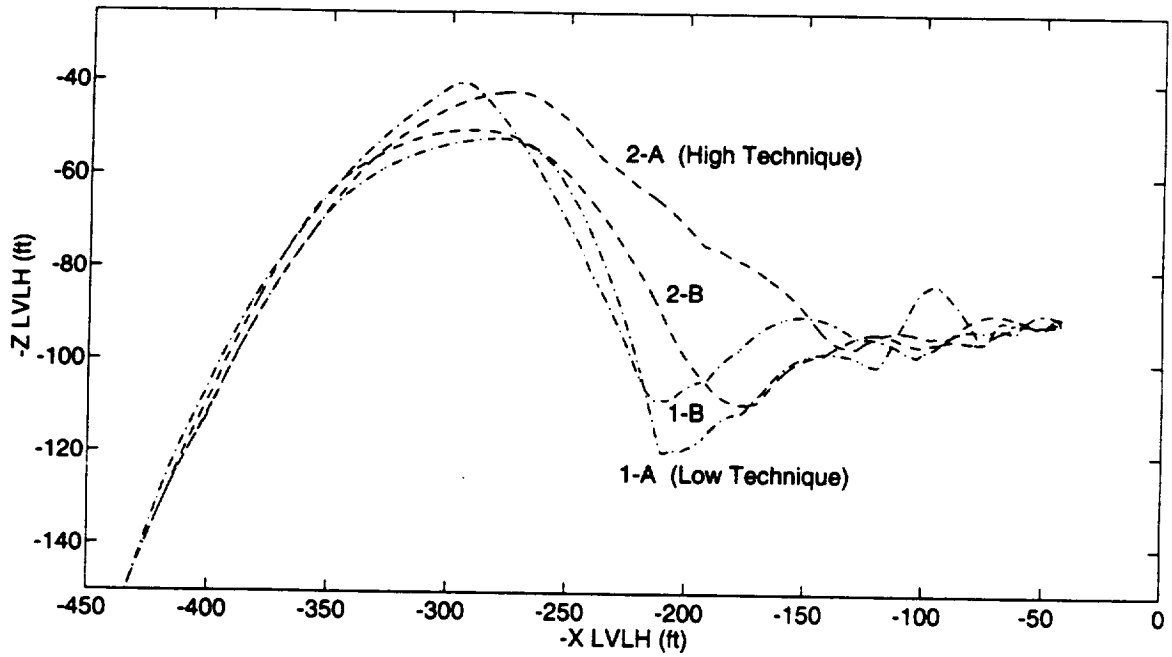

Figure 6-1 Center of mass, in-plane trajectories for the *High* and *Low* techniques

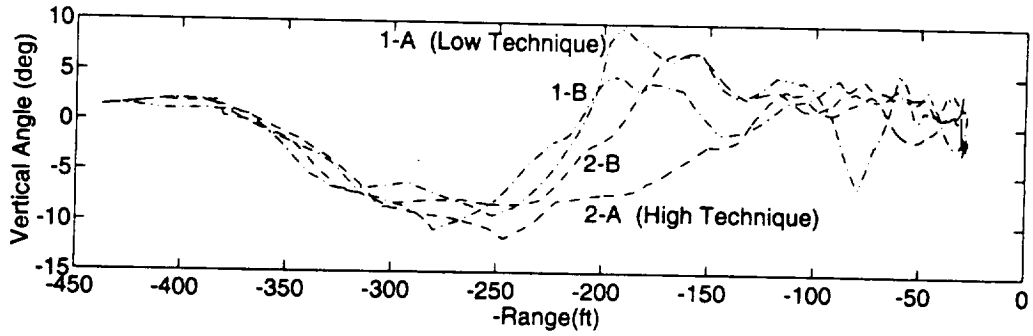

Figure 6-2 Vertical COAS angles for the *High* and *Low* techniques

Only two membership functions are changed to match these different techniques. To model the *Low* technique, $\mu(\lambda_V|R_L \text{ is } Large)$ and $\mu(\dot{\lambda}_V)$ are modified. To capture the *High* technique only $\mu(\dot{\lambda}_V)$ is adjusted. As a point of reference, Figure 6-3 shows these two membership functions used by the *Average* fuzzy pilot in Chapters 4 and 5. This chapter compares these sets with the new fuzzy sets that define the *High* and *Low* techniques.

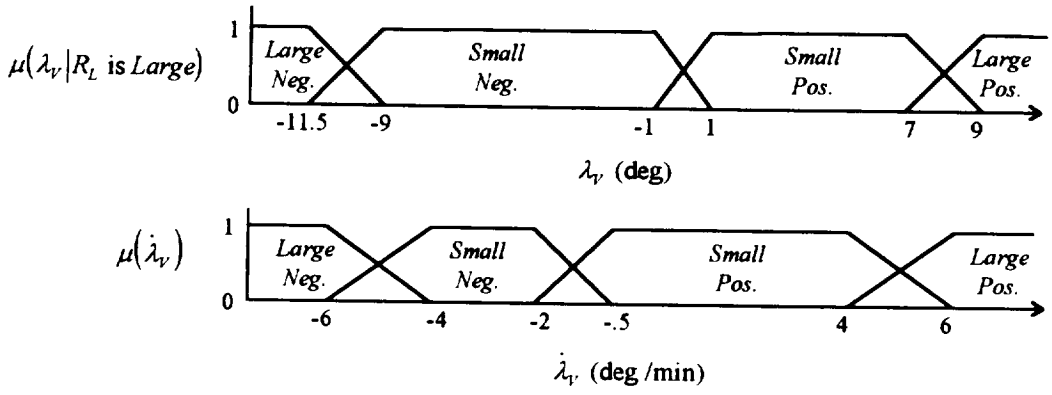

Figure 6-3 Fuzzy sets for λ_V and $\dot{\lambda}_V$ defining the *Average* technique

C-2

6.2.2 Modeling the *Low* Technique

The most significant difference with Run 1-A is the pilot does not react as quickly to the Shuttle losing altitude ($\dot{\lambda}_V > 0$) and allows the Shuttle to drop very low ($\lambda_V > 0$). This is the result of a higher individual threshold for "λ_V is *Large Positive*", "$\dot{\lambda}_V$ is *Small Positive*", and "$\dot{\lambda}_V$ is *Large Positive*". In addition, for this particular run, Pilot 1 does not allow the Shuttle to go as high on the first hop, which reflects a higher individual threshold for "λ_V is *Large Negative*".

As a first-order approximation, the four pairs of numbers defining the fuzzy boundaries for these four sets were increased, moving the sets to the right. The amount of change from the *Average* pilot model was based upon engineering judgment and observation of the trajectory from Run 1-A. Then, through approximately five more iterations, these fuzzy boundaries were modified slightly to closely match the *Low* approach. These modifications were also based upon engineering judgment, and comparison of the trajectories from the fuzzy model and Run 1-A. The resulting membership functions are shown in Figure 6-4. The four number pairs that differ from the *Average* pilot model are shown in large bold type along the abscissa.

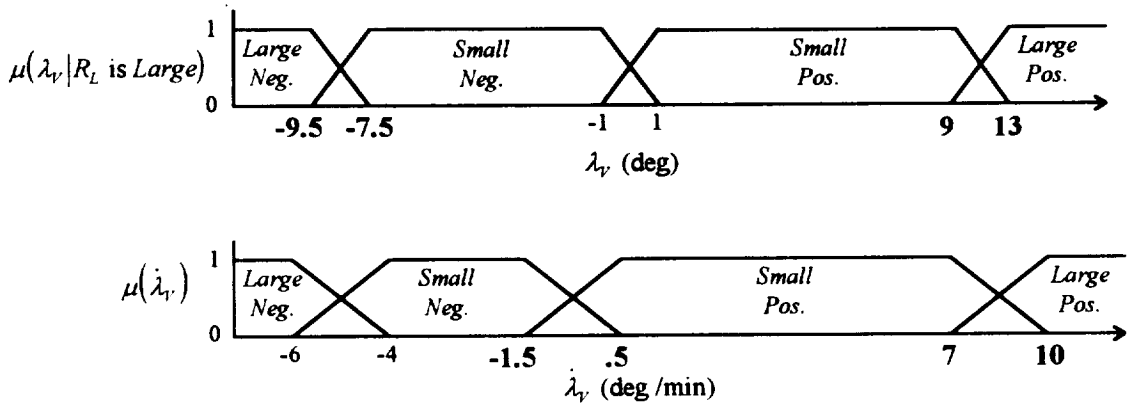

Figure 6-4 Fuzzy sets for λ_V and $\dot{\lambda}_V$ defining the *Low* technique

In some cases, when modeling relatively abrupt pilot transitions, the iterative process resulted in crisper boundaries between sets (the pair of numbers defining a boundary are closer together). For example, the boundary between "λ_V is *Large Negative*" and "λ_V is *Small Negative*" spans only 2 , from -9.5 to -7.5 . However, for the *Average* pilot this same boundary spanned 2.5 . In other cases, the new set boundaries are slightly fuzzier than the *Average* pilot, which models a more gradual control response from Pilot 1 in that particular operating region.

These new fuzzy definitions result in the in-plane trajectory shown in Figure 6-5. This figure compares the trajectories from the fuzzy pilot model and Run 1-A, showing both trajectories and the location of their X THC commands. These trajectories are very similar. Perhaps more importantly, the fuzzy model makes the X burns in the same general location as the human pilot. Also notice, neither pilot applies a +X burn to reduce $\dot{\lambda}_V$ as they are coming down from the first hop. This is a unique characteristic of the *Low* technique.

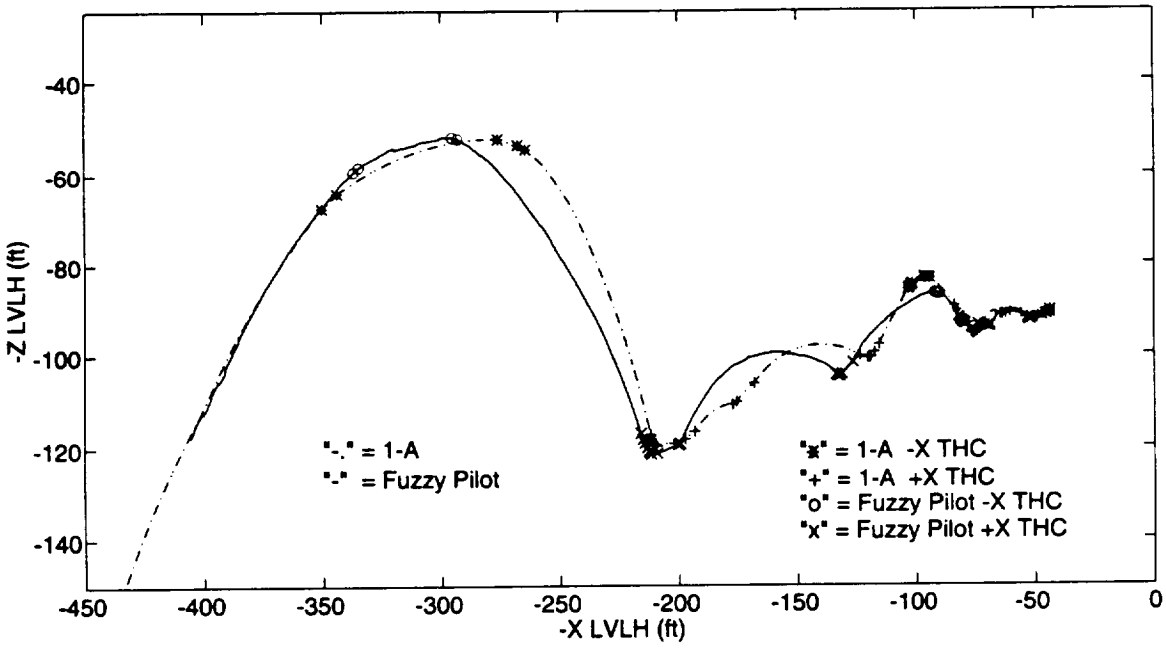

Figure 6-5 Center of mass, in-plane trajectories for the *Low* technique

Figure 6-6 gives a comparison of λ_V as a function of $-R_L$ for the fuzzy model and Run 1-A. These plots are also very similar and further demonstrate the fuzzy model's ability to match the *Low* technique.

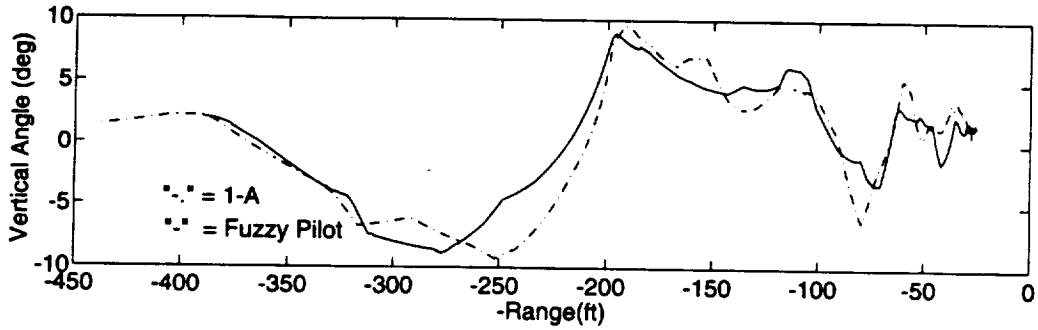

Figure 6-6 Vertical COAS angle for the *Low* technique

Because only the parameters affecting the X axis were adjusted for this demonstration, other comparisons between these two runs are somewhat irrelevant and are not included. For example, parameters used to control $\dot{R}_L$ with ±Z THC pulses were not changed. Because +Z burns require significantly more jet time and fuel than other burns, the *Low* pilot model uses essentially the same total THC jet on time and fuel as the *Average* pilot model.

6.2.3 Modeling the *High* Technique

In contrast to the *Low* technique, which does not make any +X burns to reduce $\dot{\lambda}_V$, the *High* technique makes a number of +X commands to slow $\dot{\lambda}_V$ when coming "down" from the first hop. This technique results in a very gradual descent, and is modeled by reducing the pilot's threshold for "$\dot{\lambda}_V$ is *Large Positive*". The *High* technique also does not make as many -X burns as the Shuttle approaches the top of the first hop. This characteristic is captured by reducing the threshold for "$\dot{\lambda}_V$ is *Large Negative*". Figure 6-7 shows these changes to the membership function for $\dot{\lambda}_V$. Again, the numbers on the abscissa that have

been changed are shown in large bold type. All other parameters are identical to the *Average* fuzzy pilot model, presented in Chapters 4 and 5.

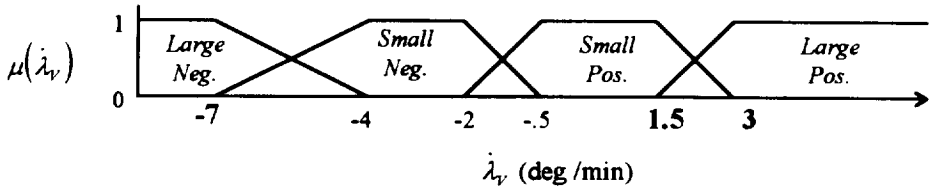

Figure 6-7 Fuzzy sets for $\dot{\lambda}_V$ defining the *High* technique

Figure 6-8 shows the resulting in-plane trajectory. Both pilots fly a very similar approach, and make a number of +X burns between 250 and 150 ft on the x axis. These burns reduce $\dot{\lambda}_V$ and result in a higher approach trajectory. Figure 6-9 compares the vertical COAS angles for the same two runs. These plots are also very similar varying by at most two or three degrees.

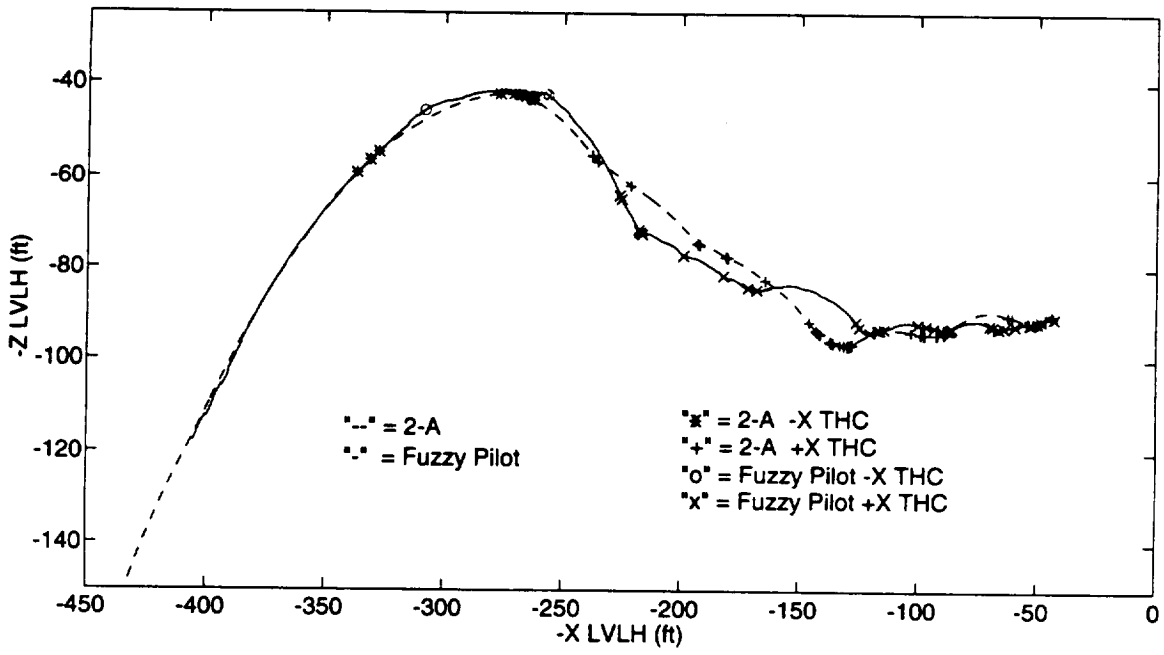

Figure 6-8 Center of mass, in-plane trajectories for the *High* technique

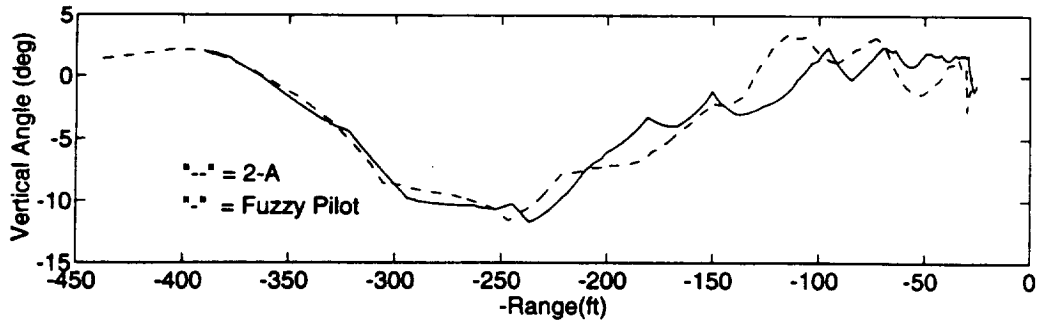

Figure 6-9 Vertical COAS angle for the *High* technique

6.3 CONCLUSIONS

This chapter demonstrates the fuzzy model's ability to emulate different individual piloting techniques, which is an important requirement for any proposed pilot model. It is particularly important to identify and model the extreme piloting techniques. These techniques define the range of potential pilots, and will likely determine the maximum plume loads on the Station. After modeling the extreme piloting techniques, a methodology for varying the model's parameters over many runs could be designed to statistically match the performance of a broad spectrum of human pilots.

As a demonstration of the fuzzy pilot's ability to model different techniques, a relatively *High* and *Low* approach were "duplicated". These different techniques did not require additional logic, but were modeled using new definitions for fuzzy terms such as "λ_y is *Large Negative*", "$\dot{\lambda}_y$ is *Large Positive*", etc.. The fuzzy model did a very good job of matching these extreme techniques. The trajectories were similar, and the THC commands were in the same general location as the man-in-the-loop runs. This was accomplished by changing only two membership functions used by the fuzzy pilot. When comparing their in-plane orbital motion, these simulations were certainly much closer than

any of the other man-in-the-loop runs, including one by the same pilot. This demonstrates that a straight forward process of selecting the fuzzy model's parameters provides the means to accurately model a spectrum of potential human pilots.

Chapter 7 : Evaluating the Fuzzy Pilot from a Number of Initial Conditions

7.1 Overview

Up to this point, the fuzzy pilot model has been tested from only one initial condition. This raises the logical question, "Does the model respond well from a number of different initial conditions, without being readjusted for each run?". This chapter answers this question, evaluating the fuzzy pilot from eight different initial conditions using the exact same fuzzy set definitions. The model's performance is compared with Pilot 2's results from the same initial conditions.[1] This comparison shows the fuzzy model does respond well, displaying human characteristics from a number of different conditions.

This study also provides insight into the variability of individual human pilots. Because the parameters used by the fuzzy pilot remain constant, the techniques modeled do not change. Therefore, the model provides a set of control runs against which the man-in-the-loop simulator data can be compared. This comparison shows the extent a

[1] This constitutes all of Pilot 2's simulations to this particular Station configuration. Because other pilots did not use these same initial conditions, results are only compared with one human pilot.

human pilot's techniques vary between different runs. After matching one run by the human pilot, variations between subsequent runs by the fuzzy model and the human pilot may be attributed to variabilities in the human's techniques.

Unfortunately, these eight runs could not be performed using the same fuzzy sets from Chapters 4 and 5. Those sets were used to model an average human pilot flying to Station Configuration 4, using a piloting rule that defined an approach corridor with COAS angles up to ±10°. Because NASA's database does not include any other runs to SC-4, this chapter compares the pilot model with man-in-the-loop runs to SC-2. These simulations were created using a new requirement that only allows COAS angles of up to ±8°. Therefore, one run by Pilot 2 was used to adjust the fuzzy pilot and determine the new fuzzy sets necessary to model this piloting rule. Then seven more simulations were performed from different initial conditions using the exact same fuzzy sets.

The chapter describes the changes necessary to model the human pilot when flying with a smaller approach corridor. The aggregate results from the pilot model are compared with the aggregate results by Pilot 2 to SC-2 using the same eight initial conditions. These comparisons are identical to those made in Chapter 5, with some additional analysis of the model's THC frequency response. Following these results, some conclusions are made about the fuzzy pilot model.

7.2 Modifications to Fly a Smaller Approach Corridor

7.2.1 New Sets for the X THC Decision Logic

Almost all of the necessary changes to the fuzzy pilot model affect the translation burns in the X_{Body} axis. Using the old piloting rule, pilots often reached the limit for the vertical COAS angle, allowing $|\lambda_V| \approx 10°$. Although the new piloting rule is not a significant

change, pilots almost never get close to the limit of $|\lambda_V| = 8°$. Instead, they generally stay within $|\lambda_V| \leq 5°$. Because this is a significant difference, the functions for $\mu(\lambda_V | R_L \text{ is } Large)$ and $\mu(\dot{\lambda}_V)$ were adjusted by reducing the magnitude of the numbers along the abscissa. These new membership functions are shown in Figure 7-1. The numbers that differ from the *Average* pilot model in Chapters 4 and 5 are shown in large bold type. Because the human pilots' performance for *Small* ranges is similar to the previous runs, $\mu(\lambda_V | R_L \text{ is } Small)$ and $\mu(R_L)$ were not modified.

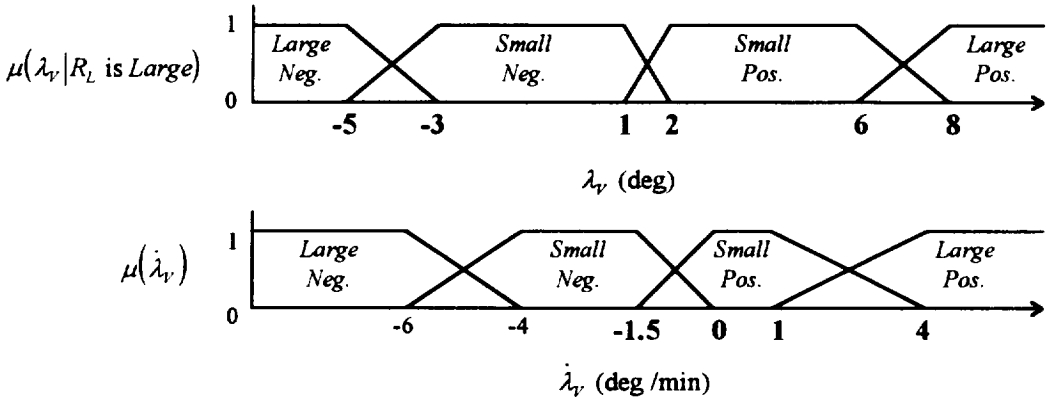

Figure 7-1 New fuzzy sets for λ_V and $\dot{\lambda}_V$

The crisp conclusions, determining the required X burn sizes were also changed slightly. Because of the smaller approach corridor, human pilots are not as inclined to make large +X corrections. Therefore, all of the model's conclusions specifying +X burns were reduced slightly. However, flying this smaller approach corridor, human pilots do make -X commands very quickly to reduce $|\dot{\lambda}_V|$ as the Shuttle approaches the top of the first hop. As a result, the burn size required when "λ_V is *Small Negative* and $\dot{\lambda}_V$ is *Large Negative*" was increased in magnitude. These changes are shown on the vertical COAS phase plane in Figure 7-2. This phase plane is similar to those in Chapter 4. The required burn sizes are shown in each grid, and the gray areas indicate where the fuzzy sets overlap. The changes from the previous pilot model are shown in bold type.

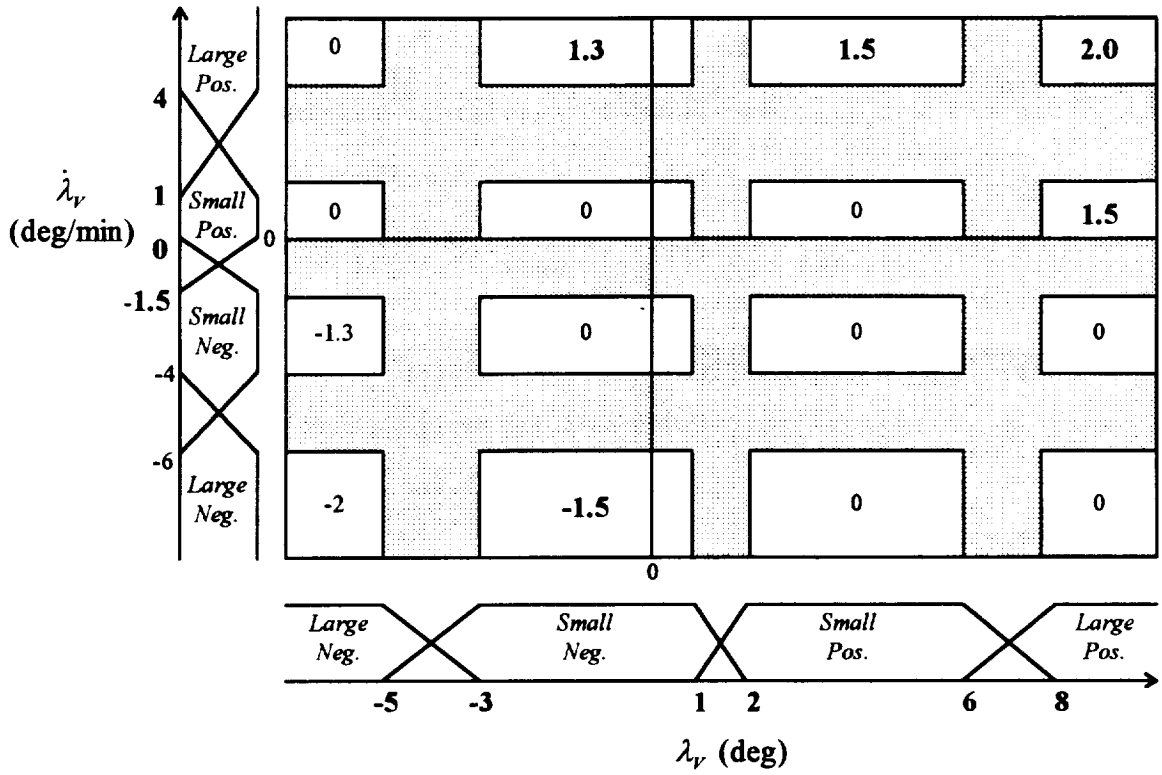

Figure 7-2 New X THC burn size for *Large* ranges

To reduce the possibility the pilot model would overcontrol with successive X burns, it was also necessary to make a small change to the membership function for the Shuttle's pitch rate, $\dot{\theta}$. The previous limits defined a pitch rate to be completely *High* if the attitude rate with respect to the LVLH frame had a magnitude greater than $4.5\frac{\text{deg}}{\text{min}}$. It was completely *Low* if the rate was less than $1.5\frac{\text{deg}}{\text{min}}$. For a few sample runs to SC-2, these values still resulted in too many successive X burns by the pilot model. Therefore, the parameters were reduced slightly to $4\frac{\text{deg}}{\text{min}}$ and $1\frac{\text{deg}}{\text{min}}$ respectively. Figure 7-3 shows these new fuzzy sets for pitch rate. To be consistent with the universal pointing display, which presents inertial attitude rates, the function accounts for the pitch rate bias of $-0.067\frac{\text{deg}}{\text{sec}}$ due to the rotating LVLH frame. Figure 7-3 also uses units of $\frac{\text{deg}}{\text{sec}}$, which conforms with the universal pointing display.

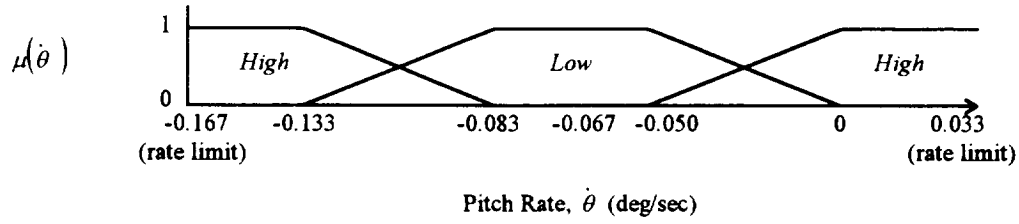

Figure 7-3 New fuzzy sets for inertial pitch rate

7.2.2 New Sets for the Y THC Decision Logic

Because the previous pilot model already flew a relatively small approach corridor in the horizontal axis, there is only one change required that affects the model's Y THC burns. This minor change makes the membership function for the Shuttle's roll rate identical the new membership function for pitch rate, with one exception. Because the LVLH rotation rate is purely about the Shuttle's pitch axis, the membership function for inertial roll rate does not have a bias term. It is therefore symmetric about zero. This membership function is depicted graphically in Figure 7-4.

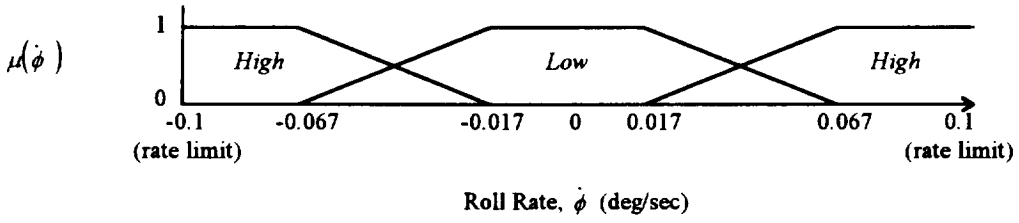

Figure 7-4 New fuzzy sets for inertial roll rate

7.2.3 New Sets for the Z THC Decision Logic

Only two modifications are needed for the fuzzy sets used by the Z THC decision logic. Both changes allow a slightly slower approach. Instead of defining R_L to be completely *Large* outside 300 ft, it is now completely *Large* outside 350 ft. In addition, for *Medium*

ranges the parameters defining a *Fast* approach are decreased slightly in magnitude. These two changes, shown in bold type in Figure 7-5, allow the pilot model to closely match the man-in-the-loop data to SC-2. The functions for $\mu(\dot{R}_L|Large)$ and $\mu(\dot{R}_L|Small)$ remain the same as the previous model, for runs to SC-4.

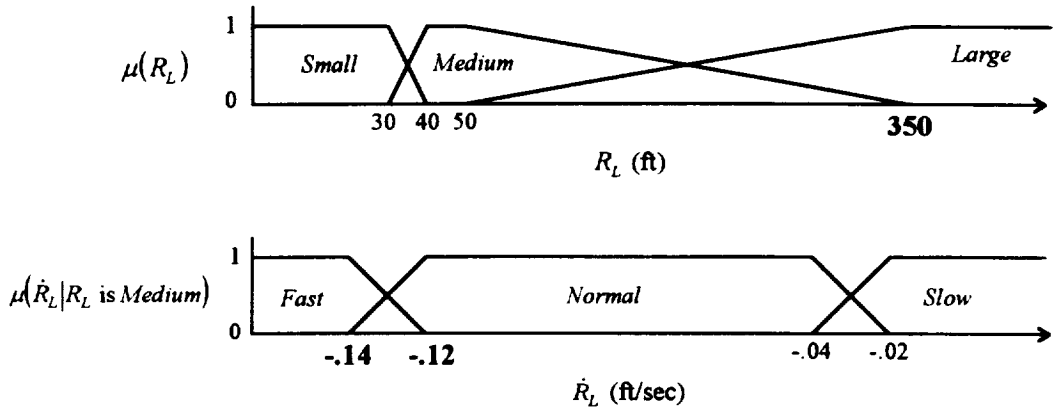

Figure 7-5 New fuzzy sets for R_L and $\dot{R}_L$ for the Z axis

7.2.4 Selection of DAP mode and Low Z/Norm Z Transition

The fuzzy model presented in Chapters 4 and 5, for approaches to SC-4, switched from Low Z to Norm Z once inside $R_L = 100$ ft. This point corresponds to the requirement for no Norm Z burns outside $R_P = 75$ ft. The transition from DAP A to DAP B was also made based on this threshold. The pilot model uses these same numbers when flying the eight runs to SC-2, with two slight modifications.

The first change, adds a small standard deviation of five feet to this transition point. This models the slight variability associated with a human operator. The second modification adds some simple logic to determine when it is acceptable to switch to DAP B. The new model will only select DAP B mode if R_L is less than the transition point, and the total output specifying the burns for the X and Y axes is 0. This prevents the fuzzy pilot from switching DAP modes right before a DAP A burn might be commanded; then

immediately making a number of successive, smaller DAP B burns. Instead, once inside the transition point, if the model is about to make a burn in DAP A mode, the transition to DAP B is delayed. Once the DAP A burn is complete or no longer anticipated, the model then switches to DAP B mode. This new logic is more consistent with the man-in-the-loop data, and only affects the model's performance if the Shuttle is near the edge of the COAS corridor when $R_L \approx 100$ ft. This situation did not occur for any of the previous OFS simulations, but it did happen in a few sample OFS runs to SC-2. Therefore, the new logic was added to prevent multiple DAP B burns immediately after switching DAP modes.

7.2.5 Frequency of THC Burns

One final change to the fuzzy model was necessary to produce a THC frequency response similar to a human pilot. The original model skipped one cycle after a THC command, thus waiting 1.92 seconds before deciding if another burn was necessary. For a large sample of runs, this would result in a disproportionate number of translation burns that were approximately two seconds apart. Very few burns would be three or four seconds apart, and absolutely no burns would be within one second of each other. This distribution of THC commands is not typical of the human pilot tendencies observed in the man-in-the-loop data, and real pilots do not consistently wait 1.92 seconds after making a THC burn. Therefore, a Gaussian distribution is added to model the short wait time after a THC command before re-evaluating the Shuttle's state. This wait time has a mean of three seconds and a standard deviation of one second. The small variance allows the pilot model's frequency response to be more similar to a human's response.

7.3 RESULTS

The modifications outlined in the previous section were based upon iterations attempting to match just one of Pilot 2's runs. Using these identical fuzzy set boundaries, all eight runs by Pilot 2 to SC-2 were flown by the pilot model. This section compares these aggregate results from the human pilot and the fuzzy model in five general areas. The first four comparisons are identical to those made in Chapter 5. The fifth comparison analyzes the model's frequency of THC commands along each axis. These five categories are listed below:

1. Trajectories and pilot sensory data
2. Location of THC commands
3. Total time, fuel consumed, and THC activity
4. Adherence to the piloting rules and final miss distance
5. Frequency of THC commands

7.3.1 Trajectories and Pilot Sensory Data

The two graphs on page 120 compare the center of mass, in-plane trajectories from the man-in-the-loop data and the fuzzy pilot model. Page 121 compares their out-of-plane trajectories, and page 122 compares their range rate vs. range profiles. Because each simulator stored different data, the range rate plots for the man-in-the-loop runs show the exact value of $\dot{R}_L$, without any noise, and the plots for the fuzzy model show the filtered value for $\dot{R}_L$. The final sensory comparison, on page 123, shows their vertical and

horizontal COAS angles as a function of range. For all of these plots, the fuzzy model used the same eight initial conditions as the human pilot.[1]

These comparisons show the fuzzy model does perform well from a number of initial conditions, without being adjusted. It handles all eight initial conditions in a very similar manner as the human pilot. The trajectories are typical of the man-in-the-loop data, and the sensory information, supplied by the laser and COAS, also compares well with the simulations by the human. However, there are some differences that were expected.

Because the fuzzy pilot's parameters were held constant, the model flew all eight runs using the exact same techniques. As a result there is less variability with the fuzzy model than with the eight man-in-the-loop runs. This difference is evident on a few plots, but it is most noticeable when comparing their vertical COAS angles on page 123. Notice, the fuzzy pilot is extremely consistent between 200 and 40 feet. Over this range, there is a well-defined line below which the Shuttle never descends, and λ_V never gets above this line. In contrast, the human pilot varies considerably more, and on one occasion lets $\lambda_V > 9$. This consistency of the fuzzy model was expected because it used the exact same parameters for all eight runs. Despite this difference, the fuzzy model did perform well, and exhibited average human performance characteristics for all of the initial conditions.

[1] The initial conditions may appear to be slightly different, because the pilot model does not begin storing data for plots until approximately 80 seconds into the run. Despite the different appearance, the simulations do begin at the same initial conditions.

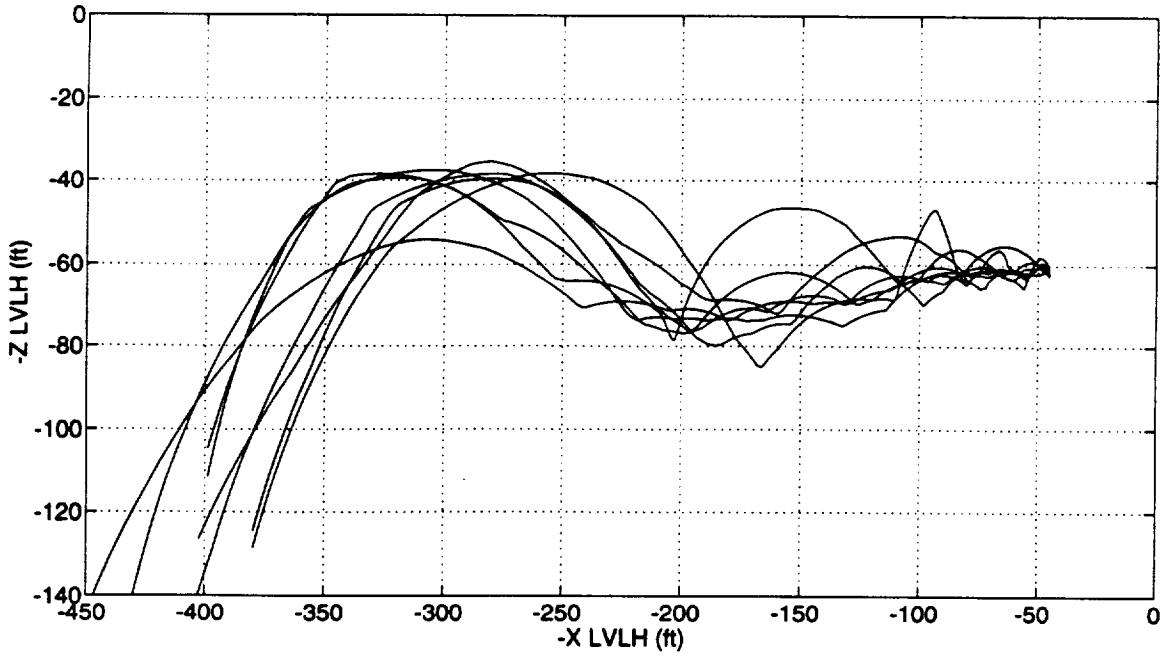

Figure 7-6 Man-in-the-loop, center of mass, in-plane trajectories

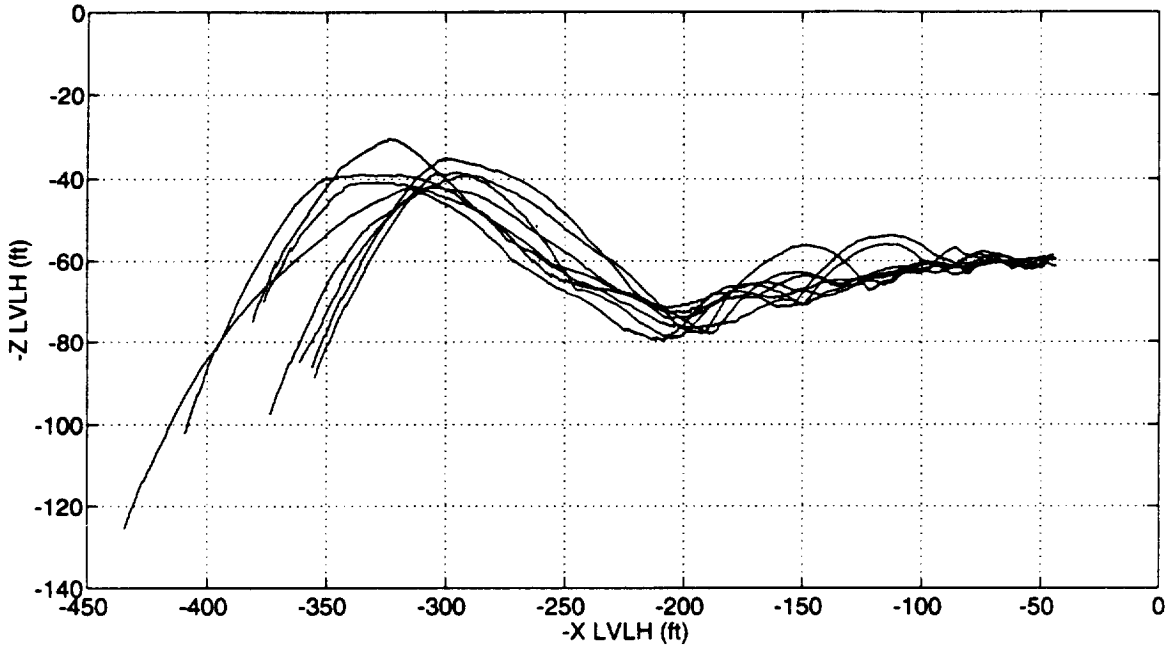

Figure 7-7 Fuzzy model, center of mass, in-plane trajectories

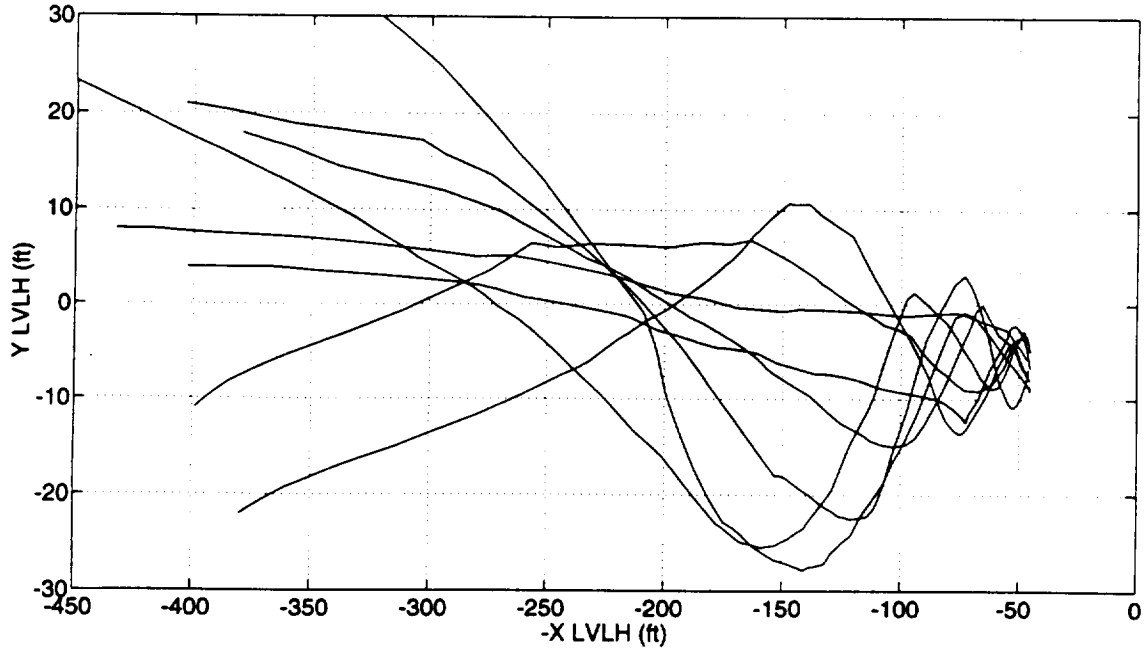

Figure 7-8 Man-in-the-loop, center of mass, out-of-plane trajectories

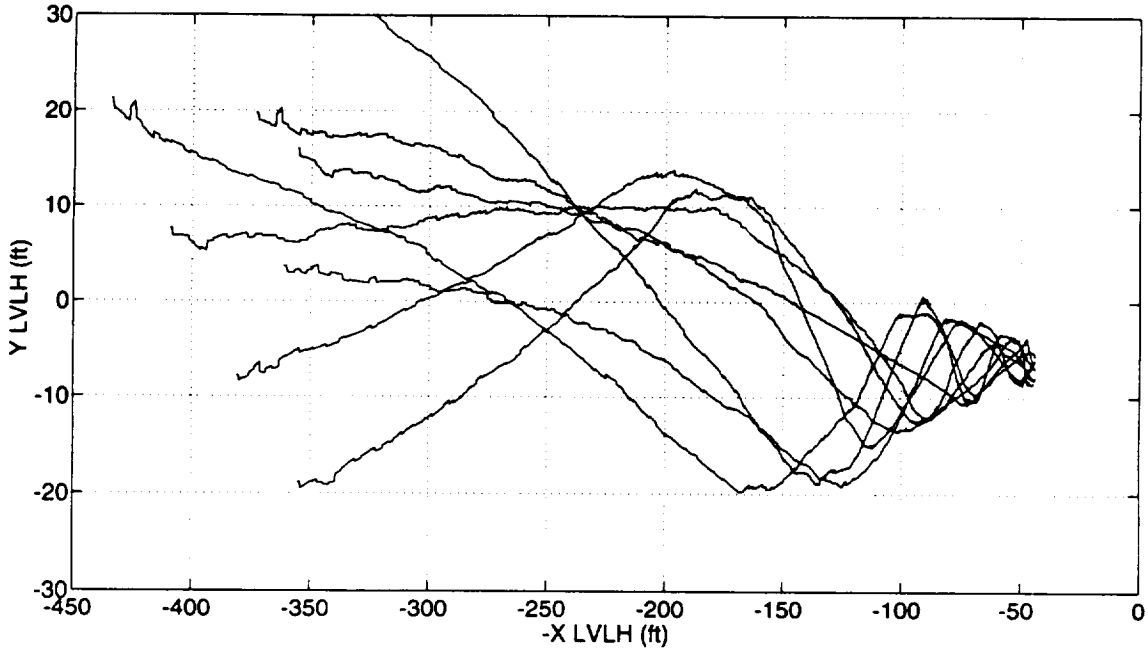

Figure 7-9 Fuzzy model, center of mass, out-of-plane trajectories

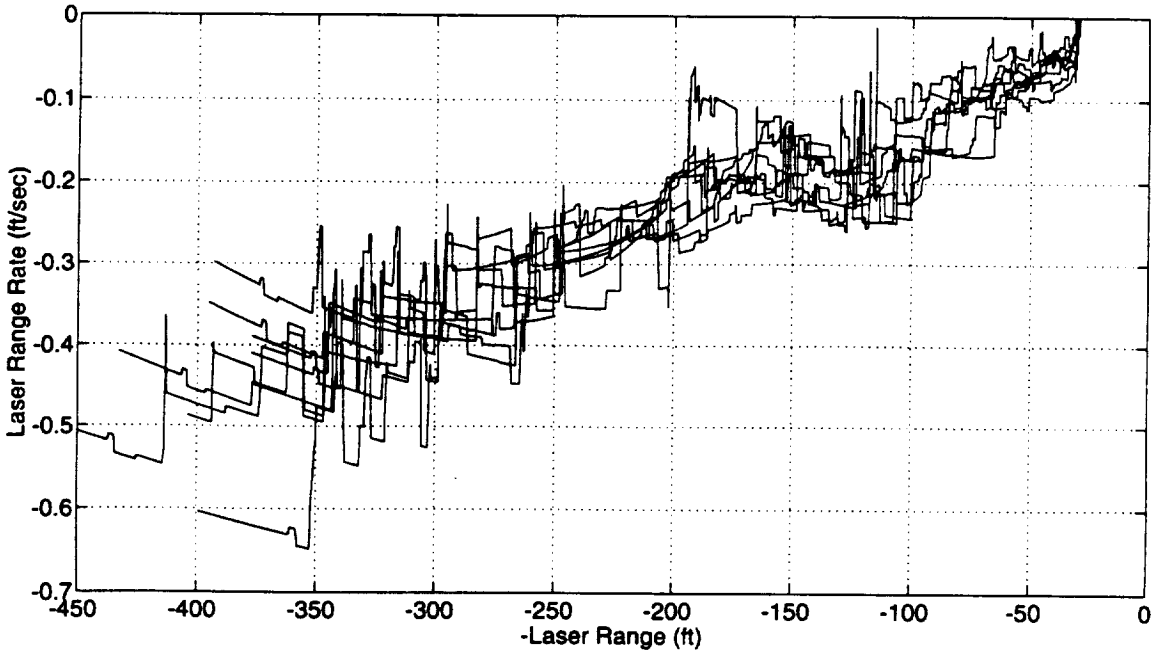

Figure 7-10 Man-in-the-loop range rate vs. range profiles

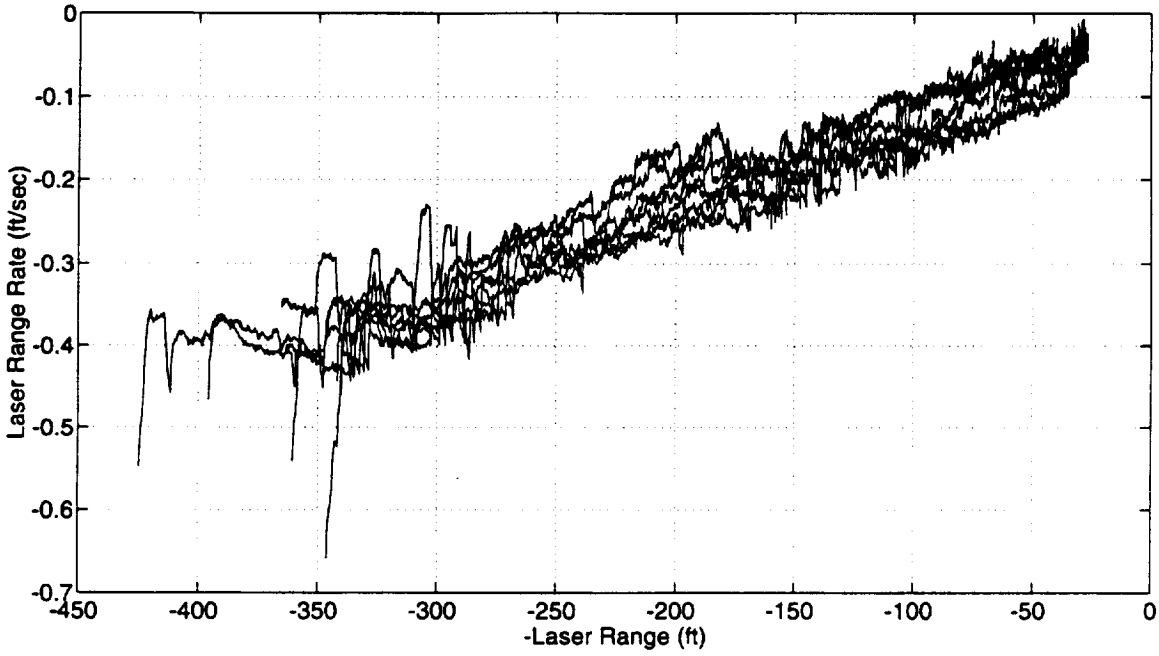

Figure 7-11 Fuzzy model range rate vs. range profiles

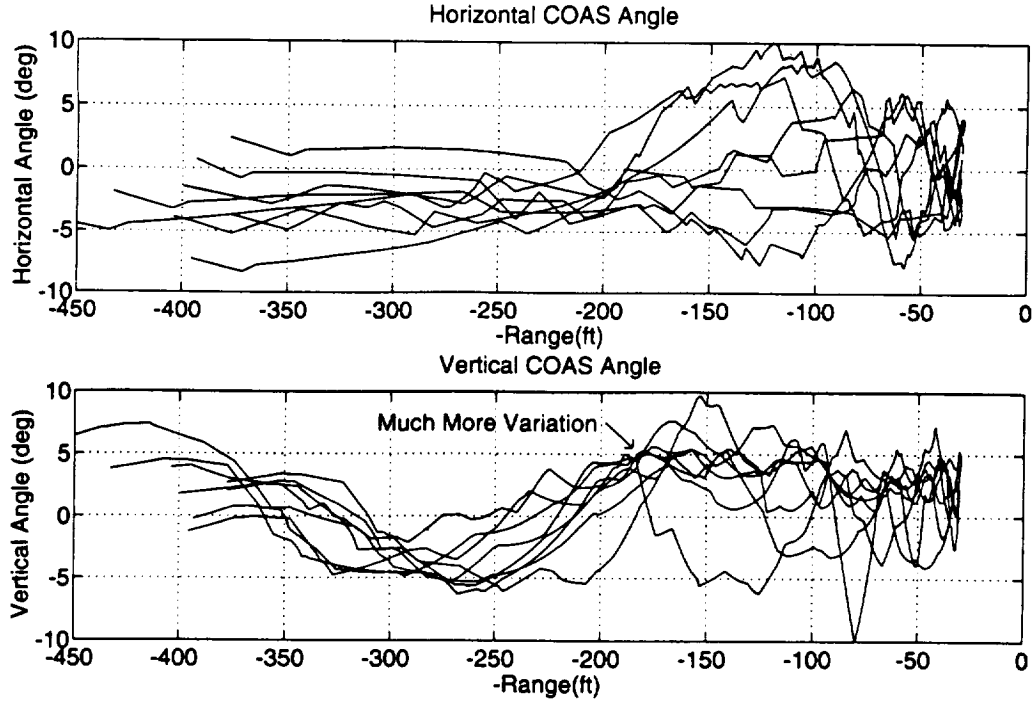

Figure 7-12 Man-in-the-loop COAS angles

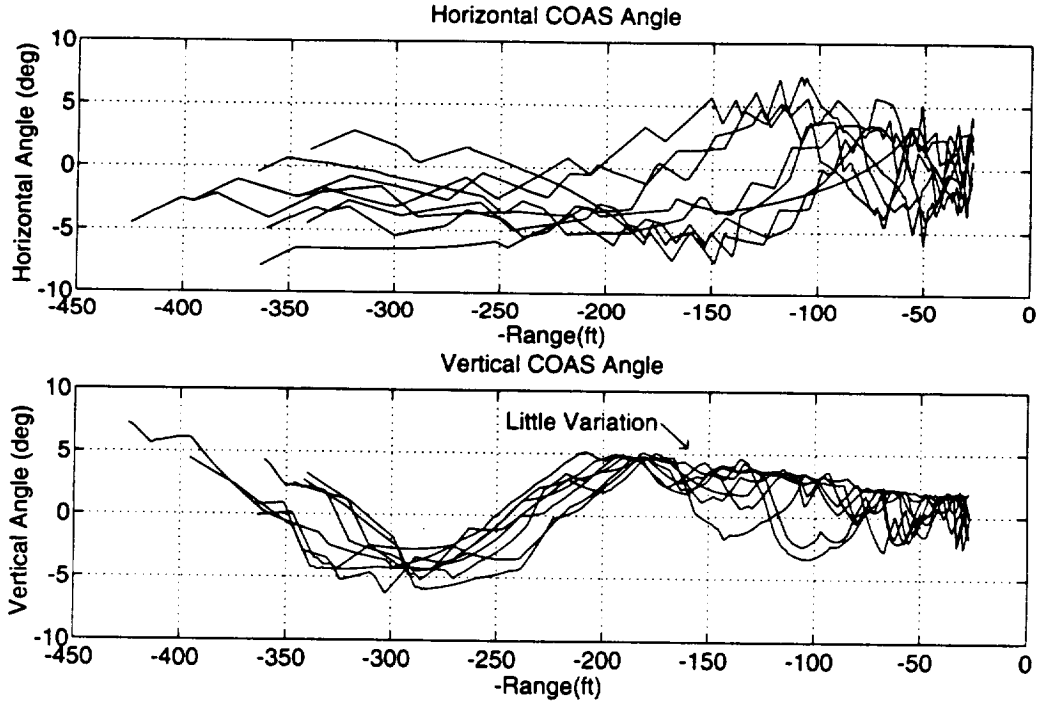

Figure 7-13 Fuzzy model COAS angles

7.3.2 Location of THC Commands

The next three plots compare the location of all the X, Y, and Z THC burns by the fuzzy pilot model and the human pilot. For each plot, the human's THC commands are indicated by an "o", and the fuzzy pilot's commands are indicated with a "+". All three of these plots show the fuzzy model's burns are in the same location as a majority of the burns made by the human pilot. The only notable difference is the human pilot's X THC commands span slightly more space than the X burns made by the fuzzy pilot. This difference is most likely a result of the consistency of the fuzzy model, discussed previously. If the fuzzy sets were statistically varied, the model would be more similar to a real human pilot. However, the purpose of this chapter is to demonstrate the fuzzy model's ability to handle a number of initial conditions, using the same parameters for each run. This results in the same techniques for each simulation, which produces average results when compared to a number of man-in-the-loop runs.

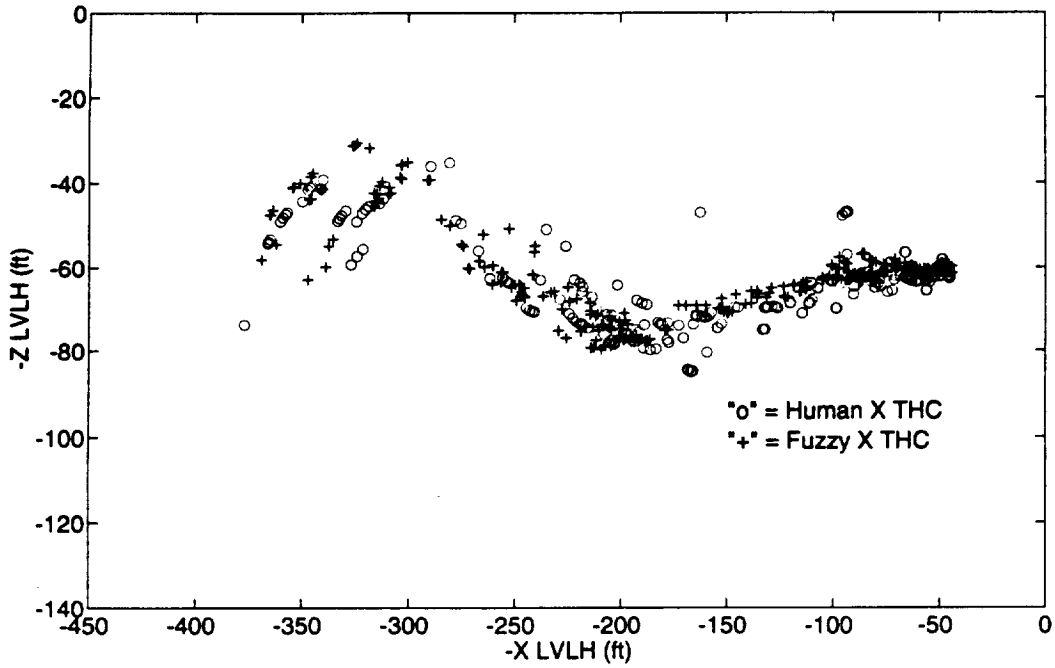

Figure 7-14 Location of the X THC commands

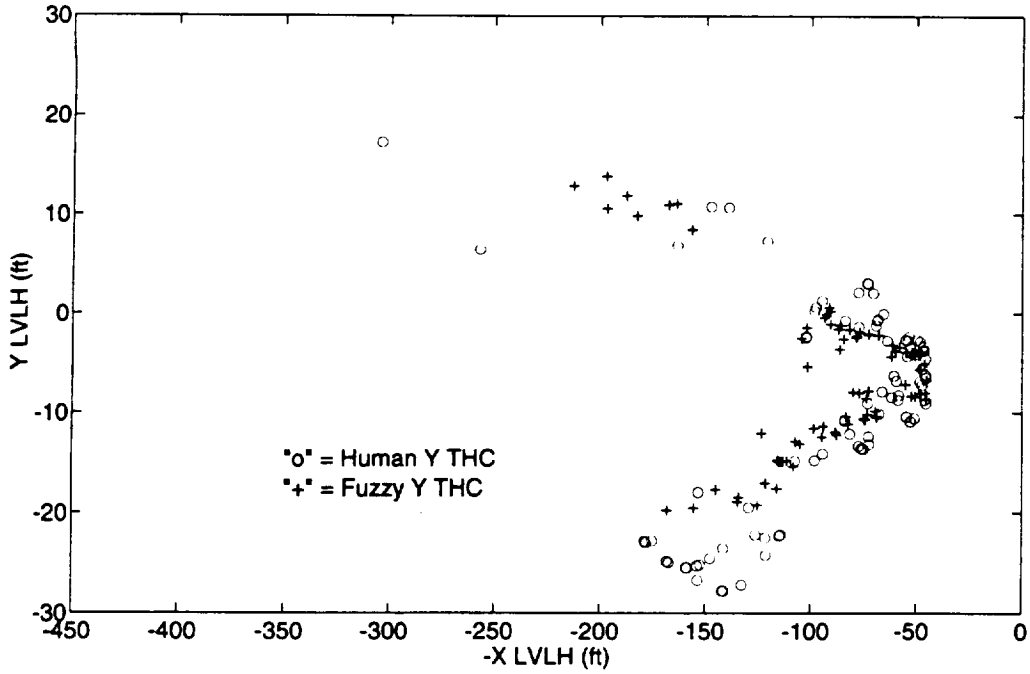

Figure 7-15 Location of the Y THC commands

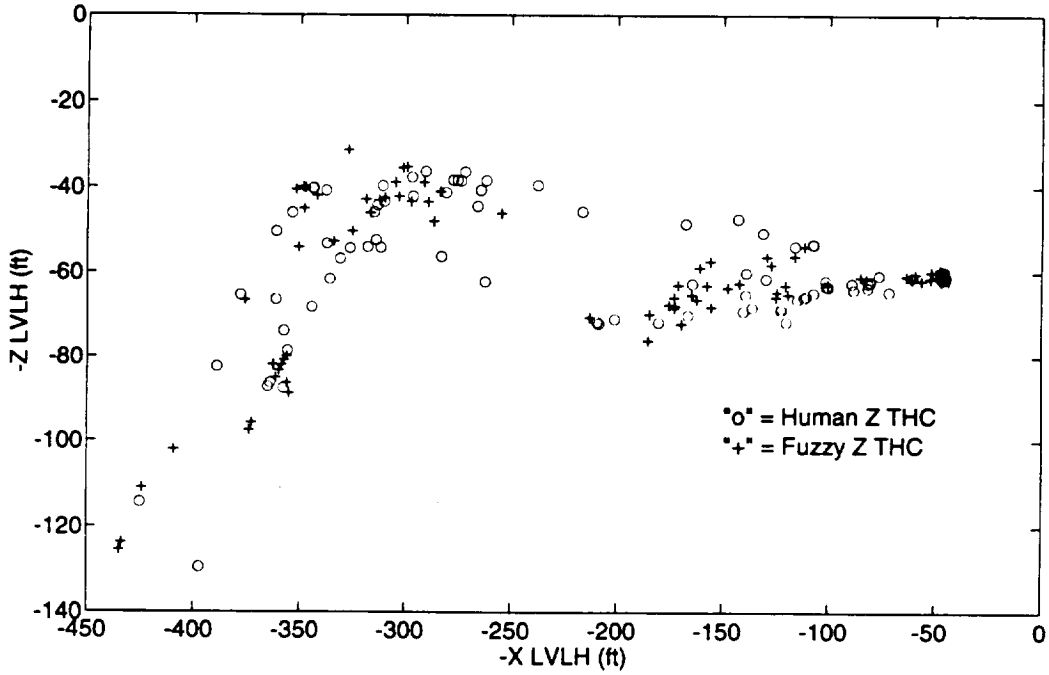

Figure 7-16 Location of the Z THC commands

7.3.3 Total Time, Fuel, and THC Activity

Table 7-1 compares the statistics for the total time, fuel consumed, and THC activity from the man-in-the-loop runs and the fuzzy pilot simulations. It has a similar format to Table 5-1, with the first three rows listing the total values, and all other rows comparing the various burns in the X, Y, and Z axes.

Looking at the total numbers in the first three rows, the average simulation by the fuzzy model was extremely close to the average man-in-the-loop run. On average the fuzzy pilot's simulations lasted only 33 seconds longer, consumed 7.1 lb. more of fuel, and left the THC jets on for 0.99 seconds less than the human pilot. These numbers equate to percentage differences of only 1.6%, 3.2%, and -1.7% respectively. Not only are these average numbers very similar, but so are the values for each individual run. The three figures on page 128, show a comparison of these performance numbers for all eight initial conditions (labeled 1-6, 29, and 30). These bar graphs indicate different initial conditions affect both pilots in the same way. The initial conditions that required more time, fuel, or jet activity from the human operator, required the same from the fuzzy pilot. This indicates the fuzzy model is a good predictor of the human's overall performance from a number of initial conditions, in terms of simulation time, fuel requirements, and translation jet on time.

The fuzzy model also had very similar performance to the human pilot, when comparing the THC activity for each axis. For the X axis, the fuzzy model used an average of 0.48 seconds more jet time than the human pilot; for the Y axis it used 0.08 seconds less; and the fuzzy model averaged using 0.39 seconds less jet time for the Z axis. These differences equate to only 3.9%, -3.4% and -0.9% deviation from the average man-in-the-loop run. The standard deviation for the THC jet on time was also very close for the Y and Z axes. However, in the X axis, the fuzzy pilot was more consistent than the human pilot, and had a THC jet on time σ less than half the σ of the human pilot.

Table 7-1 Comparison of total time, fuel and THC activity

	Man-in-the-loop Ave	σ	Fuzzy Pilot Ave	σ	Difference of Averages
Total Numbers					
Total Time (sec)	**2,105.6**	261.1	**2,138.9**	227.1	**33.3**
Total Fuel Consumed (lb.)	**221.8**	51.2	**228.9**	43.7	**7.1**
Total THC Jet on Time (sec)	**59.59**	14.27	**58.60**	12.11	**-0.99**
X THC PULSES:					
±X THC Jet on Time (sec)	**12.28**	**2.08**	**12.76**	**0.94**	**0.48**
Number of ±X THC Pulses	**33.00**	6.28	**41.50**	4.78	8.50
Number of +X THC	**26.75**	4.13	**35.25**	3.53	**8.50**
DAP A +X	**17.75**	3.01	**14.25**	0.89	**-3.50**
DAP B +X	**9.00**	4.27	**21.00**	3.46	**12.00**
Number of -X THC	**6.25**	3.15	**6.25**	2.43	0
DAP A -X	**4.12**	1.73	**4.88**	1.36	0.76
DAP B -X	**2.12**	2.42	**1.38**	1.60	-0.74
Y THC PULSES:					
±Y THC Jet on Time (sec)	**2.36**	**1.30**	**2.28**	**1.40**	**-0.08**
Number of ±Y THC Pulses	**11.25**	5.65	**10.25**	5.55	-1.00
Number of +Y THC	**6.75**	4.23	**5.25**	2.91	-1.50
DAP A +Y	**0.75**	1.16	**1.00**	1.19	0.25
DAP B +Y	**6.00**	3.38	**4.25**	2.49	-1.75
Number of -Y THC	**4.50**	2.07	**5.00**	2.73	0.50
DAP A -Y	**1.00**	1.07	**1.00**	1.60	0
DAP B -Y	**3.50**	1.77	**4.00**	2.33	0.50
Z THC PULSES:					
±Z THC Jet on Time (sec)	**43.95**	**12.63**	**43.56**	**12.67**	**-0.39**
Number of ±Z THC Pulses	**11.87**	3.23	**10.25**	2.31	-1.62
Number of +Z THC	**10.50**	2.14	**8.87**	2.30	-1.63
Low Z					
DAP A Low Z	**7.38**	2.13	**7.38**	2.20	0
DAP B Low Z	**0**	0	**0**	0	0
Norm Z					
DAP A Norm Z	**0.25**	0.46	**0.25**	0.46	0
DAP B Norm Z	**2.87**	1.36	**1.25**	0.89	-1.62
Number of -Z THC	**1.38**	1.51	**1.38**	0.92	0
DAP A -Z	**0**	0	**0**	0	0
DAP B -Z	**1.38**	1.51	**1.38**	0.92	0

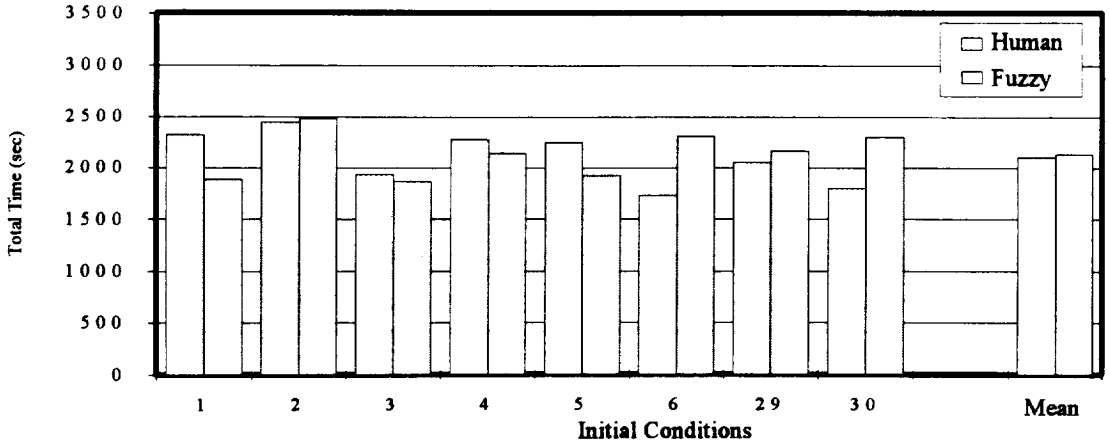

Figure 7-17 Comparison of simulation time

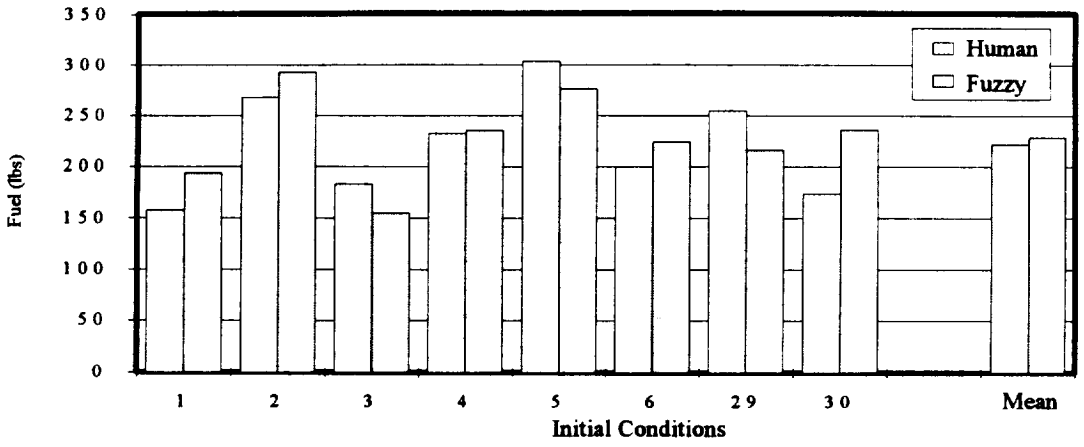

Figure 7-18 Comparison of fuel consumed

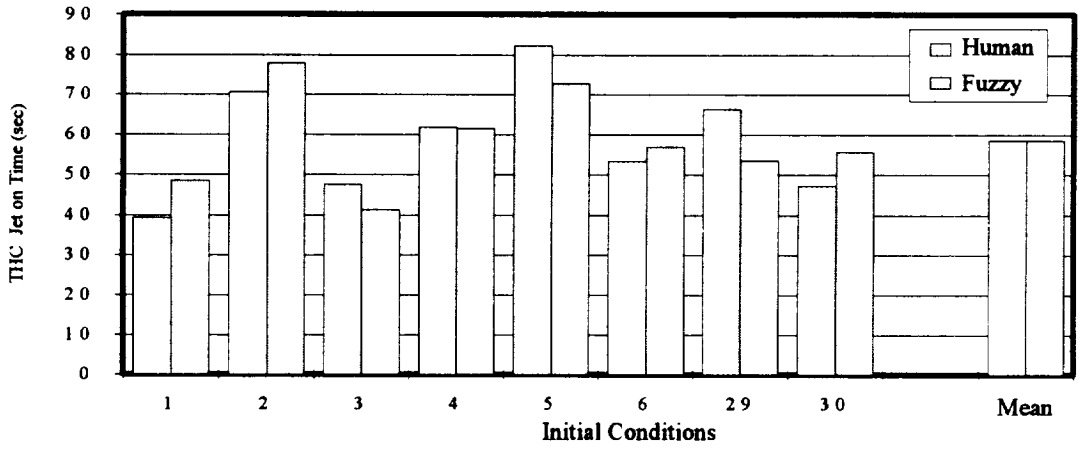

Figure 7-19 Comparison of THC jet on time

The model also made approximately the same number of each type of individual burn (DAP A/B, Positive/Negative, Low Z/Norm Z) as the human in all three axes. The model did a particularly good job of duplicating the human's response in the Z axis, matching the human pilot exactly in six of the nine types of Z burns. The only category where the pilot model differed significantly from the human was for the average number of various +X burns. However, this minor discrepancy may have been prevented if the model had waited slightly longer before switching to DAP B mode. Notice, the difference between the average number of DAP A +X burns is -3.5, but the difference for the number of burns in DAP B mode is +12. Because a DAP A burn is three times as large as a DAP B burn, these two discrepancies almost cancel each other. In other words, if the fuzzy model had averaged 4 more DAP A +X burns in place of 12 DAP B +X burns, it would have produced almost identical results as the human pilot.

The easiest way for the model to produce more X burns in DAP A is to switch to DAP B at a later point in the run. This would correct the slight discrepancy in the X axis. However, it would also probably result in a difference with the Y axis. If the transition point was reduced, the model would most likely make too many Y burns in DAP A mode, and to few Y burns in DAP B, when compared with the human's results. A better solution is to incorporate the ability to switch back and forth between DAP modes. This capability is not included in the present software model, but it could be added by simply using a different transition point for each axis. For example, instead of switching to DAP B for all three axes when $R_L \approx 100$ ft, a transition point around 80 ft could be used for the X axis. With this logic, at ranges between approximately 100 ft and 80 ft the model would make Y burns in DAP B mode, but switch back to DAP A for the X burns. This behavior has been observed by some human pilots. Adding this capability to the pilot model would likely produce slightly closer results to the man-in-the-loop data.

7.3.4 Adherence to Piloting Rules and Miss Distance

The first two sections of Table 7-2 list the average performance for the fuzzy model and Pilot 2 relative to the piloting requirements for COAS angles and range rate. In the first section, comparing COAS angles, the fuzzy pilot and human pilot differ by 1° or less in six of the eight categories. In the other two categories they are only off by -1.8° and -2.7°. In the second section, comparing the pilots' adherence to the range rate requirements, the numbers are also very close. The most significant difference in these first two sections is the man-in-the-loop runs have slightly higher standard deviations. This difference is most pronounced for the maximum $\lambda_{\dot{r}}$ inside 25 ft. For this parameter the human pilot had a σ twelve times larger than the fuzzy model. This is due to the variability associated with a human operator. In contrast, the fuzzy model used the exact same techniques for each run, and as a result had very little variation, particularly in the vertical axis.

The miss distances, shown in the third section of Table 7-2 are defined in the same way they were in Chapter 5. For the pilot model, this distance is calculated after the Shuttle manipulator arm brakes the YZ LVLH plane, resulting in every simulation missing by 0 ft in the X_{LVLH} direction. For the man-in-the-loop runs the final miss distance had to be determined by the minimum port-to-port distance during the entire simulation. Using these slightly different definitions, the fuzzy model and human pilot still produced similar results. In each axis the fuzzy model's miss distance was within 1.6 ft of the human's, and it averaged missing by only a foot less than the average human simulation. This is another example of the fuzzy pilot's ability to handle a number of different initial conditions and produce similar results to an average man-in-the-loop run.

Table 7-2 Comparison of adherence to piloting rules and final miss distance

PARAMETER	Rule or Ideal	Man-in-the-loop Ave	Man-in-the-loop σ	Fuzzy Pilot Ave	Fuzzy Pilot σ	Difference of Averages
COAS ANGLES:						
Port-to-Port Range > 25						
Minimum λ_V (deg)	-8	-5.9	1.8	-5.0	0.8	0.9
Maximum λ_V (deg)	8	6.9	1.5	5.1	0.9	-1.8
Minimum λ_H (deg)	-8	-6.1	1.8	-5.9	1.5	0.2
Maximum λ_H (deg)	8	5.8	3.6	5.2	1.6	-0.6
Port-to-Port Range < 25						
Minimum λ_V (deg)	-5	-1.2	2.2	-1.4	1.0	-0.2
Maximum λ_V (deg)	5	4.7	1.2	2.0	0.1	-2.7
Minimum λ_H (deg)	-5	-4.0	0.9	-3.4	1.3	0.6
Maximum λ_H (deg)	5	3.8	1.0	2.8	0.9	-1.0
RANGE RATE:						
Port-to-Port Range > 100 ft:						
Max neg. deviation from $\frac{-R_L}{1000}$ ($\frac{ft}{sec}$)	-.1	-.12	.02	-.10	.01	.02
Max pos. deviation from $\frac{-R_L}{1000}$ ($\frac{ft}{sec}$)	.1	.04	.04	.03	.02	-.01
Port-to-Port Range < 100 ft:						
Min $\dot{R}_L$ (max closure rate) ($\frac{ft}{sec}$)	-.2	-.21	.03	-.18	.03	.03
MISS DISTANCE:						
X_{LVLH} (ft)	0	1.6	0.5	0	0	-1.6
Y_{LVLH} (ft)	0	-0.6	0.9	-1.0	0.9	-0.4
Z_{LVLH} (ft)	0	1.0	0.8	-0.2	0.7	-1.2
Total (RMS) Miss Distance (ft)	0	2.3	0.6	1.3	0.7	-1.0

7.3.5 Frequency of THC Commands

The final evaluation of the fuzzy model compares its frequency of THC commands with the response from the human pilot. This was not practical in earlier chapters, which only evaluated one simulation. However, given a sample size of eight simulations, it is now a worthwhile comparison. It is also a very important comparison because the frequency of jet firings is a critical factor in determining the dynamic loads on the Station's solar panels. Therefore, the pilot model should match a human's general THC command frequency characteristics.

The figures and plots used for this comparison are shown on pages 133 to 135, and require a brief explanation. Six different figures are used to compare the THC frequency response in the X, Y, and Z axes from the human and fuzzy pilot. Each of these figures is divided into three plots based upon R_L: one for ranges outside 250 ft, one for ranges between 250 ft and 100 ft, and the last plot is for ranges inside 100 ft. The x axis for each plot shows the time between successive THC burns, and has a scale from 0 to 40 seconds. The y axis shows the number of times the pilot waited a specified length of time. This value is shown as an average over all eight runs. For example, Figure 7-20 shows the frequency of THC commands applied by Pilot 2 in the X_{Body} axis. The third plot in this figure is used for $R_L < 100$ ft. It shows the human averaged 1.5 X burns that were between two and three seconds from the pervious X burn. This was the most common time interval for this range. The plot also shows relatively few burns were made within 20 to 40 seconds of the previous burn. Because the number of THC commands that are separated by more than 40 seconds continues decreasing for larger time intervals, points outside 40 seconds are not shown. All six figures used to evaluate the frequency response from the human pilot and the fuzzy pilot model use this same format.

A few conclusions can be made by comparing the three plots in Figure 7-20 with those in Figure 7-21, showing the fuzzy model's response. In general these plots are

similar. They all have more points plotted between two and five seconds than for any other time interval. This indicates the dominant frequency for both pilots is approximately one THC pulse every three seconds. Both pilots also do not make many burns within a 20 to 40 second time interval from the previous X burn.

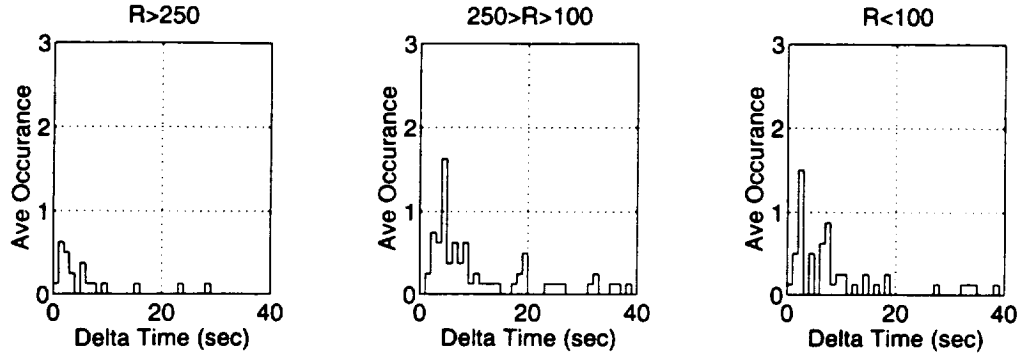

Figure 7-20 Human pilot's frequency response for the X axis

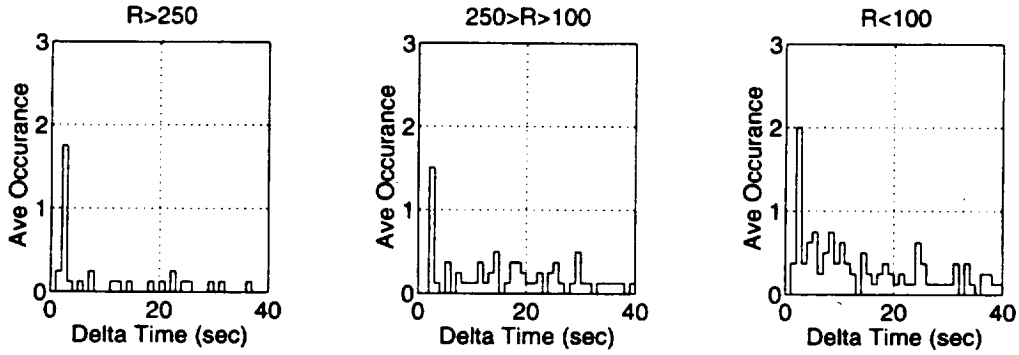

Figure 7-21 Fuzzy model's frequency response for the X axis

The most notable difference between the two pilots' frequency response, is the comparison of the first plots in each figure, for $R_L > 250$ ft. For this range, the fuzzy model made slightly more burns at a two to three second time interval than the human pilot. However, this was only a difference of one more burn for each run, which could be the result of too small of a sample of initial conditions.

The fuzzy model also did a good job of matching the human's frequency of Y THC commands. Referencing the first plots in Figure 7-22 and Figure 7-23, neither pilot made

any Y burns within 40 seconds of a previous Y command when $R_L > 250$ ft. For the other two plots the response is also very similar. (Notice, these figures have a much smaller scale of only one burn per simulation.)

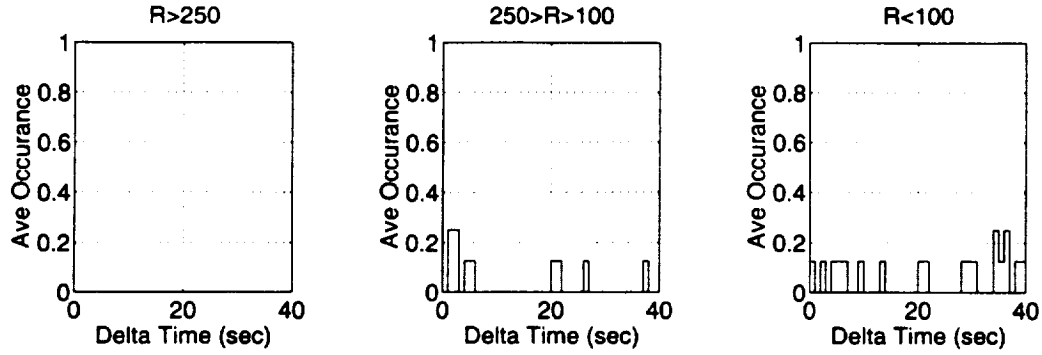

Figure 7-22 Human pilot's frequency response for the Y axis

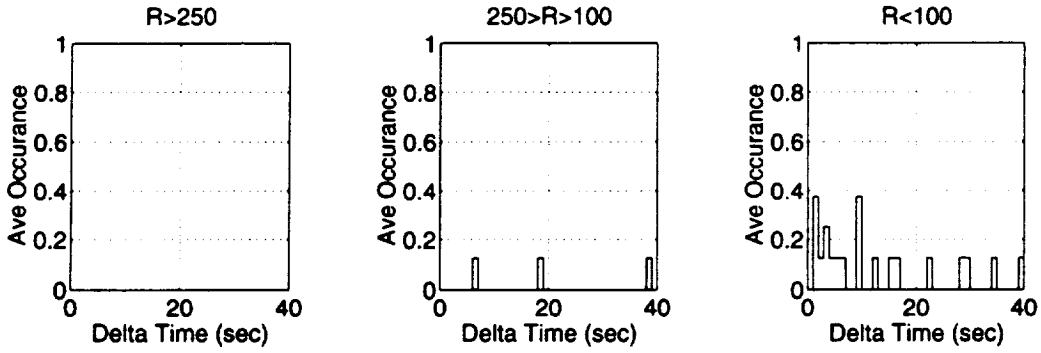

Figure 7-23 Fuzzy model's frequency response for the Y axis

The fuzzy model's frequency of Z THC commands also compares well with the human's response. There are only two general discrepancies. For ranges outside 250 feet, the fuzzy pilot model made an average of 0.6 more burns than the human at a Δt of two to three seconds. Secondly, for ranges inside 100 feet, the human pilot made a total of five burns, that were within 20 seconds of the previous Z command. However, for this range the fuzzy pilot did not make any burns within 20 seconds of the previous Z burn.

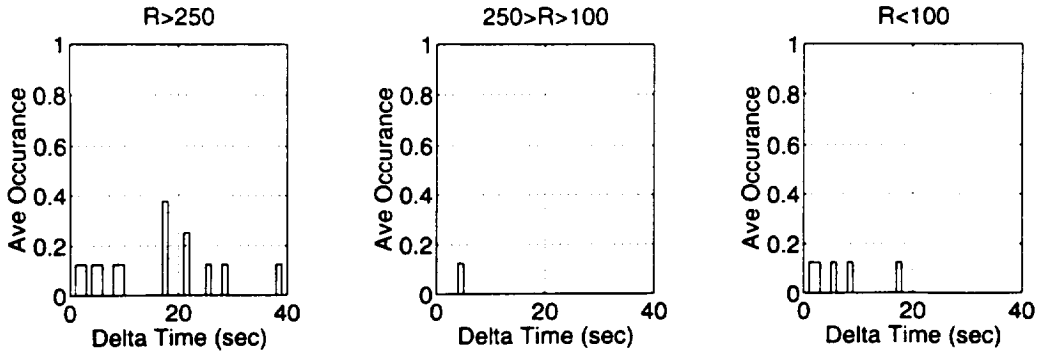

Figure 7-24 Human pilot's frequency response for the Z axis

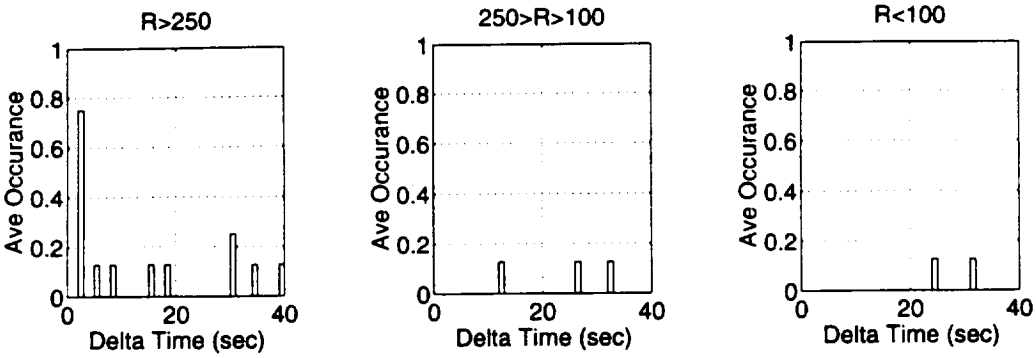

Figure 7-25 Fuzzy model's frequency response for the Z axis

For all three axes, only minor differences were noted when comparing the frequency of THC commands from the fuzzy model and the human pilot. These differences could be due to the relatively small number of simulations used in this comparison or the consistent parameters used by the pilot model. Given a larger sample of simulations, and some pilot model variability the frequency response may be more similar. The slight difference could also be attributed to the arbitrary selection of dividing the three plots in each figure into ranges outside 250 feet, between 250 ft and 100 ft, and inside 100 ft.

7.4 CONCLUSIONS

This chapter demonstrates the fuzzy model is very robust and can perform well from a number of different initial conditions without being readjusted for each run. The fuzzy model produced average results when compared with a human pilot from the same eight initial conditions.

One area of improvement for the pilot model was also identified. This slight change would incorporate different DAP mode transition points for each axis, which would model the human pilots' ability to switch back and forth between DAP modes. With this modification, the model would make slightly more X burns in DAP A, and still make most of the Y burns in DAP B, producing results that are more similar to a human pilot.

This chapter also demonstrates the need to vary the pilot model's fuzzy sets between runs to capture the natural variability of human pilots. Because the fuzzy sets were held constant, the pilot model used the exact same techniques for each simulation. As a result, the model was more consistent than the human pilot. This consistency was necessary to show the robust qualities of the pilot model, and would also be very beneficial for any future parametric studies. However, an extremely consistent model is not desirable for the immediate requirement of supplementing NASA's man-in-the-loop data base. For this task the pilot model needs to vary its techniques by changing some fuzzy set boundaries. This would model slight differences in the techniques used by a human pilot for different simulations.

It is probably not necessary to vary every membership function, only a few critical ones. The most important function to vary is $\mu(\lambda_r)$, which directly affects the model's control response in the vertical axis. Statistically changing this function between extremes should correct the model's lack of variability evident in the vertical COAS plots and the location of X THC commands. It should also correct the model's small σ for the X THC

jet on time and the maximum λ_v inside 25 ft. These changes would enable the model to closely match the variation associated with a human pilot over a large sample of simulations.

Chapter 8 : Conclusions

8.1 Summary of Research

A software pilot model has been developed for Space Shuttle proximity operations utilizing fuzzy logic. This model is designed to duplicate a human pilot's performance. It uses only the sensory data available to a real pilot, and its decision logic is based upon existing piloting rules and techniques and analysis of man-in-the-loop simulations. Because of its ability to produce a large sample of simulations with typical human results, this pilot model should be suitable for supplementing NASA's database of man-in-the-loop simulations to various Space Station assembly stages. The model could therefore support the on going analysis of the Shuttle jet plume effects on the Space Station. In addition, the model can easily be modified to incorporate new piloting rules or techniques. As a result, the model is a valuable tool for performing parametric analysis of proposed changes to NASA's existing procedures.

The fuzzy pilot model was developed incrementally, beginning with a simple model that did not account for the effect of the Shuttle's attitude motion on the pilot's view through the COAS. This three degree-of-freedom model produced reasonable results while flying a three DOF Shuttle simulator, demonstrating the benefits of a fuzzy logic

controller. However, when flying a realistic six DOF Shuttle, the model misinterpreted the Shuttle's attitude motion as translational motion relative the Space Station. This resulted in unnecessary X and Y translation burns.

To correct this problem additional logic was added, which accounts for the Shuttle's attitude motion using the same simple techniques used by real pilots. This six degree-of-freedom model produced average results when compared with four man-in-the-loop runs from the same initial condition. It was much more representative of the human's performance than a similar pilot model based upon "crisp", Boolean logic. The ability of the fuzzy pilot to model extreme individual piloting techniques by adjusting fuzzy set definitions was also demonstrated.

It was also shown that the pilot model's set boundaries could be adjusted to model the new piloting rule that defines a smaller approach corridor. The pilot model was then flown from eight different initial conditions using the same fuzzy set parameters. These results were compared with a real pilot's performance. This demonstrated the model's ability to produce human-like results from a number of initial conditions. In addition, the consistent techniques used by the pilot model highlighted the variability of an individual human. This demonstrated the need to vary the fuzzy sets slightly when conducting a large sample of simulations designed to duplicate a human's performance.

8.2 Summary of Conclusions

The evolutionary process used to develop the pilot model, was outlined in Chapters 4 through 7. Each chapter analyzed a different aspect of the fuzzy controller, building upon the previous chapters' research and conclusions. These conclusions are summarized on the following page:

Chapter 4:

- Fuzzy logic is a suitable means of modeling a human pilot during proximity operations. It allows the pilot model to operate with vague and conflicting goals using a number of simple linguistic rules. The conclusions from these rules can be combined resulting in a single output. This is a good model of a human pilot's ability to perform trade-offs between vague and opposing objectives.
- Despite the initial success of the fuzzy pilot model, additional logic was needed to account for the effect of the Shuttle's attitude motion on the pilot's view through the COAS.

Chapter 5:

- The additional logic, enabling the model to account for attitude motion when interpreting COAS data, prevented the model from overcontrolling with successive X and Y THC commands.
- The six DOF fuzzy pilot model can duplicate an average human's performance.
- The fuzzy model is much more similar to the man-in-the-loop data than another model based upon traditional logic.

Chapter 6:

- The fuzzy model is able to match different individual piloting techniques by redefining fuzzy terms. This gives the model the potential to capture the individual techniques of a broad range of possible pilots, which is a necessary requirement for supplementing NASA's database.

Chapter 7:

- The fuzzy pilot is also able to model new piloting rules by redefining fuzzy terms. This capability will be important if preliminary analysis indicates the existing rules are inadequate for Space Station rendezvous missions.
- The pilot model can produce average human results from a number of initial conditions.

- The pilot model should incorporate different DAP A to DAP B transition points for each axis. This would more accurately model a human pilot's ability to switch back and forth between DAP modes during a simulation, and would produce results that are more similar to a human pilot.
- Because the piloting parameters were held constant, the model was very consistent. This will be beneficial for future parametric studies. However, for the current requirement of supplementing NASA's plume loads database, a realistic representation of human variability is required. This can best be achieved by varying the fuzzy sets between extreme techniques.

8.3 Recommendations for Additional Work

8.3.1 Improvements to the Current Fuzzy Pilot Model

Two areas need to be addressed before the fuzzy pilot model is able to produce large Monte Carlo studies. First, the model should incorporate the ability to switch DAP modes at different points for each axis. This relatively minor change would model the human pilots' tendency to use DAP A for more X burns and DAP B for more Y burns.

Another area that requires further research involves statistically varying the fuzzy sets between runs. This is necessary to model a range of potential pilots. There are a number of ways this could be accomplished. One possible method is to begin by "matching" a number of man-in-the-loop runs one-by-one, using the same iterative process used in this thesis. This is a time consuming task, requiring approximately seven iterations for each run.[1] After closely duplicating approximately 20 to 30 man-in-the-loop

[1] A more systematic method of identifying piloting techniques and matching individual runs without manual iterations would be beneficial in reducing the time required for this process. Unfortunately, the author does not know of any such methods that can produce reasonable results.

simulations, create a covariance matrix of all their piloting parameters. This matrix would account for the correlation between different piloting techniques. Using this covariance matrix, a "new" software pilot could be generated for every simulation. This would enable the model to capture a broad range of potential pilots, not just the 20 to 30 pilots that were initially modeled.

Using this basic methodology and the fuzzy pilot model presented in this thesis, Draper Laboratory intends to conduct large sample Monte Carlo studies of proximity operations to various Space Station assembly stages. As needed, Draper Laboratory will also use this fuzzy pilot model for parametric studies for analysis of potential new piloting rules or techniques.

8.3.2 Long Term Potential of a Fuzzy Pilot Model

The fuzzy pilot model has the ability to meet NASA's short term requirements. It could supplement their man-in-the-loop database and would also be useful for analyzing proposed new piloting requirements or techniques. In addition, there are a number of long term benefits for the fuzzy pilot model.

Because the model is designed to mimic a human pilot, it has the potential to be a suitable pilot aide or autonomous pilot. Research in this area could include information from other navigation sensors not available to a human pilot, which should improve its performance. This work would be similar to some previous work by NASA described in Chapter 1, with the exception that this model would still be based primarily upon actual human performance. It would therefore perform in a manner acceptable to a human operator. This is one of the essential requirements for any aircraft autopilot system, and it is also important for a proximity operations autopilot or pilot aide.

Other improvements could be made to the pilot model that would not detract from its acceptability as a pilot aide or autopilot. For example, the model could command burns at an optimum frequency to minimize dynamic plume loads on the Station. This minor

change would produce superior results, which would still be very reasonable and readily accepted by a human operator.

Appendix A: The Clohessy-Wiltshire Equations of Motion

The Clohessy-Wiltshire equations describe the relative motion between two point masses that are both in orbit about a larger body.[7] This portion of the thesis derives these equations and their solution, choosing the two point masses to be the Shuttle and a target vehicle, with the earth as the third large body. A number of assumptions are made in their derivation. These are summarized below:

1. All three bodies are treated as point masses, and the mass of the Shuttle and target vehicle is negligible compared to the earth's mass.
2. The earth's gravitational field is the only force acting on the Shuttle and the target.
3. The target is in a circular orbit.
4. The distance between the Shuttle and the target is small compared to their distance from the earth.

Newton's gravitational law defines the magnitude of force between two point masses, m_1 and m_2, as

$$F = \frac{Gm_1m_2}{R_{12}} \tag{A-1}$$

Where G is the universal gravitational constant, and R_{12} is the distance separating the two bodies. This force acts along the vector $\mathbf{R}_{12} = \mathbf{R}_2 - \mathbf{R}_1$. The force on each body

expressed in vector form is:

$$\mathbf{F}_1 = \frac{Gm_1m_2}{R_{12}^3}(\mathbf{R}_2 - \mathbf{R}_1) \qquad \mathbf{F}_2 = \frac{Gm_1m_2}{R_{12}^3}(\mathbf{R}_1 - \mathbf{R}_2) \tag{A-2}$$

Applying Newton's second law, $\mathbf{F} = m\ddot{\mathbf{R}}$, yields two differential equations describing the bodies' motion in an inertial reference frame.

$$\ddot{\mathbf{R}}_1 = \frac{Gm_2}{R_{12}^3}(\mathbf{R}_2 - \mathbf{R}_1) \qquad \ddot{\mathbf{R}}_2 = \frac{Gm_1}{R_{12}^3}(\mathbf{R}_1 - \mathbf{R}_2) \tag{A-3}$$

The relative motion of m_2 with respect to m_1 is found by differencing these two equations.[1]

$$\ddot{\mathbf{R}}_2 - \ddot{\mathbf{R}}_1 = \frac{-G(m_1 + m_2)}{R_{12}^3}(\mathbf{R}_2 - \mathbf{R}_1) \tag{A-4}$$

Defining $\mathbf{R} = \mathbf{R}_{12} = \mathbf{R}_2 - \mathbf{R}_1$ and $\mu = G(m_1 + m_2)$, the fundamental differential equation describing the gravitational motion of m_2 with respect to m_1 is

$$\ddot{\mathbf{R}} + \frac{\mu}{R^3}\mathbf{R} = 0 \tag{A-5}$$

Using this equation, the motion of the Shuttle and the target vehicle can be found with respect to the center of the earth

$$\begin{aligned} &\text{Space Shuttle:} && \ddot{\mathbf{R}}_S + \frac{\mu}{R_S^3}\mathbf{R}_S = 0 \\ &\text{Target Vehicle:} && \ddot{\mathbf{R}}_T + \frac{\mu}{R_T^3}\mathbf{R}_T = 0 \end{aligned} \tag{A-6}$$

Where m_1 is the earth's mass and m_2 is either the mass of the Shuttle or the target, so $\mu = G(m_1 + m_2) \approx Gm_1$.[1]

Defining $\mathbf{r} = \mathbf{R}_S - \mathbf{R}_T$, the Shuttle's motion with respect to the target is

$$\ddot{\mathbf{r}} = \ddot{\mathbf{R}}_S - \ddot{\mathbf{R}}_T = \frac{\mu}{R_T^3}\left(\mathbf{R}_T - \frac{R_T^3}{R_S^3}\mathbf{R}_S\right) \tag{A-7}$$

In LVLH coordinates[1], the three vectors are

$$\mathbf{r} = \begin{bmatrix} x \\ y \\ z \end{bmatrix} \qquad \mathbf{R}_T = \begin{bmatrix} 0 \\ 0 \\ -R_T \end{bmatrix} \qquad \mathbf{R}_S = \mathbf{r} + \mathbf{R}_T = \begin{bmatrix} x \\ y \\ z - R_T \end{bmatrix} \tag{A-8}$$

and the ratio

$$\frac{R_T^3}{R_S^3} = \frac{R_T^3}{\left(x^2 + y^2 + (z - R_T)^2\right)^{\frac{3}{2}}} \tag{A-9}$$

This fraction can be expanded as a binomial series.

$$\frac{R_T^3}{R_S^3} = R_T^3\left((R_T - z)^{-3} - \tfrac{3}{2}(R_T - z)^{-5}(x^2 + y^2) + H.O.T.\right) \tag{A-10}$$

Further expanding the two $(R_T - z)$ terms using the binomial series yields

$$\begin{aligned} (R_T - z)^{-3} &= R_T^{-3} + 3R_T^{-4}z + \text{H.O.T} \\ (R_T - z)^{-5} &= R_T^{-5} + 5R_T^{-6}z + \text{H.O.T} \end{aligned} \tag{A-11}$$

Substituting these expressions into Equation A-10, and multiplying through by R_T^3,

$$\frac{R_T^3}{R_S^3} = 1 + 3\frac{z}{R_T} - \frac{3}{2}(x^2 + y^2)\left(\frac{1}{R_T^2} + 5\frac{z}{R_T^3}\right) + \text{H.O.T.} \tag{A-12}$$

Because $R_T >> r$, all of the second order terms involving $\frac{X}{R_T}$, $\frac{Y}{R_T}$, or $\frac{Z}{R_T}$ can be neglected.

[1] The LVLH coordinate frame is described in Section 3.3.

This leaves

$$\frac{R_T^3}{R_S^3} \approx 1+3\frac{z}{R_T} \tag{A-13}$$

Substituting this into Equation A-7, and remembering $\mathbf{R_S} = \mathbf{R_T} + \mathbf{r}$

$$\ddot{\mathbf{r}} = \frac{\mu}{R_T^3}\left(\mathbf{R_T} - \left(1+3\frac{z}{R_T}\right)(\mathbf{R_T}+\mathbf{r})\right) \tag{A-14}$$

Collecting similar terms this expression reduces to

$$\ddot{\mathbf{r}} = \frac{\mu}{R_T^3}\left(-\mathbf{r} - 3\frac{z}{R_T}\mathbf{R_T} - 3\frac{z}{R_T}\mathbf{r}\right) \tag{A-15}$$

Because $\frac{z}{R_T}\mathbf{r} << 1$, the last term is neglected, and the differential equation of the Shuttle's motion relative to the target vehicle becomes

$$\ddot{\mathbf{r}} = \frac{\mu}{R_T^3}\left(-\begin{bmatrix} x \\ y \\ z \end{bmatrix} - \frac{3z}{R_T}\begin{bmatrix} 0 \\ 0 \\ -R_T \end{bmatrix}\right) = \frac{\mu}{R_T^3}\begin{bmatrix} -x \\ -y \\ 2z \end{bmatrix} \tag{A-16}$$

The position vector $\mathbf{r}$ can also be differentiated directly. Its first and second derivatives are

$$\begin{aligned} \dot{\mathbf{r}} &= \mathbf{r}' + \boldsymbol{\omega} \times \mathbf{r} \\ \ddot{\mathbf{r}} &= \mathbf{r}'' + 2(\boldsymbol{\omega} \times \mathbf{r}') + (\dot{\boldsymbol{\omega}} \times \mathbf{r}) + \boldsymbol{\omega} \times (\boldsymbol{\omega} \times \mathbf{r}) \end{aligned} \tag{A-17}$$

where $\mathbf{r}'$ and $\mathbf{r}''$ are the first and second derivatives of the position vector observed in the rotating LVLH frame, and $\boldsymbol{\omega}$ is the coordinate frame's angular velocity vector with respect to an inertial frame.

If the target is in a circular orbit, $\boldsymbol{\omega}$ will be constant so Euler's term, $(\dot{\boldsymbol{\omega}} \times \mathbf{r})$, drops out. The angular velocity vector is in the $-\hat{\mathbf{i}}_Y$ LVLH direction, and

$$\omega = \begin{bmatrix} 0 \\ -\omega \\ 0 \end{bmatrix} \quad \mathbf{r}' = \begin{bmatrix} x' \\ y' \\ z' \end{bmatrix} \quad \omega \times \mathbf{r}' = \begin{bmatrix} -\omega x' \\ 0 \\ \omega x' \end{bmatrix} \quad \omega \times (\omega \times \mathbf{r}) = \begin{bmatrix} -\omega^2 x \\ 0 \\ \omega^2 z \end{bmatrix} \tag{A-18}$$

Substituting these terms into Equation A-17, the second derivative of the position vector may be written

$$\ddot{\mathbf{r}} = \begin{bmatrix} x'' \\ y'' \\ z'' \end{bmatrix} + 2\omega \begin{bmatrix} -z' \\ 0 \\ x' \end{bmatrix} + \omega^2 \begin{bmatrix} -x \\ 0 \\ -z \end{bmatrix} \tag{A-19}$$

Set the right side of this equation equal to the right side of Equation A-16, and note for circular orbits R_T is the semimajor axis. Therefore, from Kepler's third law $\frac{\mu}{R_T^3} = \omega^2$.

$$\omega^2 \begin{bmatrix} -x \\ -y \\ 2z \end{bmatrix} = \begin{bmatrix} x'' \\ y'' \\ z'' \end{bmatrix} + 2\omega \begin{bmatrix} -z' \\ 0 \\ x' \end{bmatrix} + \omega^2 \begin{bmatrix} -x \\ 0 \\ -z \end{bmatrix} \tag{A-20}$$

This is rewritten as three separate equations, and the notation " ′ " is replaced with the more conventional " ˙ ". The resulting constant-coefficient, second order differential equations describe the relative motion of two point masses in a rotating LVLH frame. These are the Clohessy-Wiltshire equations.

$$\begin{aligned} \ddot{x} &= 2\omega\dot{z} \\ \ddot{y} &= -\omega^2 y \\ \ddot{z} &= -2\omega\dot{x} + 3\omega^2 z \end{aligned} \tag{A-21}$$

The second equation is uncoupled from the other two equations. Its solution is of the form $y = A\cos\omega t + B\sin\omega t$ where A and B are determined by the initial conditions: $y(0) = y_0$ and $\dot{y}(0) = \dot{y}_0$. Using this approach, y and $\dot{y}$ are

$$\begin{aligned} y &= y_0 \cos\omega t + \frac{\dot{y}_0}{\omega} \sin\omega t \\ \dot{y} &= -y_0 \omega \sin\omega t + \dot{y}_0 \cos\omega t \end{aligned} \tag{A-22}$$

The equations governing the in-plane orbital motion are coupled and are slightly more difficult to solve. Integrating the first equation from A-21 yields $\dot{x} = 2\omega z + C$. The constant of integration can be determined from the initial conditions: $x(0) = x_0$, $z(0) = z_0$, $\dot{x}(0) = \dot{x}_0$, and $\dot{z}(0) = \dot{z}_0$.

$$\dot{x} = 2\omega z - 2\omega z_0 + \dot{x}_0 \tag{A-23}$$

Substitute this expression for $\dot{x}$ into the third equation from A-21.

$$\ddot{z} = -2\omega(2\omega z - 2\omega z_0 + \dot{x}_0) + 3\omega^2 z$$

$$\ddot{z} = -\omega^2 z + 4\omega^2 z_0 - 2\omega\dot{x}_0 \tag{A-24}$$

The solution for this equation will be of the form $z = A\cos\omega t + B\sin\omega t + C$, where A, B, and C are determined by the initial conditions, $z(0) = z_0$, $\dot{z}(0) = \dot{z}_0$, and $\ddot{z}(0) = -2\omega\dot{x}_0 + 3\omega^2 z_0$. This results in the following expressions for z and $\dot{z}$.

$$\begin{aligned} z &= \left(\frac{2\dot{x}_0}{\omega} - 3z_0\right)\cos\omega t + \frac{\dot{z}_0}{\omega}\sin\omega t + 4z_0 - 2\frac{\dot{x}_0}{\omega} \\ \dot{z} &= \dot{z}_0\cos\omega t - (2\dot{x}_0 - 3\omega z_0)\sin\omega t \end{aligned} \tag{A-25}$$

Substitute the expression for z into Equation A-23, and collect the common terms.

$$\dot{x} = 2\dot{z}_0\sin\omega t + (4\dot{x}_0 - 6\omega z_0)\cos\omega t + 6\omega z_0 - 3\dot{x}_0 \tag{A-26}$$

Because each coefficient is a constant, this equation can be integrated directly. Then the constant of integration is evaluated at the initial condition, $t = 0$.

$$x = -\frac{2\dot{z}_0}{\omega}\cos\omega t + \left(\frac{4\dot{x}_0}{\omega} - 6z_0\right)\sin\omega t + (6\omega z_0 - 3\dot{x}_0)t + \left(x_0 + 2\frac{\dot{z}_0}{\omega}\right) \tag{A-27}$$

The six equations for x, y, z and their first derivatives can be combined in a transition matrix. For simplicity, the terms $\cos\omega t$ and $\sin\omega t$ have been replaced with "C"

and "S" respectively.[19] This is the solution to the Clohessy-Wiltshire equations in matrix form.

$$\begin{bmatrix} x \\ y \\ z \\ \dot{x} \\ \dot{y} \\ \dot{z} \end{bmatrix} = \begin{bmatrix} 1 & 0 & 6\omega t - 6\mathrm{S} & \frac{4\mathrm{S}}{\omega} - 3t & 0 & \frac{2}{\omega}(1-\mathrm{C}) \\ 0 & \mathrm{C} & 0 & 0 & \frac{\mathrm{S}}{\omega} & 0 \\ 0 & 0 & 4-3\mathrm{C} & -\frac{2}{\omega}(1-\mathrm{C}) & 0 & \frac{\mathrm{S}}{\omega} \\ 0 & 0 & 6\omega(1-\mathrm{C}) & 4\mathrm{C}-3 & 0 & 2\mathrm{S} \\ 0 & -\omega\mathrm{S} & 0 & 0 & \mathrm{C} & 0 \\ 0 & 0 & 3\omega\mathrm{S} & -2\mathrm{S} & 0 & C \end{bmatrix} \begin{bmatrix} x_0 \\ y_0 \\ z_0 \\ \dot{x}_0 \\ \dot{y}_0 \\ \dot{z}_0 \end{bmatrix} \qquad \text{(A-28)}$$

References

1. Battin, Richard, An Introduction to the Mathematics and Methods of Astrodynamics, American Institute of Aeronautics and Astronautics, New York, 1987.

2. Bellman, R.E., and L.A. Zadeh, "Decision-Making in a Fuzzy Environment", *Management Science*, vol. 17, 1970, pp. B-141-164.

3. Berenji, Hamid, Yashvant Jani, and Robert Lea, "Approximate Reasoning-Based Learning and Control for Proximity Operations and Docking in Space", Proceedings of the AIAA conference on Guidance, Navigation and Control, New Orleans, LA, August 1991.

4. Brown, Robert, Robert Polutchko, and Pete Kachmar, "Proximity Operations Pilot Model", Presented to NASA JSC Rendezvous & Proximity Operations Working Group by the Charles Stark Draper Laboratory, ESB-93-402, Shuttle-93-025, June 10, 1993.

5. Chu, Julia, Lockheed Corp. at NASA, JSC, fax to Robert Polutchko, C.S. Draper Laboratory, "Docking Angular Alignment Checklist", December 10, 1992.

6. Chu, Julia, Lockheed Corp. at NASA, JSC, fax to Pete Kachmar, C.S. Draper Laboratory, "Docking Angular Alignment Checklist", March 10, 1993.

7. Clohessy, W. H. and R. S. Wiltshire, "Terminal Guidance System for Satellite Rendezvous", *Journal of Aerospace Sciences*, vol. 27, September 1960, pp. 653-658, 674.

8. Cunningham, Glen, Erik Horstkotte, and Daniel Bochsler., "Integrating Fuzzy Logic Technology into Control Systems". AIAA Conference Paper 91-2802, 1991, pp. 1699-1702.

9. Fill, Thomas, "R&POWG Piloting Analysis Action Item 1 Analysis/Conclusions", Presented to NASA JSC Rendezvous & Proximity Operations Working Group by the Charles Stark Draper Laboratory, ESB-94-03, Shuttle-94-006, Feb. 10, 1994.

10. "Introduction to Rendezvous Guidance, Navigation and Control (GN&C)", STSOC-TM-001498, Rockwell International, Mission Operations Directorate, Flight Software Product and Verification Division, January, 1993.

11. Knapp, Roger, "A Fuzzy-Based Attitude Controller for Flexible Spacecraft with On/Off Thrusters", Master of Science Thesis, Department of Aeronautics and Astronautics, Massachusetts Institute of Technology, May 93.

12. Kosko, Bart and Satoru Isaka, "Fuzzy Logic", *Scientific American,* July 93, pp. 76-80.

13. Larkin, Lawrence, Industrial Applications of Fuzzy Control, edited by M. Sugeno. "A Fuzzy Logic Controller for Aircraft Flight Control", Elsevier Science Publishing Company, New York, 1985, pp. 87-103.

14. Le, Thomas Quan, Chair Rendezvous & Proximity Operations Working Group, NASA, Johnson Space Center, Phone interview by author, Houston, Texas, January 1994.

15. Lea, Robert, "Automated space vehicle control for rendezvous proximity operations", *Telematics and Informatics,* vol. 5, no. 3, pp. 179-185, 1988.

16. Lea, Robert, "Applications of fuzzy sets to rule-based expert system development", *Telematics and Informatics,* vol. 6, nos. 3-4, pp. 403-406, 1989.

17. Lea, Robert, Jeffrey Hoblitt, and Yashvant Jani, and "A Fuzzy Logic Based Spacecraft Controller for Six Degree of Freedom Control and Performance Results", Proceedings of the AIAA conference on Guidance, Navigation and Control, New Orleans, LA, August 1991.

18. Lea, Robert and Yashvant Jani. "Fuzzy Logic Applications to Expert Systems and Control", The Second National Technology Transfer Conference and Exposition, San Jose, CA., NASA conf. pub. 3136, vol. 2, Dec 1991, pp. 159-169.

19. Polutchko, Robert, "Cooperative Control of two active Spacecraft during Proximity Operations", Master of Science Thesis, Department of Aeronautics and Astronautics, Massachusetts Institute of Technology, August 1989.

20. "Space Shuttle Orbiter Operational Level C: Functional Subsystem Software Requirements Guidance, Navigation, and Control, Part C: Flight Control Orbit DAP", STS-83-0009F, OI-23, Rockwell International Space Systems Division, 10 February 1992.

21. "Space Shuttle Systems Handbook", JSC-11174, Revision D, Mission Operations Directorate, Systems Division, November 1987, p. 9:5-1.

22. Stephanides, Steve, "Controls Applications of Fuzzy Set Theory", Master of Science Thesis, Department of Mechanical Engineering, Massachusetts Institute of Technology, June 1992.

23. Zadeh, Lotfi, "Fuzzy Sets", *Information and Control*, vol. 8, 1965, pp. 338-353.

24. Zadeh, Lotfi, "Outline of a New Approach to the Analysis of Complex Systems and Decision Process", *IEEE Tran. Systems, Man, , and Cybernetics*, SMC-3, 1973, pp. 28-44.